Analysis and Control of Mixed Traffic Flow on a Ring with a Single Autonomous Vehicle

Vittorio Giammarino

Master of Science Thesis

TU Delft Delft University of Technology

Delft Center for Systems and Control

Analysis and Control of Mixed Traffic Flow on a Ring with a Single Autonomous Vehicle

Master of Science Thesis

For the degree of Master of Science in Systems and Control at Delft University of Technology

Vittorio Giammarino

July 11, 2019

Faculty of Mechanical, Maritime and Materials Engineering (3mE) · Delft University of Technology

Abstract

This thesis provides a theoretical framework for the arise of stop-and-go waves in platoons of Human-driven Vehicles (HVs) on a ring road topology. Possibilities and limitations for traffic control and suppression of such waves via a single Autonomous Vehicle (AV) are considered. Being HVs prone to show string instability, i.e. a type of instability caused by a disturbance acting on one of the vehicles and which is amplified throughout the platoon, the analysis starts from the observation that the standard notion of string stability on a ring road is too demanding for a mixed (human and automated) traffic scenario. Thus, after providing a new definition of string stability on a ring roadway, two directions are pursued. First, only HVs on a ring roadway are considered and their stability/instability analyzed. Second, a mixed-platoon with a single AV and the remaining HVs is placed on the ring and the AV is designed in order to ensure equilibrium stability. By means of this investigation, possibilities and limitations of traffic control via a single AV are emphasized.

Table of Contents

Acknowledgements

I would first like to thank my thesis advisor dr. Simone Baldi for his assistance during this thesis. The door of his office was always open whenever I ran into a trouble spot or had a question about my research or writing.

I would also like to thank the other experts who were involved in this research project: dr. Paolo Frasca , dr. Maria Laura Delle Monache and mr. Maolong Lyu. Without their passionate participation and input, the project could not have been successfully conducted.

I want also to acknowledge Delft University of Technology and all the employees of the DCSC department. I am gratefully indebted to this University for the several opportunities I was given and for having accompanied me in my own personal growth.

Finally, I must express my very profound gratitude to my family and to my girlfriend Justine for providing me with unfailing support and continuous encouragement throughout these years. This accomplishment would not have been so joyful without them. Thank you.

Delft, University of Technology
July 11, 2019

Vittorio Giammarino

"Just keep standing."
— *Rick Rigsby*

Chapter 1

Introduction

A traffic jam on a highway is a very familiar phenomenon that has been experienced by all the road users and which often occurs without apparent reason. It is commonly understood that a "bottleneck", like for instance on-ramps, tunnels and sags can trigger traffic jams because of the sudden increase of vehicles density on the road. Commonly, bottlenecks can cause traffic jam but they do not represent the essential origin of it. The precursor experiment of Sugiyama in 2008 [1] shows how the emergence of traffic jams can be caused by the simple interaction among vehicles, which is originated by drivers seeing other vehicles. Therefore, considering a fixed value of vehicles density, human driving style can represent the principal cause of fluctuations into traffic flow; or conversely, in congested situations, a cooperative interaction among vehicles can actually improve these scenarios.
Concerning the relation between human drivers and traffic flow, the main purpose of the aforementioned Sugiyama experiment is to provide an experimental evidence to the idea of human-triggered stop-and-go waves. Figure 1-1 shows a snapshot of the setup used in [1], a circular single-lane roadway, which can be easily interpreted as a model for an infinite road in which the dynamics are repeated any N vehicles. In this specific case, 22 vehicles drive on a ring road topology of $230m$ of circumference. Despite Sugiyama gives a first experimental evidence, earlier works such as [2, 3] already endorsed the idea that human behavior can originate traffic phases and eventually trigger stop-and-go waves with a remarkable impact in terms of fuel consumption and time. To tackle or at least to mitigate this problem, the development of traffic control systems and strategies has gained a central role in the past 20 years.

1-1 Prior research on traffic control

In the recent past, different traffic control infrastructures have been developed with the aim to reduce traffic congestion and improve the drivers experience on the roadways. Examples of these technologies are ramp metering systems, which prevent situations of critical density on the highways, and variable speed limit systems, which are useful to prevent the exponential

Figure 1-1: A snapshot of the experiment on a circular road [1]. In this case, the circumference is 230m, and the number of vehicles is 22.

growth of queue and traffic jams [4, 5, 6]. Nowadays, the transportation system is undergoing a major transition from full Human-driven Vehicle (HV) to Autonomous Vehicle (AV). As automation increases, new opportunities are arising to use AVs to control traffic flow. Attempts have been done trying to explore adaptive cruise control [7, 8] and, when the mutual vehicles communication is enabled, cooperative adaptive cruise control [9, 10] to influence the vehicular traffic by smoothing the flow or increasing its rate. In these cases the traffic flow is controlled by means of platoon control. In platooned traffic, all vehicles on the roadway are considered equipped with control and communication technology, and they can be centrally controlled to achieve stability. This ideal situation allows the vehicles to travel with extremely short spacing while maintaining stable flow dynamics. Although AV-only systems will be of great interest for the far future, before that, a long period of mixed HV-AV will occur and in the near future a really small number of AVs will drive on our roadways. This situation is more complicated in terms of theoretical stability analysis; however, it is more interesting in order to obtain short-term achievements in traffic control. As a matter of fact, this thesis focuses on this specific case where a small penetration rate of AVs is available for traffic control purposes.
Concerning this mixed HV-AV scenario, quite recent field experiments [11] have shown how a well designed single AV is in fact able to achieve stability for a finite number of HVs on a ring. This endorses the idea that is in fact possible to obtain satisfying results also with a very small penetration rate. Also in this case, the experiments have been performed on the

ring road setup in Fig. 1-1. Fig. 1-2 shows a snapshot of the field experiment [11] in which the red arrow points out the AV and the graph below depicts the evolution in time of the traffic flow. Clearly, when the AV is active, the traffic flow appears remarkably smoother than in the only HVs cases.

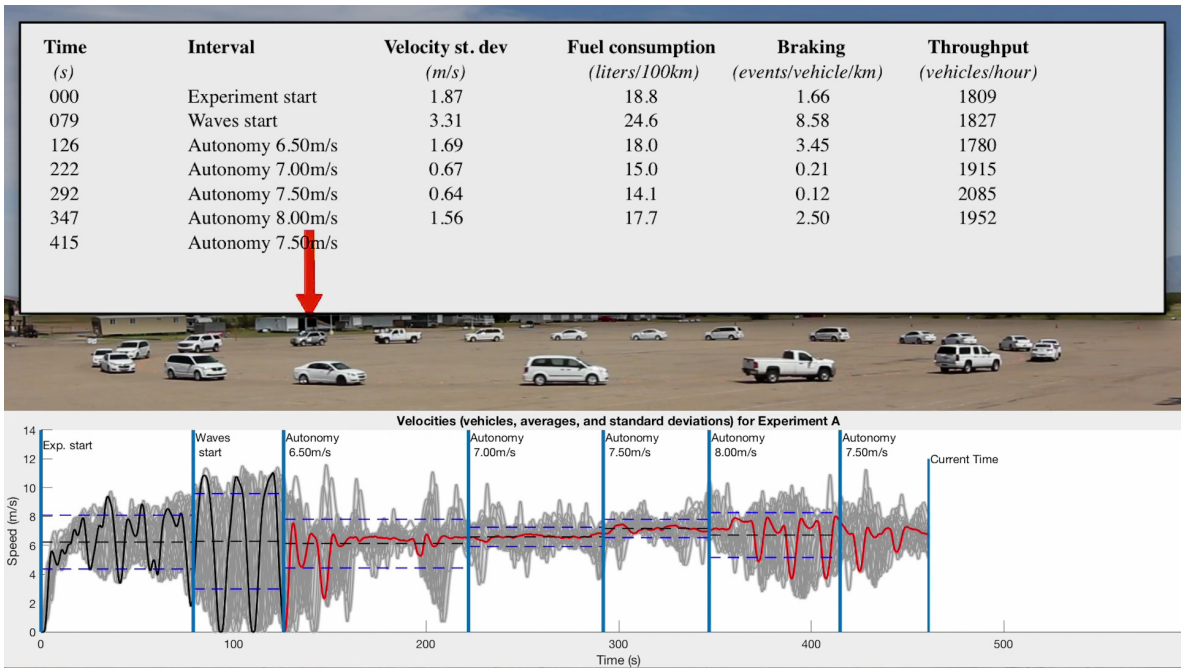

Figure 1-2: This Figure is directly taken from [11] and shows the ring road setup with 21 HVs and a single AV (red arrow). The AV is activated at about $t = 126s$ and it is able to remarkably improve the traffic flow.

1-2 Motivation of the research

The main problems identified prior the development of this work, which motivate also the thesis, are:

- An *absence of a theoretical framework* by means of systems theory *for the two aforementioned experiments*. Linear Time Invariant (LTI) systems theory is the first candidate to consider, due to the possibility of getting analytic results both in time and frequency domain. Generally, vehicles dynamics is modeled by means of non-linear models, this in order to take into account the drivers' rationality and avoid crashes between vehicles. What is missing is the evaluation of the linearized version of these models at their equilibrium and, moreover, the study of both [1, 11] using LTI systems theory in order to understand better what kind of (in)stability is observed in the two experiments.
- For practical reasons, the two experiments have been performed on a ring road topology which is somehow related to the more common string roadway. However, for the same number of vehicles N, the two topologies have undeniably a different structure and therefore, it seems reasonable investigating *if the more common definitions adopted for the stability on a string can actually be used on a ring.*

- Finally, from a practical point of view, although some AVs designs are available, most of these have been formulated by means of an empirical analysis [11, 12]. These AVs can accomplish good results in terms of traffic flow stabilization; however, *the reasons which lead to these results have to be identified*. Consequentially, it is believed that with a proper analysis, more performing designs and more awareness can be achieved.

1-3 Thesis contribution

This thesis work tries, first of all, to establish a theoretical framework for the analysis of traffic flow via a single AV. Given the ring road setup in Fig. 1-1, stability analysis will be performed first on a homogeneous HVs platoon and then on a mixed HVs-AV platoon. Thus, new definitions of stability on a ring are introduced and finally, exploiting this theoretical analysis, different AV controllers are designed and tested in order to understand to what extent a single AV is able to stabilize an otherwise unstable platoon.

In summary, the thesis will provide the following contributions

- Give a theoretical framework of the experiments performed in [1] and [11] linearizing the non-linear vehicle dynamics and then exploiting the LTI systems theory. The results obtained in the linear world are eventually validated through non-linear simulation.
- Give a new stability definition which is also suitable for heterogeneous/mixed platoon and that can be exploited in the analysis of the ring road topology.
- Propose new AV designs and strategies in order to accomplish stability for the platoon on the ring road topology. Through this last section, possibilities and limitations of traffic flow control via a single autonomous vehicle are explored.

1-4 Outline

This thesis work is divided in six main chapters. After the introduction, Chapter 2 focuses on the Sugiyama's experiment [1] and on how to model the HVs in order to recreate, in the most realistic way, what is observed. The most common car following models in literature are considered, analyzed and finally a model for the HV is determined.
Chapter 3 introduces the different notions of stability for a platoon of vehicles: namely, Lyapunov stability, string stability and string stability on a ring (ring stability) both for a homogeneous and mixed platoon.
In Chapter 4, the HV car following model chosen in Chapter 2 is considered in the ring setup with N vehicles. A necessary and sufficient condition and an only sufficient condition for Lyapunov stability are obtained. Then, after ensuring Lyapunov stability, ring stability is investigated.
Finally, in Chapter 5 controllability and stabilizability of the system at the equilibrium are inquired in order to determine what can be achieved via a single AV. Afterwards, two different designs for the AV: a Proportional-Integral (PI) with saturation controller and a H_∞ controller are developed and different strategies to control an otherwise unstable platoon are introduced. Moreover, the designs are validated through non-linear simulations of the platoon on a ring.

As last, in the conclusive chapter a summary of all the work is drawn and possible future works presented.

Chapter 2

Modeling Human Drivers

The experiment of Sugiyama et al. [1] reports the first experimental verification of a traffic jam generated in absence of a bottleneck and caused by humans' driving behavior. The human drivers, either braking too often or reacting slowly, enhance fluctuations in the traffic flow which end up generating stop-and-go waves. Sugiyama's test was important to validate the mathematical model developed prior the experiment and to provide an evidence of traffic jams as collective phenomenon.
As a matter of fact, during the 1990s, a new approach to study traffic flow was introduced: the interaction among vehicles was for the first time investigated as a dynamical phenomenon of a many-particle system. In other words, traffic flow evolution was considered similar to fluid mechanics or other fields of physics, where the macroscopic aspect evolves due to the collective motion of interactive particles [13, 14]. Hence, according to these studies, the microscopic interactions among vehicles cause changes in the macroscopic traffic features making possible a shift from a stable free flow state to a highly oscillatory jam state. Consequentially, models, also known as Car-Following (CF) models, able to show the arise of traffic jams have been developed.
Thus, the main topic of this chapter is the analysis of some of the CF models developed before the Sugiyama's experiment. Few of the most used in literature are here introduced both mathematically and qualitatively and finally, one of them is selected in order to be used in the aforementioned ring scenario simulation.
To summarize, in Section 2-1 a generic introduction to CF models and their linearization is given; then, Sections 2-2, 2-3 and 2-4 consider respectively the Optimal Velocity model, the Follow The Leader and the Intelligent Driver Model. Finally, Section 2-5 describes the Optimal Velocity-Follow the Leader model which represents the actual model used in this thesis for the Human-driven Vehicle (HV)s dynamics simulation.

2-1 An Introduction to Car-Following model framework

The starting point of this section is the standard situation depicted in Fig. 2-1. A single lane of traffic is considered with the vehicles labelled 1,2, etc., in the downstream direction.

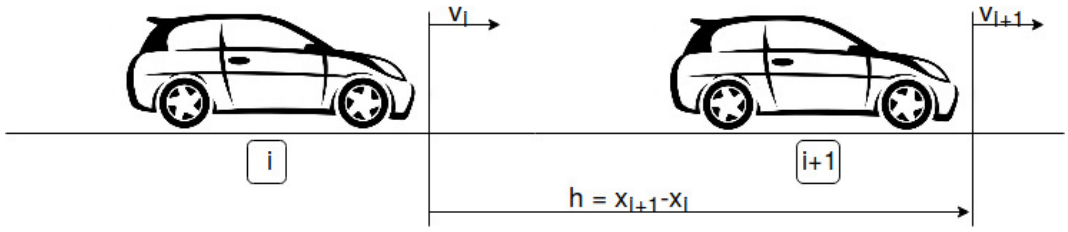

Figure 2-1: General scheme and notation for car following models.

Positions and velocities are denoted as $x_i(t)$ and $v_i(t) \geq 0$, respectively, and this notation involves front-to-front spacing $h_i(t) = x_{i+1}(t) - x_i(t) > 0$ of consecutive vehicles, commonly referred to as the headway. Note that overtaking is neglected in our framework.
In their simplest form, CF models consist of a set of coupled differential equations, in general non-linear, for the trajectory of each vehicle, which typically supplements the kinematic relations $\dot{x}_i = v_i$ with a model

$$\dot{v}_i = f(h_i, \dot{h}_{i+1}, v_i) \tag{2-1}$$

which describes how drivers accelerate/decelerate in response to the motion of the vehicle in front, to their headway and their own velocity. The equilibrium of (2-1) is found computing

$$f(h_*, 0, v_*) = 0 \quad \text{for all} \quad h_* > 0. \tag{2-2}$$

At h_* all the vehicles drive steadily with the same dynamics, this solution is known as uniform flow. As mentioned, one of the purpose of the thesis work is to show how Linear Time Invariant (LTI) systems theory can be used to analyze the non-linear traffic behavior and additionally, try to exploit this analysis to stabilize the flow by means of an Autonomous Vehicle (AV). Considering now small perturbations to the equilibrium, by setting $h_i = h_* + \tilde{h}_i(t)$ and $v_i = v_* + \tilde{v}_i(t)$, where $\tilde{h}_i$ and $\tilde{v}_i$ are small. Assuming f is sufficiently smooth, the linearization of the most common CF models yields

$$\dot{\tilde{v}}_i = (D_h f)\tilde{h}_i + (D_{\dot{h}} f)\dot{\tilde{h}}_i + (D_v f)\tilde{v}_i, \tag{2-3}$$

where the partial derivatives Df are evaluated at constant equilibrium arguments $(h_*, 0, v_*)$ and necessary constraints for rational driver behavior are

$$D_h f, D_{\dot{h}} f \geq 0 \quad \text{and} \quad D_v f \leq 0. \tag{2-4}$$

Note that equation (2-3) can be re-expressed in the form

$$\begin{aligned} \dot{v}_i &= (D_h f)(h_i - h_*) + (D_{\dot{h}} f)(\dot{h}_i - 0) + (D_v f)(v_i - v_*) \\ \dot{v}_i &= (D_h f)h_i - (D_{\dot{h}} f - D_v f)v_i + D_{\dot{h}} f v_{i+1} - (D_v f v_* + D_h f h_*) \\ \dot{v}_i &= \alpha_1 h_i - \alpha_2 v_i + \alpha_3 v_{i+1} - \alpha_4. \end{aligned} \tag{2-5}$$

A really broad class of CF models can be obtained and linearized as illustrated in (2-3). Exploiting (2-3) and using the Laplace transform, frequency domain analysis can be used in order to study linear stability of the traffic flow.
The next sections introduce some of the main CF models available in literature.

2-2 Optimal Velocity (OV) Model

The Optimal Velocity model has been theorized for the first time in literature in 1995 by Bando et al. [13]. Their purpose was to developed a model able to properly describe the dynamical evolution of congestion. Afterwards, the model has been further improved with the introduction of drivers delay response to the stimulus (cf. [17]).
The first assumption made for this model is that each vehicle has a legal velocity V and that each driver responds to a stimulus from the vehicle ahead. Each human driver should control the acceleration by putting on or getting off the accelerator and the brakes in such a way that he can maintain the legal safe velocity according to the motion of the preceding vehicle. Then, the dynamical equation of the system is obtained as,

$$\dot{v}_i = a(V(\Delta x_i) - v_i). \tag{2-6}$$

In eq. (2-6), $\Delta x_i = h_i = x_{i+1} - x_i$ is the headway and a is a constant representing the driver's sensitivity, which for simplicity is always considered independent of i. The legal velocity $V(\Delta x_i)$ is a non-linear function which is able to describe the drivers behavior on the roadway. That is, when the headway becomes too short the velocity must be reduced and become small enough to prevent crashing into the preceding vehicle. On the other hand, when the headway becomes bigger the vehicle can move with higher velocity, although it does not exceed the maximum velocity. Therefore, V is a monotonically increasing function with an upper bound $V_{max} = V(\Delta x_i \to \infty)$. Examples of V used in [13] are

$$V(\Delta x) = \tanh(\Delta x) \tag{2-7}$$
$$V(\Delta x) = \tanh(\Delta x - 2) + \tanh(2). \tag{2-8}$$

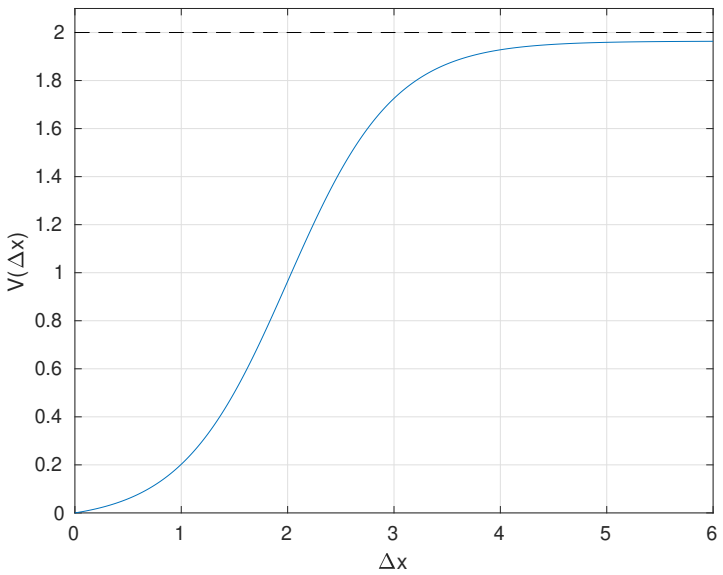

Figure 2-2: Non-linear function $V(\Delta x)$ in (2-8).

Both these functions describe approximately the desired driver behavior. For the Optimal Velocity Model (OVM), the coefficients of eq. (2-5) are

$$\alpha_1 = a\dot{V}(h_*) \quad \alpha_2 = a \quad \alpha_3 = 0 \tag{2-9}$$

and eq. (2-5) becomes

$$\dot{v_i} = a\dot{V}(h_*)h_i - av_i. \tag{2-10}$$

Despite the simplicity of the model, the OVM has been often used for numerical simulation purposes. However, one of its drawbacks is the absence of the preceding vehicle velocity v_{i+1}, which would bring advantages both from a mathematical point of view; allowing the use of the Laplace transform transfer function to determine stability, and in terms of likelihood with the reality. Neglecting the effect of the velocity difference $\Delta v = v_{i+1} - v_i$ leads to unrealistic drivers' behaviors [18].

2-3 Non-Linear Follow-The-Leader (FTL) Model

The Follow-The-Leader (FTL) model was for the first time formulated in 1960 [19] in order to provide a mathematical description of a single-lane dense traffic with no overtakes, and, as the other CF models, it is based on the assumption that each driver reacts in some specific fashion to stimulus from the car (or cars) ahead of him and/or behind him. Therefore, the basic differential equations of the FTL theory consider each driver responding to a stimulus according to a certain sensitivity. Therefore

$$\text{response} = \text{sensitivity} \times \text{stimulus}. \tag{2-11}$$

The stimulus could be a functional of the positions of a number of cars and their velocities. The response instead, has been taken as the acceleration of the vehicle, since a driver actually has a direct control of this quantity through the gas and brake pedals.
In this case, the stimulus-response differential equation is taken as

$$\dot{v_i} = \lambda(v_{i+1} - v_i) \tag{2-12}$$

with the sensitivity λ defined as

$$\lambda = a\frac{1}{(x_{i+1} - x_i)^2}. \tag{2-13}$$

With respect to the OVM, the FTL shows an acceleration that depends on both the relative velocity $\Delta v = v_{i+1} - v_i$ and the headway $h = x_{i+1} - x_i$. However, a drawback is that the acceleration becomes zero when the relative velocity is zero independently of h. This means that extremely small headways are allowed despite traveling at very high speed.
The coefficients of eq. (2-5) for the FTL model become

$$\alpha_1 = 0 \quad \alpha_2 = 2\bar{\lambda} \quad \alpha_3 = \bar{\lambda} \tag{2-14}$$

where we define for compactness $\bar{\lambda} = \frac{a}{(h_*)^2}$. Eq. (2-5) becomes then

$$\dot{v_i} = -2\bar{\lambda}v_i + \bar{\lambda}v_{i+1}. \tag{2-15}$$

Taking the Laplace transform of the signals leads to

$$\frac{v_i(s)}{v_{i+1}(s)} = \frac{\bar{\lambda}}{s + 2\bar{\lambda}} = \frac{\alpha_3}{s + \alpha_2}. \tag{2-16}$$

Given the constraints for the rational driver behavior in (2-4), $\bar{\lambda}$ turns always positive. Consequentially, the equilibrium of (2-15) turns stable, being the poles of the transfer function (2-16) always in the Left Half Plane (LHP).

2-4 Intelligent Driver Model (IDM)

The Intelligent Driver Model (IDM) belongs to the class of deterministic CF models as well as the OVM and the FTL; however, with respect to the previous two, here the mathematical complexity increases. This is the price to pay in order to have a series of remarkable advantages: the IDM (i) behaves as if accident-free because of the dependence on the relative velocity, this feature was absent in the OVM. Despite the complexity, (ii) all the model parameters have a reasonable interpretation, are known to be relevant, are empirically measurable, and have the expected order of magnitude [18], (iii) the fundamental diagram and the stability properties of the model can be easily calibrated to empirical data, (iv) an equivalent macroscopic version of the model is known [21].
Analogously to the previous models, the drivers' response is given through the vehicle acceleration which is a continuous function of its velocity v_i, the headway h and the velocity difference $\Delta v_i = v_{i+1} - v_i$:

$$\dot{v}_i = a\Big[1 - \left(\frac{v_i}{v_0}\right)^4 - \left(\frac{s^*(v_i, \Delta v_i)}{h_i}\right)^2\Big]. \tag{2-17}$$

This expression is an interpolation between the tendency to accelerate on a free road

$$\dot{v}_i(v_i) = a\Big[1 - \left(\frac{v_i}{v_0}\right)^4\Big] \tag{2-18}$$

and the tendency to brake with deceleration

$$-\dot{v}_i(h_i, v_i, \Delta v_i) = -a\left(\frac{s^*(v_i, \Delta v_i)}{h_i}\right)^2 \tag{2-19}$$

when vehicle i gets too close to its vehicle in front $i+1$. The deceleration term depends on the ratio between the "desired minimum gap" s^* and the actual headway h_i. The desired gap is expressed as

$$s^*(v_i, \Delta v_i) = s_0 + T v_i + \frac{v_i \Delta v_i}{\sqrt{4a \cdot b}} \tag{2-20}$$

and it varies dynamically with the vehicle velocity v_i and the relative velocity with the vehicle ahead Δv_i.
The coefficients that appear in the IDM not mentioned yet are: the desired velocity v_0, the safe time headway T, the maximum acceleration a, the desired deceleration b and the safe

distance s_0. Setting (2-17) equal to zero the equilibrium state equation for IDM can be obtained

$$h_* = \frac{s_0 + Tv_*}{\sqrt{1 - (\frac{v_*}{v_0})^4}}. \tag{2-21}$$

Furthermore, the coefficients for the linearized model (2-5) are

$$\alpha_1 = 2a \cdot \frac{(s_0 + Tv_*)^2}{(h_*)^3}, \tag{2-22}$$

$$\alpha_2 = \sqrt{\frac{a}{b}} \cdot \frac{v_*(s_0 + Tv_*)}{(h_*)^2} + 2a\left(\frac{2(h_*)^3}{v_0^4} + \frac{T(s_0 + Tv_*)}{(h_*)^2}\right), \tag{2-23}$$

$$\alpha_3 = \sqrt{\frac{a}{b}} \cdot \frac{v_*(s_0 + Tv_*)}{(h_*)^2}. \tag{2-24}$$

So far, among the different CF models, the IDM is probably the most complete, being function of the vehicle velocity v_i, the headway h_i and the relative velocity Δv_i with the vehicle ahead. Yet, from the mathematical point of view, the model is complicated. Hence, the purpose of the next section is to find a simpler model with though the same amount of information.

2-5 Optimal Velocity-Follow-The-Leader (OV-FTL) Model

The OV-FTL model, as the name suggests, is essentially the interpolation between the Optimal Velocity model [13] and the Follow-The-Leader [19]. The idea is to elaborate a model that, likewise the IDM, depends on the vehicle velocity v_i, the headway h and the velocity difference $\Delta v_i = v_{i+1} - v_i$. Although simpler from a mathematical point of view, the OV-FTL model represents a good trade-off between richness and simplicity [12].
The non-linear differential equation describing the acceleration is

$$\dot{v}_i = a\frac{v_{i+1} - v_i}{h_i^2} + b[V(h_i) - v_i] \tag{2-25}$$

with $V(h)$ the non-linear function determining the desired speed. With respect to the OVM, $V(h)$ is chosen as

$$V(h) = v_{max}\frac{\tanh(h - l_v - d_s) + \tanh(l_v + d_s)}{1 + \tanh(l_v + d_s)} \tag{2-26}$$

where l_v is the vehicle length and $d_s > 0$ is a safety distance between cars.

Fig 2-3 illustrates the $V(h)$ in (2-26). Note that the vehicle length l_v and the safety distance d_s are embedded in $V(h)$, this allows more realistic simulations and avoids crashes between vehicles.
The variables a and b in (2-25) are gains representing the drivers' sensitivity, they will be object of further investigation since certain coefficients combination leads to the unstable behaviors observed in [1]. The linearized version of (2-25) at the equilibrium (h_*,0,v_*) is

$$\dot{v}_i = \bar{a}(\dot{h}_i) + \bar{b}[\bar{k} \cdot (h_i) - c - v_i] \tag{2-27}$$

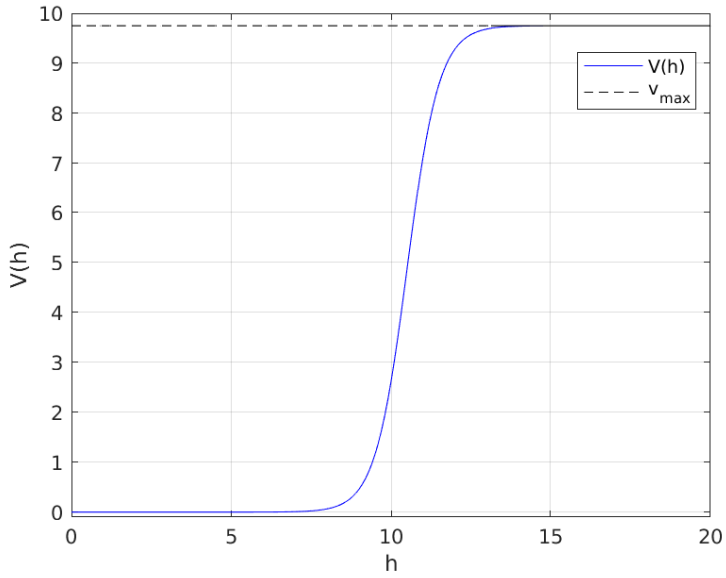

Figure 2-3: Non-linear function $V(h)$ determining the desired speed for the OV-FTL model. Note that for small headways the desired speed tends to zero, while for large it is equal to v_{max}

with $\bar{k}$, $\bar{a}$, $\bar{b}$ and c defined as follows:

$$\begin{aligned} \bar{k} &= \frac{\partial V(h_*)}{\partial h} = v_{max}\frac{1-(\tanh(h_* - l_v - d_s))^2}{1+\tanh(l_v+d_s)}, \\ \bar{a} &= \frac{a}{(h_*)^2}, \\ \bar{b} &= b, \\ c &= -\bar{k}h_* + V(h_*). \end{aligned} \tag{2-28}$$

Consequentially, the coefficients of (2-5) become:

$$\alpha_1 = \bar{b}\bar{k} \quad \alpha_2 = \bar{a} + \bar{b} \quad \alpha_3 = \bar{a}. \tag{2-29}$$

Taking the Laplace transform of (2-27) leads to the following transfer function

$$\frac{v_i(s)}{v_{i+1}(s)} = \frac{\bar{a}s + \bar{b}\bar{k}}{s^2 + (\bar{a}+\bar{b})s + \bar{b}\bar{k}} = \frac{\alpha_3 s + \alpha_1}{s^2 + \alpha_2 s + \alpha_1}. \tag{2-30}$$

The OV-FTL model has been already used for analysis purposes in [12, 22]. In addition to this, its coefficients have been calibrated with field data collected from a series of ring road experiments conducted in 2016 in Urbana, Illinois [11]. The calibration leads to

$$a = 20 \quad b = 0.5. \tag{2-31}$$

As a result, the OV-FTL model with a and b as in (2-31) will be the reference model of this thesis work and it will be used also in the further analysis.
In any case, as it has been illustrated, most of the models can be linearized by means of eq. (2-5); which means that switching among models is possible by simply changing the coefficients. Therefore, all the mathematical results can be easily generalized; conversely, non-linear simulations and the AV designs are both done considering the OV-FTL specifically.

2-6 Discussion

To summarize, this chapter provides an overview of the CF models used to determine HVs dynamics introducing the most common in literature. In this thesis work, the HVs dynamics is modeled using the Optimal Velocity-Follow the Leader (OV-FTL) since it is a good trade-off between simplicity and contained information. Additionally, a calibration of the model through real measurements is available.

Chapter 3

Stability Criteria

Stability theory plays a central role in the analysis of non-linear systems and in the evaluation of a controller design. There are different kinds of stability problems that arise in the study of multi-vehicles dynamical systems; namely, stability of an equilibrium point in the sense of Lyapunov and string stability.
Stability of an equilibrium point in the sense of Lyapunov implies the existence of an equilibrium for the vehicular platoon. If all the dynamics starting nearby the equilibrium stay nearby, such point is stable. If the solutions not only stay nearby but for $t \to \infty$ they tend to the equilibrium, the point is asymptotically stable.
On the other hand, string stability is a particular propriety of tight formations of vehicular platoons: disturbances that act on the platoon are amplified along the string of vehicles [26]. This form of instability can represent the cause of stop-and-go waves without the presence of bottlenecks on the roadway, generating therefore traffic congestion.
Hence, the purpose of this chapter is to introduce the main definitions stated in literature for these two kinds of stability. This discussion will result useful for the further analysis about the Human-driven Vehicle (HV) on a ring road and for the Autonomous Vehicle (AV) design. In particular, Section 3-1 considers Lyapunov stability formulating definition and theorems related to it. Section 3-2 gives first a qualitative definition of string stability and then it focuses on the frequency domain definitions which are handy for analysis and design. Section 3-3 deals with ring stability providing frequency domain definitions that can be used on a ring road topology and finally, Section 3-4 compares a ring roadway with a string.

3-1 Lyapunov Stability

In order to provide a stability definition in Lyapunov sense, let us consider the autonomous system:

$$\dot{\chi} = f(\chi) \tag{3-1}$$

where $f : D \to R^n$ is a locally Lipschitz map from a domain $D \subset R^n$ into R^n. Suppose $\chi_* \in D$ is an equilibrium point of (3-1); that is, $f(\chi_*) = 0$. The goal is to characterize and study the stability of χ_*.

Definition 1 (Equilibrium stability in Lyapunov sense)**.** *The equilibrium point $\chi = \chi_*$ of (3-1) is*

- *stable if, for each ϵ there is $\delta = \delta(\epsilon) > 0$ such that*

$$||\chi(0)|| < \delta \Rightarrow ||\chi(t)|| < \epsilon, \forall t \geq 0.$$

- *Unstable if it is not stable.*
- *Asymptotically stable if it is stable and δ can be chosen such that*

$$||\chi(0)|| < \delta \Rightarrow \lim_{t\to\infty} \chi(t) = \chi_*.$$

The $\epsilon - \delta$ requirements of Definition 1 states that to determine stability of an equilibrium χ_*, for any value of ϵ is possible to find a value of $\delta(\epsilon)$ such that a trajectory starting in a δ neighborhood of the origin will never leave the ϵ neighborhood.
Considering that, in a small neighborhood of the equilibrium $\chi = \chi_*$, the non-linear system (3-1) can be approximated by its linearization. A theorem that exploits the linearization to determine the stability of the equilibrium in Lyapunov sense can be formulated.

Theorem 1 (Indirect method of Lyapunov)**.** *Considering (3-1) and its equilibrium χ_*. Where $f : D \to R^n$ is a continuously differentiable and D is a neighborhood of the equilibrium. Let*

$$A = \frac{\partial f}{\partial \chi}(\chi)|_{\chi=\chi_{eq}}.$$

Then,

- *The equilibrium is asymptotically stable if $\mathfrak{Re}(\lambda_i) < 0$ for all eigenvalues of A.*
- *The equilibrium is unstable if $\mathfrak{Re}(\lambda_i) > 0$ for one or more of the eigenvalues of A.*

Theorem 1 provides a method to determine the stability of an equilibrium of (3-1) in Lyapunov sense; i.e., the system solutions goes to the equilibrium for $t \to \infty$.
On the other hand, obtaining stability in Lyapunov sense is, in traffic control field, not enough for a satisfying controller performance. Thus, the introduction of a new form of stability, known as string stability, is defined in the next section. This, in order to address the additional issues that might occur in vehicular platoon such as amplification of disturbance with the arise of stop-and-go waves.

3-2 String Stability

3-2-1 Original definition of string stability and intuitive description

The phenomenon of string (in)stability can be intuitively illustrated by using Fig 3-1. (a) in Fig 3-1 gives an example of platoon of vehicles on a road, (b-c) illustrate the response of the platoon to a disturbance. $x_i(t)$ in (b-c) is the error of the position with respect to the equilibrium, but it can be easily generalized to the vehicles velocity. In (b), it is clear how the disturbance, acting on the first vehicle, is amplified along the platoon, denoting therefore a situation of string instability. On the other hand, (c) shows a string stability situation where the disturbance is dissipated over the platoon. In both the cases, after a certain transient, $x_i(t)$ stabilizes back to the equilibrium for $t \to \infty$.

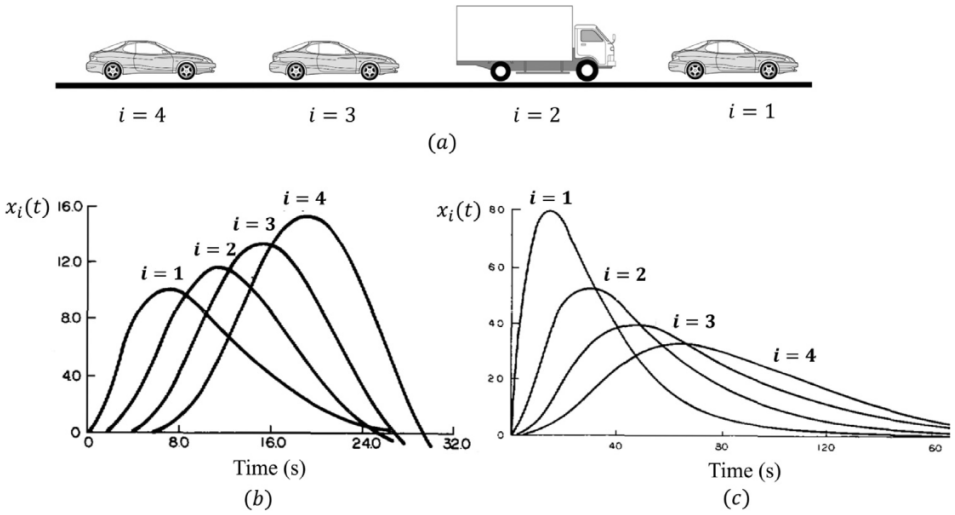

Figure 3-1: Illustration of a platoon system (a) and the qualitative description of string stability (b-c) [26], $x_i(t)$ denotes the state fluctuation (e.g., position error, velocity) of vehicle i at any time t. (b) denotes a string instability scenario, where an amplification along the platoon occurs. Whilst, (c) shows string stability. In both the cases $x_i(t)$ stabilizes at the equilibrium for $t \to \infty$, therefore, the platoon results stable in Lyapunov sense.

What intuitively illustrated in Fig. 3-1 is formalized in the original definition of string stability (OSS) [22].

Definition 2 (Original definition of String Stability (OSS))**.** *A string of vehicle is string stable if, for any set of bounded disturbance, the position (or velocity) fluctuations remain bounded and these fluctuations approach zero as* $t \to \infty$.

The main properties of Definition 2 are:

- boundedness of fluctuations of all vehicles;
- convergence of fluctuations of all vehicles.

To make the boundedness property non-trivial, it should hold for any number of vehicles in the platoon, i.e.,

- the boundedness holds for any string length.

The invariance of the bounds under the string length is an important property, as it guarantees that the notion of string stability is scalable for any number of vehicles.
In addition to this, the definition specifies that it has to be valid for any set of bounded disturbance. In literature, the commonly used types of disturbances include:

- Type I: Initial condition perturbations for the leading vehicles;
- Type II: Initial condition perturbations for all vehicles;
- Type III: External disturbances for leading vehicle;
- Type IV: External disturbances for all the vehicles;
- Type V: a combination of the previous ones.

Note that, in time domain, for certain set of disturbance the system could not show string instability while for others it could be. This is to say that is important to consider different sets of bounded disturbance.
The next section introduces frequency domain definitions which represent sufficient conditions for string stability and are convenient for theoretical analysis and design.

3-2-2 Frequency domain definition

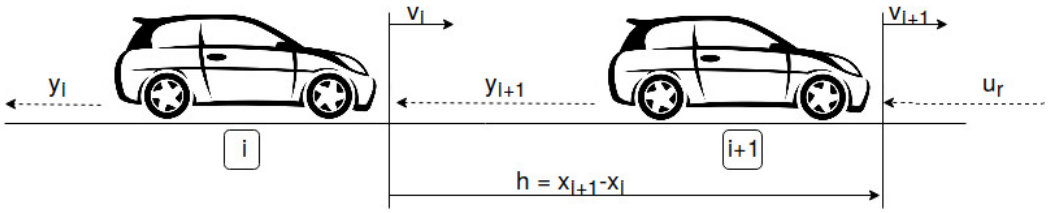

Figure 3-2: General scheme and notation for car following models. With respect to Fig. 2-1, this figure shows also the inputs and outputs (u_r, y_{i+1}, y_i) of the vehicles dynamics.

Let us recall now the standard definition of string stability in frequency domain for interconnected vehicles on a string road topology. Fig. 3-2 provides a graphical representation of the interaction between two adjacent vehicles for a simple Predecessor Following (PF) information flow topology (also known as look-ahead interconnection). Note that, different information flow topologies might require different or modified versions of the definitions stated in this section. Assuming now a linear vehicle model, such as (2-30), the response of each vehicle in the platoon to an exogenous input can be formulated as follows

$$y_i(s) = P_i(s)u_r(s), \tag{3-2}$$

where $y_i(s)$ and $u_r(s)$ are respectively the Laplace transforms of the vehicle output $y_i(t)$ and the exogenous input $u_r(t)$ in Fig. 3-2, with $s \in \mathbb{C}$. In (3-2), $y_i(s)$ and $u_r(s)$ are respectively the output of the i-th vehicle and an exogenous input acting on the $i+1$-th vehicle (e.g. a disturbance); $P_i(s)$ is the transfer function between these signals.
For simplicity, we will consider zero initial conditions. From (3-2) it directly follows that

$$y_i(s) = \Gamma_i(s) y_{i+1}(s). \tag{3-3}$$

In (3-3), $\Gamma_i(s)$ is the transfer function between two adjacent vehicles output which is equivalent to

$$\Gamma_i(s) = P_i(s) P_{i+1}^{-1}(s). \tag{3-4}$$

Note that this definition requires the existence of P_{i+1}^{-1} and for the HV models considered, P_{i+1}^{-1} always exists. A platoon is said to be "homogeneous" if all vehicles have identical dynamics [27], otherwise it is heterogeneous. Considering now for simplicity only Type III disturbance, the block diagram representation for N-vehicles PF platoon depicted in Fig. 3-2 is given in Fig 3-3.

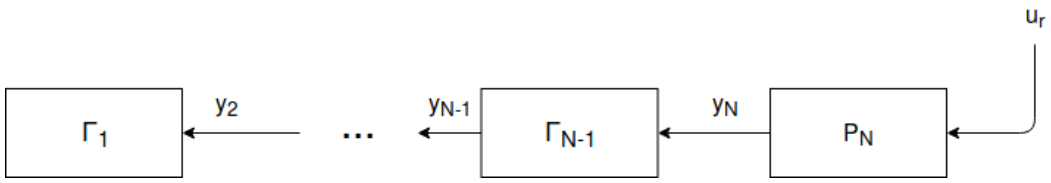

Figure 3-3: Block Diagram representation of a platoon of vehicles on a string.

The string interconnection in Fig 3-3 leads to the following transfer function:

$$y_i(s) = P_N(s) \prod_{j=i}^{N-1} \Gamma_j(s) u_r(s). \tag{3-5}$$

At this point, a definition of strong frequency domain string stability as given in [28] can be provided.

Definition 3 (Strong frequency domain string stability (SFSS))**.** *Let (3-5) represent a linear one-vehicle look-ahead interconnected system whose input-output relation is described by (3-2). Assume $P_i(s)$ invertible, for all $i \in \{1, \dots, N\}$. Then the system (3-5) is said to be* strong string stable *if*

$$||P_N(j\omega)||_\infty \quad \textit{is finite;} \tag{3-6}$$
$$||\Gamma_i(j\omega)||_\infty \leq 1 \quad \forall i \in \{1, \dots, N-1\}, \quad \forall N. \tag{3-7}$$

This definition considers that the amplification of the disturbance never occurs between each vehicle i and its predecessor $i+1$. If it happens, the platoon is string unstable.
A relaxed definition of Definition 3 is provided in [29] and it is also known as Eventual Stability Definition (ESS).

Definition 4 (Eventual Stability Definition (ESS)). *Let (3-5) represent a linear one-vehicle look-ahead interconnected system whose input-output relation is described by (3-2). Assume $P_i(s)$ with the poles in the Left Half Plane (LHP) for all $i \in \{1, \dots, N\}$. Then the system (3-5) is said to be* eventual string stable *if there exist $m < N$ such that*

$$||P_N(j\omega)||_\infty \quad \textit{is finite;} \tag{3-8}$$

$$||P_i(j\omega)||_\infty \leq ||P_{i+1}(j\omega)||_\infty \quad \forall i < m < N, \quad \forall N. \tag{3-9}$$

The ESS definition states that if there exists a value $m < N$ such that for $i < m$ the disturbance is no longer amplified, the platoon can be considered eventual string stable. This definition allows amplification of the disturbance for $i > m$ and it is particularly suitable for platoons of HV with a unique AV.
Although the frequency domain definitions are convenient for theoretical analysis, they present few limitations that are briefly presented. First of all, the linear assumption on the platoon system requires a perfect prior knowledge of the vehicular dynamics. Secondly, only type III disturbance is considered, requiring therefore further analysis for the other types. Finally, the H_∞-norm only captures the signals in a perspective energy (L_2 norm), but not in their maximal amplitude (i.e. L_∞).
In order to handle all the types of disturbances and to provide a significant definition form L_2 and L_∞ norms, another form of string stability, known as L_p string stability (LPSS) is introduced as stated in [28]. The following cascaded state-space system is considered:

$$\begin{aligned} \dot{\chi}_N &= f_r(\chi_N, u_r), \\ \dot{\chi}_i &= f_i(\chi_{i+1}, \chi_i), \\ y_i &= h(\chi_i), \end{aligned} \tag{3-10}$$

where u_r is the external input on the leading vehicle, χ_i the state for each vehicle $i \in \{1, \dots, N\}$ and y_i is the output signal.

Definition 5. *(L_p string stability (LPSS)): Consider the interconnected system (3-10). Let χ be the state vector and χ_* the constant equilibrium solution of (3-10) for $u_r = 0$. The system (3-10) is said string stable if there exist a class $\mathcal{K}$ functions α and β such that, for any initial disturbance $\chi(0)$, where $\chi = (\chi_0, \dots, \chi_N)$ is the state vector, and any exogenous input u_r.*

$$||y_i(t) - h(x_*)||_{L_p} \leq \alpha(||u_r(t)||_{L_p}) + \beta(||\chi(0) - \chi_*||), \quad \forall i \in \{1, \dots, N\} \textit{ and } \forall N \in \mathbb{N}. \tag{3-11}$$

If, in addition, with $\chi(0) = \chi_*$ it also holds that

$$||y_i(t) - h(\chi_*)||_{L_p} \leq ||y_{i+1}(t) - h(\chi_*)||_{L_p}, \quad \forall i \in \{1, \dots, N-1\} \textit{ and } \forall (N-1) \in \mathbb{N}. \tag{3-12}$$

The system 3-10 is strictly L_p string stable with respect to the disturbance $u_r(t)$.

With this definition both L_2 and L_∞ norms and types I, II and III disturbances are addressed. Providing, as a result, a rigorous and complete definition of string stability for linear-systems. In [25], several other definitions are presented in order to make the notion of string stability as much general as possible. However, for the sake of our analysis, those provided in this section are enough to compare the string scenario with the ring road experiment in [11].

3-3 Ring Stability

In this section, the concept of string stability on a ring road topology is considered; for brevity it is defined as ring stability.
As already mentioned in the introduction, one of the main purpose of this thesis is to provide a theoretical framework for the two experiments in [1, 11] which were both performed on a ring road topology. Few of the questions that the thesis would like to address are:

- To what extent ring and string topology differ between each other?
- Is it possible to exploit definitions of string stability on a ring road?

In order to answer to these queries, an analysis of the ring topology with the formulation of ring stability definitions is done in the following sections.

3-3-1 Strong Ring Stability

Assuming linear vehicle model, as it is done for the string, and considering type III disturbance; the block diagram representation for N-vehicles PF platoon on a ring road topology is given in Fig 3-4.

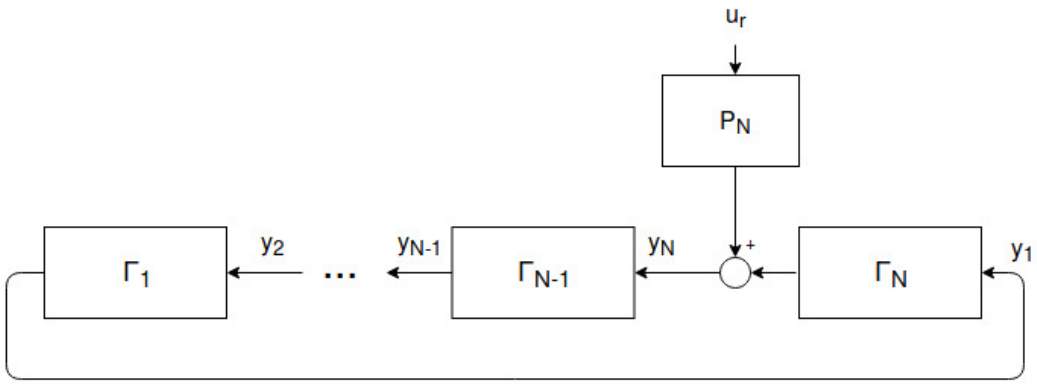

Figure 3-4: Block Diagram representation of a platoon of vehicles on a ring.

At first glance, Fig 3-4 is a closed loop version of the string block diagram in Fig. 3-3. As a result, the transfer function from u_r to the output y_i is:

$$y_i(s) = F_i^{(N)}(s)u_r(s), \tag{3-13}$$

$$F_i^{(N)}(s) = \begin{cases} \frac{1}{1-\prod_{j=1}^{N}\Gamma_j(s)}P_N(s), & \text{if} \quad i = N \\ \frac{\prod_{j=i}^{N-1}\Gamma_j(s)}{1-\prod_{j=1}^{N}\Gamma_j(s)}P_N(s), & \text{otherwise.} \end{cases} \tag{3-14}$$

Clearly, considering the same number of vehicles N on both the topologies, ring and string present different structures and the same definitions are not directly applicable on both. The main difference between the two topologies is the poles distribution in the complex plane

by varying the number N of vehicles. The transfer functions to be considered are (3-5) and (3-14).
In the first case, the string in (3-5), the poles location does not vary in function of N. If the single vehicles transfer functions in (3-4) has the poles in the LHP then can be easily proved that also (3-5) has all the poles in the LHP.
Conversely, the poles distribution of (3-14) in the complex plane varies according to N. Consequentially, the fact that the single vehicle transfer functions in (3-4) have the poles in the LHP does not ensure that (3-14) has all the poles in the LHP. Therefore, the equilibrium might become Lyapunov stable or unstable according to the number of vehicles N on the ring. Thus, scaling stability results on the ring for different N is harder than on the string road topology and it requires stronger assumptions.
In [30] a definition of Strong Ring Stability (SRS) for a homogeneous platoon is stated. For a homogeneous platoon, $F_i^{(N)}(s)$ in (3-13) is

$$F_i^{(N)}(s) = \frac{\Gamma^{N-i}(s)}{1-\Gamma^N(s)} P_N(s). \tag{3-15}$$

Definition 6 (Strong Ring Stability (SRS))**.** *Consider a homogeneous platoon $F_i^{(N)}(s)$ defined in (3-15) for all i, N with $i \leq N$ and assume $||\Gamma||_\infty \leq 1$. Then, the platoon is said to be* strong ring stable *if there exists $c > 0$ such that $||F_i^{(N)}(s)||_\infty \leq c$ for all $i, N, i \leq N$.*

The condition $||\Gamma||_\infty \leq 1$ is a sufficient condition to ensure that $F_i^{(N)}(s)$ has all its poles in the open-left-half plane [30]. As a result, Definition 6 becomes scalable for all $N \in \mathbb{N}$. Assuming $||\Gamma||_\infty \leq 1$ is quite a strong assumption, since it is equivalent to assume SFSS on a string road.
Despite the scalability property assumes great relevance when platooned traffic design is the final purpose, in order to explain the experiments in [1, 11] the scope of Definition 6 is too narrow. It is important to remark that both in [1, 11] the HV driving style generates stop-and-go waves in the platoon, which are related to $||\Gamma||_\infty > 1$ for all the HVs. In addition to this, even though $||\Gamma||_\infty \leq 1$ is sufficient to ensure asymptotic stability, it is not a necessary condition. This means that, for certain N, there must be cases where, despite $||\Gamma||_\infty > 1$, $F_i^{(N)}(s)$ has all its poles in the open-left-half plane. These Lyapunov stable cases with $||\Gamma||_\infty > 1$ are ignored by Definition 6. Clearly, Definition 6 cannot be used for the thesis goals and therefore, a new original definition of ring stability is stated in order to deal with heterogeneous and mixed platoons and for cases in which $||\Gamma||_\infty > 1$.

3-3-2 Weak Ring Stability

Being human vehicles naturally prone to exhibit $||\Gamma||_\infty > 1$, the assumption made in SRS of $||\Gamma||_\infty \leq 1$ cannot be done for mixed platoons, i.e. platoons with both HV and AV. This is the reason why it becomes relevant to look for a weaker version of ring stability, where scalability with respect to N cannot be ensured, thereby addressing all the cases not considered in Definition 6.

Definition 7 (Weak Ring Stability (WRS))**.** *Fix N and consider $F_i^{(N)}(s)$ defined in (3-14) for all i with $i \leq N$. Assume that $F_i^{(N)}(s)$ has all its poles in the open-left-half plane. Then, the platoon is said to be* weakly ring stable *if $||F_i^{(N)}||_\infty \leq ||F_{i+1}^{(N)}||_\infty$ for all i, with $i \leq N$.*

Definition 7 states that, for a fixed N, the peaks of the transfer functions (3-14), from the exogenous disturbance to the output of each vehicle, should decrease in their magnitude throughout the platoon. Physically, this means that the effect of the disturbance is not amplified (in terms of its energy). Notably, as compared to Definition 6, we have that Definition 7: can address heterogeneous platoons, covers those cases where the equilibrium is Lyapunov stable, although $||\Gamma_i||_\infty > 1$, covers those cases where the effect of the disturbance is not amplified for platoons of fixed size, although a uniform bound over N cannot be mathematically ensured.

3-4 Ring vs String Topology

Considering the same number of vehicles N on both the ring and the string, the two topologies show different properties and therefore they cannot be directly compared. However, being the ring the closed loop version of the string, they are related. In summary,

- The ring corresponds to a string with number of vehicles $\bar{N} >> N$ where the N vehicles are repeated a certain number of times according to the time span of the experiment.
- It is relevant to study the ring topology since the obtained results can be opportunely translated into the more realistic scenario of the string roadway.
- However, for the same number of vehicles N the common string stability definitions of Section 3-2 cannot be directly used and therefore new definitions have been formulated.

3-5 Discussion

To summarize, this chapter formulates the main definitions for Lyapunov, string and ring stability. These are exploited in the next chapters for the sake of our analysis.
The novelty of the chapter, which is also a thesis contribution, is the new definition of Weak Ring Stability which, since considers HVs strong frequency string unstable (Definition 3), has to renounce to uniformity with respect to N, the overall number of vehicles in the platoon. Additionally, weak ring stability definition is also suitable for heterogeneous and mixed platoons as opposed to the strong ring stability definition which was originally aimed to only homogeneous platoons.

Chapter 4

Human Drivers Traffic Scenario

This chapter goes into the merits of the Sugiyama's experiment in [1], where a certain number of Human-driven Vehicle (HV)s N are placed on a ring road topology. First of all, in Section 4-1 the HVs are modeled by using the Optimal Velocity-Follow the Leader (OV-FTL) described in Chapter 2; the model is briefly refreshed for sake of clarity.
In Section 4-2, the N vehicles are considered on the ring road and the properties of the overall system are investigated. In particular, the properties and the theorems of the circulant matrices (see Appendix A) are exploited in order to determine a necessary and sufficient condition in Section 4-3 and an only sufficient condition in Section 4-4 for the Lyapunov stability of the equilibrium. Furthermore, Section 4-5 investigates ring stability by means of numerical analysis and finally, Section 4-6 draws conclusions on the Sugiyama's experiment.

4-1 Human Vehicle Model

The model of the HVs is taken to be the OV-FTL. This choice is due to the fact that this model has already been calibrated in [11] to match the macroscopic properties of the traffic observed in [1]. The model seems therefore fitting quite well the purpose of this analysis. However, other Car-Following (CF) models can be used without losing generality. The OV-FTL has been introduced in Section 2-5 (Eq. (2-25)). Being the vehicles on a ring, the equilibrium of the platoon is

$$\begin{aligned} x_{i+1} - x_i &= h_* = \frac{l_r}{N}, \\ \dot{x}_i &= \dot{x}_{i+1} = v_* = V(h_*), \end{aligned} \tag{4-1}$$

where l_r represents the circumference of the ring and N the overall number of vehicles. Thus, linearizing the HVs dynamics around this equilibrium results in the following transfer function

$$\Gamma(s) = \frac{v_i(s)}{v_{i+1}(s)} = \frac{\bar{a}s + \bar{b}\bar{k}}{s^2 + (\bar{a} + \bar{b})s + \bar{b}\bar{k}} = \frac{\alpha_3 s + \alpha_1}{s^2 + \alpha_2 s + \alpha_1}. \tag{4-2}$$

The transfer function in (4-2) is derived by taking y_i in (3-3) equal to v_i the vehicle velocity and the definitions of the coefficients in (4-2) can be found in (2-28). It can be verified that the same transfer function is obtained using $y_i = v_i - v_{i-1}$ which is another typical way to check string stability [28, 32].
Note that (4-2) broadly appears in literature (cf. [31] and reference therein) for both analysis and synthesis problems.
Despite in reality the HV traffic is heterogeneous, i.e. each vehicle has different dynamics, it is common to consider a worst case scenario homogeneous traffic for the sake of the mathematical analysis. For the values of a and b in (2-31) for instance, the human behavior is highly unstable and generates naturally stop-and-go waves. An Autonomous Vehicle (AV) which stabilizes the worst case, even though for a homogeneous platoon, works also for a heterogeneous platoon.

4-2 State-space formulation

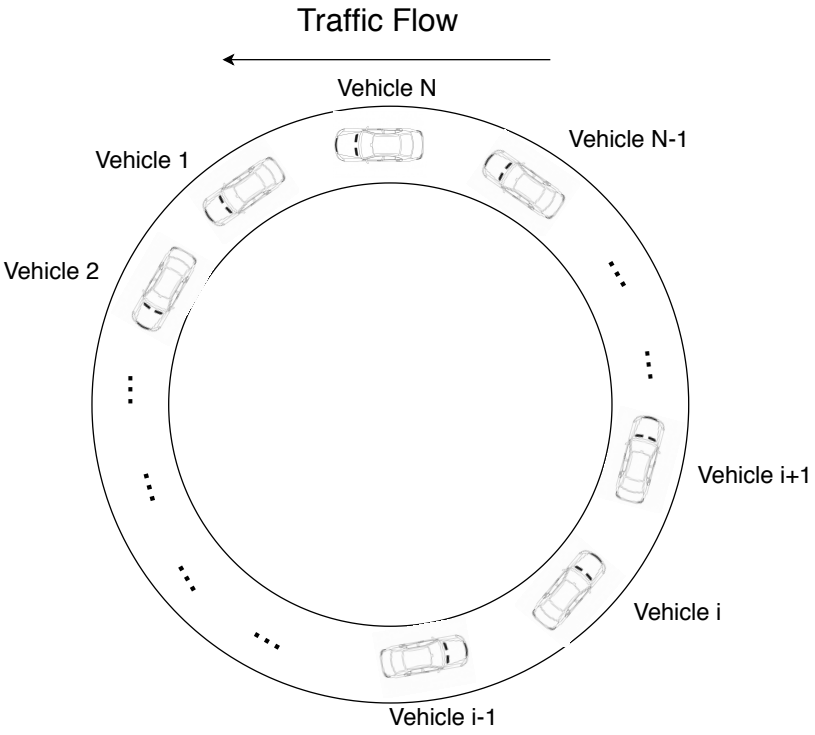

Figure 4-1: Schematic model of the ring road topology.

Fig 4-1 shows a schematic sketch of the N vehicles on the ring and therein the used notation.

The state space formulation of Fig 4-1 for the linearized system (2-27) is

$$\begin{bmatrix} \dot{\chi}_1 \\ \vdots \\ \dot{\chi}_{N-1} \\ \dot{\chi}_N \end{bmatrix} = \underbrace{\begin{bmatrix} A_1 & A_2 & & O \\ & \ddots & \ddots & \\ & & A_1 & A_2 \\ A_2 & & & A_1 \end{bmatrix}}_{A} \begin{bmatrix} \chi_1 \\ \vdots \\ \chi_{N-1} \\ \chi_N \end{bmatrix} + \underbrace{\begin{bmatrix} 0 \\ 0 \\ \vdots \\ B_r \end{bmatrix}}_{B} u_r; \tag{4-3}$$

where:

$$A_1 = \begin{bmatrix} 0 & 1 \\ -\alpha_1 & -\alpha_2 \end{bmatrix} \quad A_2 = \begin{bmatrix} 0 & 0 \\ \alpha_1 & \alpha_3 \end{bmatrix} \quad B_r = \begin{bmatrix} 0 \\ 1 \end{bmatrix}. \tag{4-4}$$

Where $\chi_i = \begin{bmatrix} x_i & v_i \end{bmatrix}^T$, x_i is the position of the vehicle i and v_i is the corresponding velocity. Note that, B in (4-3) is given, in this case, by the fact that type III disturbances are considered as in most of the definitions provided in Chapter 3. For different kinds of disturbances, or exogenous inputs, B changes accordingly.
Matrix A in (4-3) is clearly block circulant, some of the properties of this familiy of matrices can be found in Appendix A and in [33]. A in (4-3) can be re-written in a more compact way by using its generating matrix

$$A = \text{circ}(A_1, A_2, 0_{2x2}, \dots 0_{2x2}) \tag{4-5}$$

$$A = \text{circ}\Big(\begin{bmatrix} 0 & 1 \\ -\alpha_1 & -\alpha_2 \end{bmatrix}, \begin{bmatrix} 0 & 0 \\ \alpha_1 & \alpha_3 \end{bmatrix}, 0_{2x2}, \dots 0_{2x2} \Big) \tag{4-6}$$

where $0_{2\times 2}$ is a 2×2 matrix of zeros.

4-3 Necessary and Sufficient condition for Lyapunov Stability

In this section, a necessary and sufficient condition for asymptotic stability of the linearized state-space (4-3) equilibrium is given in the following Theorem.

Theorem 2. *Consider the linear state-space* (4-3)*, its equilibrium* (4-1) *is asymptotically stable if and only if*

$$-\frac{1}{2}\gamma_i \pm \left(\frac{\sqrt{(\gamma_i^2 - \phi_i^2 - r_i)^2 + (\eta_i + 2\gamma_i\phi_i)^2} + \gamma_i^2 - \phi_i^2 - r_i}{2} \right)^{1/2} < 0, \tag{4-7}$$

with

$$\gamma_i = \alpha_2 - \alpha_3 \cdot \cos\left(\frac{2\pi(i-1)}{N}\right), \tag{4-8}$$

$$\phi_i = -\alpha_3 \cdot \sin\left(\frac{2\pi(i-1)}{N}\right), \tag{4-9}$$

$$r_i = 4\alpha_1 \cdot \left(1 - \cos\left(\frac{2\pi(i-1)}{N}\right)\right), \tag{4-10}$$

$$\eta_i = 4\alpha_1 \cdot \sin\left(\frac{2\pi(i-1)}{N}\right), \tag{4-11}$$

for all $i \in \{1, \dots, N\}$. *Where* N *is the number of vehicles driving on the ring roadway.*

Proof. The platoon equilibrium (4-1) is asymptotically stable if and only if the eigenvalues of (4-3) are located in the open Left Half Plane (LHP). Being (4-3) a block circulant matrix, eq.(A-12) can be used to find an analytical expression of its eigenvalues. Therefore

$$\Lambda_i = A_1 + w^{i-1}A_2, \tag{4-12}$$

$$\Lambda_i = \begin{bmatrix} 0 & 1 \\ \alpha_1(w^{(i-1)} - 1) & -\alpha_2 + w^{(i-1)}\alpha_3 \end{bmatrix}, \tag{4-13}$$

$$\Lambda_i - \lambda I_{2x2} = \begin{bmatrix} -\lambda & 1 \\ \alpha_1(w^{(i-1)} - 1) & -\alpha_2 + w^{(i-1)}\alpha_3 - \lambda \end{bmatrix}, \tag{4-14}$$

$$\lambda^2 + (\alpha_2 - \alpha_3 \cdot w^{(i-1)})\lambda - \alpha_1(w^{(i-1)} - 1) = 0, \tag{4-15}$$

with $w = \exp(2\pi j/N)$ and $i \in \{1, \dots, N\}$. The eigenvalues of Λ_i are

$$\lambda_{i,\pm} = \frac{-\alpha_2 + \alpha_3 w^{(i-1)}}{2} \pm \frac{1}{2}\Big((\alpha_2 - \alpha_3 w^{(i-1)})^2 + 4\alpha_1(w^{(i-1)} - 1)\Big)^{1/2}, \tag{4-16}$$

where the square root of a complex number $a + jb$, with $b \neq 0$, is defined as

$$(a + jb)^{1/2} = \sqrt{\frac{|a + jb| + a}{2}} + j\mathrm{sgn}(b)\sqrt{\frac{|a + jb| - a}{2}}. \tag{4-17}$$

To ensure asymptotically stability we require that:

$$Re\frac{-\alpha_2 + \alpha_3 w^{(i-1)}}{2} \pm Re\frac{1}{2}\Big((\alpha_2 - \alpha_3 w^{(i-1)})^2 + 4\alpha_1(w^{(i-1)} - 1)\Big)^{1/2} < 0, \tag{4-18}$$

which is equivalent to

$$-\frac{1}{2}\gamma_i \pm \left(\frac{\sqrt{(\gamma_i^2 - \phi_i^2 - r_i)^2 + (\eta_i + 2\gamma_i\phi_i)^2} + \gamma_i^2 - \phi_i^2 - r_i}{2}\right)^{1/2} < 0, \tag{4-19}$$

with

$$\gamma_i = \alpha_2 - \alpha_3 \cdot \cos\left(\frac{2\pi(i-1)}{N}\right), \tag{4-20}$$

$$\phi_i = -\alpha_3 \cdot \sin\left(\frac{2\pi(i-1)}{N}\right), \tag{4-21}$$

$$r_i = 4\alpha_1 \cdot \left(1 - \cos\left(\frac{2\pi(i-1)}{N}\right)\right), \tag{4-22}$$

$$\eta_i = 4\alpha_1 \cdot \sin\left(\frac{2\pi(i-1)}{N}\right). \tag{4-23}$$

□

Remark 1. Few observations can be done based on this result. First of all, for $i = 1$, A in (4-3) has one zero-eigenvalue (it can be easily seen in (4-16)). This zero-eigenvalue is due to the ring structure itself and in particular by the fact that $x_N - x_1 = (x_2 - x_1) + \cdots + (x_N - x_{N-1})$. It is easy to show that, by means of a change of basis in (4-3), the zero-eigenvalue disappears. Moreover, as shown and discussed in [32] a (structural) zero-eigenvalue does not compromise the stability of the system and therefore it can be neglected for the purpose of Lyapunov analysis. Therefore, although the presence of one zero-eigenvalue, since it is structural, the indirect method of Lyapunov (Theorem 1) and Theorem 2 can be applied to study Lyapunov stability of the system for the remaining $2N - 1$ eigenvalues of A.
Secondly, the necessary and sufficient condition obtained in (4-7) is fairly complicated to be further developed and exploited for an eventual design. As a result, the next section will formalize an analytical sufficient condition for Lyapunov stability on the ring. By means of numerical examples, the limits of the sufficient condition are afterwards pointed out.

4-4 Sufficient condition for Lyapunov Stability

A sufficient condition to ensure asymptotic stability on the ring is given in the following theorem. This theorem comes directly from analysis in [34].

Theorem 3. *Consider the linear state space* (4-3)*, its equilibrium* (4-1) *is asymptotically stable if*

$$\alpha_2^2 - \alpha_3^2 - 2\alpha_1 \geq 0. \tag{4-24}$$

That, considering the OV-FTL model by plugging (2-29) *in* (4-24)*, becomes*

$$2\bar{a} + \bar{b} \geq 2\bar{k} \tag{4-25}$$

Proof. Considering eq.(4-15) to determine the eigenvalues of (4-3) and substituting the expression of w with its actual definition $w = \exp(2\pi j/N)$ the following is obtained

$$\frac{\alpha_1 + \alpha_3\lambda}{\alpha_1 + \alpha_2\lambda + \lambda^2} = e^{\frac{(N-1)(i-1)}{N} \cdot 2\pi j} \quad i \in \{1, \ldots, N\}, \tag{4-26}$$

$$H(\lambda) = e^{\frac{(N-1)(i-1)}{N} \cdot 2\pi j}. \tag{4-27}$$

Note that $w^{(N-1)(i-1)} = e^{\frac{(N-1)(i-1)}{N} \cdot 2\pi j}$ is the i-th complex root of $|w^{(N-1)(i-1)}| = (w^{(N-1)(i-1)})^N = 1$, indicating that for all the eigenvalues λ of A, the values of $H(\lambda)$ constitute N unit roots. As N changes, $H(\lambda)$ corresponds to different unit roots. Hence, if all the roots of $|H(\lambda)| = 1$ have negative real part, then the solutions of (4-26), i.e., the eigenvalues of matrix A (4-3) have negative real part. The conclusion is that, by ensuring that all the roots of $|H(\lambda)| = 1$ have negative real part is necessary and sufficient to guarantee an asymptotic stable equilibrium [34].
Let us now compute $|H(\lambda)| = 1$. Consider $\lambda = a + jb$

$$\begin{aligned} |H(\lambda)| &= 1, \\ |H(a+jb)| &= 1, \end{aligned} \tag{4-28}$$

$$a^4 + Da^3 + Ea^2 + Fa + G = 0, \tag{4-29}$$

with

$$D = 2\alpha_2, \tag{4-30}$$

$$E = -2b^2 + 2\alpha_1 + \alpha_2^2 - \alpha_3^2, \tag{4-31}$$

$$F = -2\alpha_1\alpha_3 + 2\alpha_1\alpha_2 + 2\alpha_2 b^2, \tag{4-32}$$

$$G = -\alpha_3^2 b^2 + b^4 - 2\alpha_1 b^2 + \alpha_2^2 b^2. \tag{4-33}$$

Eq. (4-29) has to be solved in order to find a condition on a such that $a < 0$ for all λ, where λ is an eigenvalue of A in (4-3). Eq. (4-29) is complicated to be solved analytically; however, by exploiting certain properties of $H(\lambda)$, the sufficient condition for the equilibrium stability is found.
Indeed, $H(\lambda)$ is a meromorphic function, which in complex analysis [35] means that, given an open subset D of the complex plane, the function is holomorphic on all D except for the poles of the functions. Since α_1 and α_2 are always positive because of the necessary constraints for a rational driver behavior (2-4), (2-5), (2-29), the poles of $H(\lambda)$ are always in the left half plane, indicating that $H(\lambda)$ is holomorphic in the Right Half Plane (RHP).
Holomorphic means that the function is complex differentiable at every point of the considered subset. Exploiting the Maximum Modulus Principle [35], which states that the maximum value of an holomorphic function is along the edge of its domain, i.e., the imaginary axis for the open RHP, it is proved that if $|H(jb)| \leq 1$ for all $b \in \mathbb{R}$ does not exist any $\lambda = a + jb$ with $a > 0$ such that $|H(\lambda)| = 1$.
Consequentially, all the eigenvalues of A in (4-3) are in the open LHP.
Thus, condition $|H(jb)| \leq 1$ becomes

$$\begin{aligned} |H(jb)| &\leq 1, \\ \alpha_3^2 b^2 - b^4 + 2\alpha_1 b^2 - \alpha_2^2 b^2 &\leq 0, \\ \alpha_3^2 - b^2 + 2\alpha_1 - \alpha_2^2 &\leq 0, \\ -\alpha_3^2 + b^2 - 2\alpha_1 + \alpha_2^2 &\geq 0. \end{aligned} \tag{4-34}$$

In the worst case scenario $b = 0$, therefore

$$\alpha_2^2 - \alpha_3^2 - 2\alpha_1 \geq 0. \tag{4-35}$$

Considering the OV-FTL model by plugging (2-29) in (4-24), the stability criterion becomes

$$2\bar{a} + \bar{b} \geq 2\bar{k}. \tag{4-36}$$

□

Remark 2. Note that, despite the used method is different, the conclusion in (4-34) is essentially the same obtained in [30] to ensure Lyapunov stability in the Strong Ring Stability (SRS) definition (Chapter 3). Analogously, the condition is also the same required to ensure Strong frequency domain string stability (SFSS) (Definition 3, Chapter 3).
Although (4-24) provides a simple analytical result to check asymptotic stability of the platoon solution, it is quite conservative and does not consider the number of vehicles on the ring. In the coming section, by means of numerical analysis, the conservativeness of (4-24) is determined.

4-5 Numerical Evaluation of Lyapunov and Weak Ring Stability

This section investigates, by means of numerical analysis, Lyapunov stability and Weak Ring Stability (WRS) of the A's equilibrium, with A as in (4-3), for different combinations of a and b in (2-28) and by varying the number of vehicles N on the ring. In order to do this numerically, few variables for the HV model in (2-25) and (2-26) have to be determined beforehand. Tab. 4-1 shows these choices.

Table 4-1: Standard values used for the numerical analysis.

.

Variable name	Symbolic name	Value
Vehicle Length	l_v	$4.5m$
Maximum vehicle velocity	v_{max}	$9.75m/s$
Safety distance	d_s	$6m$

In addition to this, A in (4-3) is obtained by linearization of (2-25) at the equilibrium (4-1). For the sake of coherence, varying the number of vehicles (N) on the ring requires also changing the ring length (l_r) proportionally, this in order to keep the same equilibrium and the same linearization. By choosing a referential equilibrium also $\bar{k}$ in (2-28) is automatically fixed. Tab. 4-2 shows the referential values by which the equilibrium is computed. Note that all the variables introduces in Tab. 4-1 and Tab. 4-2 are in compliance with the Sugiyama experiment in [1].

4-5-1 Lyapunov Stability

Lyapunov stability is checked by using the necessary and sufficient condition for Lyapunov stability (Theorem 2) on (4-3) for different N vehicles. The main purpose of this analysis is to show how the sufficient condition for Lyapunov stability in (4-25) (Theorem 3) is actually

Table 4-2: Referential values to compute the equilibrium (4-1).

Variable name	Symbolic name	Value
Ring Length	l_r	$260m$
Number of vehicle	N	22
Linearization of V in (2-26) at equilibrium	$\bar{k}$	1.2163

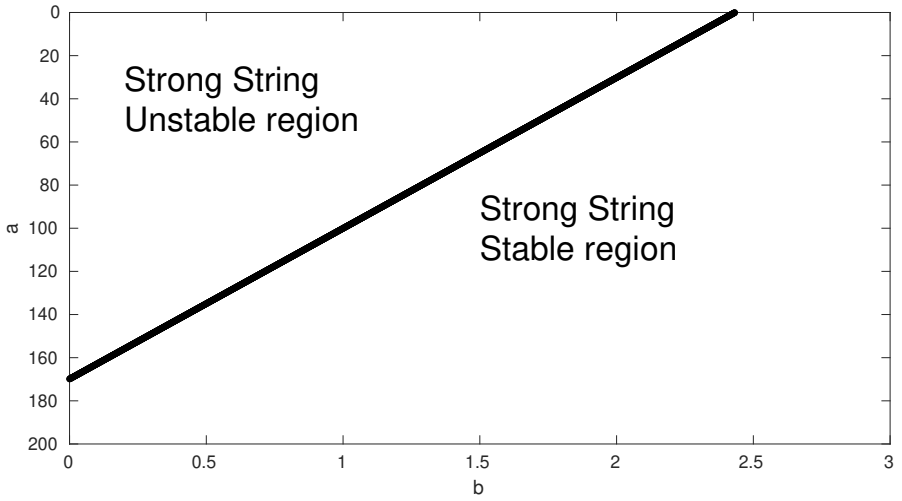

Figure 4-2: The red line shows the bound computed using the sufficient condition of Lyapunov stability (eq. (4-25)). The right-bottom area (where $2\bar{a} + \bar{b} > 2\bar{k}$) corresponds to $||\Gamma||_\infty \leq 1$ and therefore where the equilibrium is always Lyapunov stable for all N.

very conservative.

Fig. 4-2 shows the bound obtained by using eq. (4-25) (Theorem 3) for the sufficient condition of Lyapunov stability. The right-bottom area (where $2\bar{a} + \bar{b} > 2\bar{k}$) shows always a Lyapunov stable equilibrium for all N on the ring and it corresponds to the area in which $||\Gamma||_\infty \leq 1$ with Γ in (4-2). Note that Fig. 4-2 is expressed in terms of a and b as originally found in the non-linear model (2-25), their relation with $\bar{a}$ and $\bar{b}$ is stated in (2-28).

In the same (a,b)-plane, Fig. 4-3 illustrates instead, the number of vehicles N that makes the equilibrium (4-1) Lyapunov unstable, which means that at least an eigenvalue of A has positive real part.

The color-bar on the right side of Fig. 4-3 indicates a certain color associated with a number N of vehicles. For instance, the blue area on the top-left is related to $N = 3$; therefore, for this portion of the (a,b)-plane, A in (4-3) has an eigenvalue with positive real part for $N = 3$. Increasing $N = 5$, not only the area already unstable for $N = 3$ keeps being unstable, but also an additional area (light-blue) turns Lyapunov unstable. Thus, a greater portion of the (a,b)-plane shows, for $N = 5$, a Lyapunov unstable equilibrium. It is possible to appreciate how the unstable area in Fig. 4-3 increases proportionally to N and for $N \to \infty$ it converges to condition in (4-25).

For $N << \infty$, eq. (4-25) does not take into account the several cases in which, despite

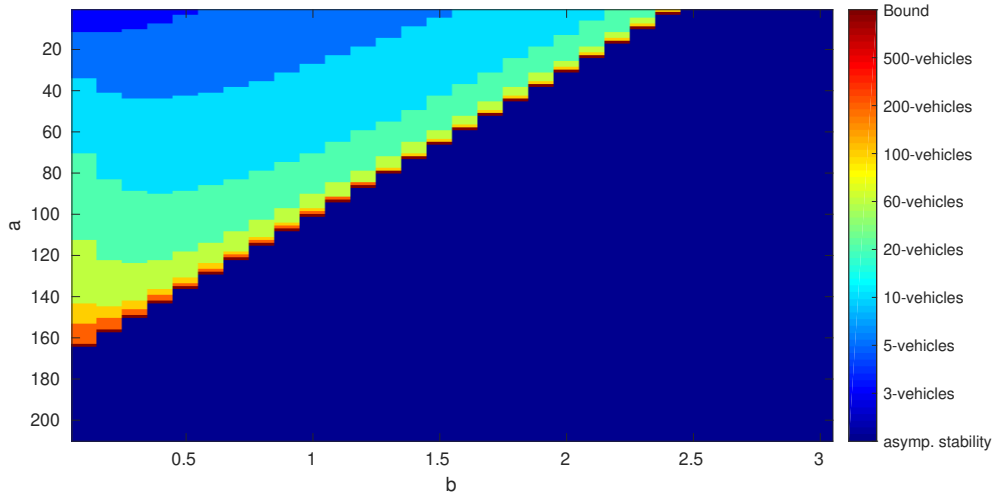

Figure 4-3: This Figure illustrates graphically what obtained applying the Indirect Lyapunov method to determine Lyapunov stability of the equilibrium in the (a,b)-plane. The color-bar on the right side associates a certain color with a number N of vehicles for which the aforementioned equilibrium (4-1) is Lyapunov unstable. For $N \to \infty$ the unstable (a,b)-space tends to eq. (4-25) which is the bound in Fig. 4-2.

$||\Gamma||_\infty > 1$, the equilibrium of (4-3) is in fact Lyapunov stable.

4-5-2 Ring Stability

This section investigates the definitions of SRS (Definition 6, Chapter 2) and WRS (Definition 7, Chapter 2) for the HVs homogeneous platoon on the ring roadway (Fig. 4-1).
Given the linear vehicle dynamics Γ, as in (4-2), and a type III disturbance acting on the N-th vehicle (see Fig. 3-4 for the block diagram representation), the transfer function $F_i^{(N)}(s)$ from disturbance to i-th vehicle velocity is

$$F_i^{(N)}(s) = \frac{\Gamma^{N-i}(s)}{1-\Gamma^N(s)} P_N(s). \tag{4-37}$$

Definition 6 of strong ring stability assumes $||\Gamma||_\infty \leq 1$ which ensures Lyapunov stability. From this assumption, it can actually be shown that the highest peak is always obtained for $F_N^{(N)}$ and, consequentially, this also allows a uniform bound c such that $||F_i^{(N)}(s)||_\infty \leq c$ for all $i, N, i \leq N$.

Remark 3. Assuming $||\Gamma||_\infty \leq 1$ is reasonable in a platooned traffic scenario, where the headway between vehicles can be arbitrarily influenced. However, being impossible to control the human vehicles behavior, $||\Gamma||_\infty \leq 1$ cannot be ensured in the Sugiyama experiment [1]. This motivates the formulation of Definition 7 of weak ring stability, which, by renouncing to uniformity with respect to N, does not require $||\Gamma||_\infty \leq 1$. It is therefore interesting to study what happens when the equilibrium is Lyapunov stable and $||\Gamma||_\infty > 1$. Note that this means studying the platoon in the top-left of Fig 4-2, where the sufficient condition (4-25) is

not met. As a result, Fig. 4-3 (which exploits Theorem 2) is used to determine if, fixed N, the equilibrium is Lyapunov stable and only afterwards, WRS is analyzed.

4-5-3 Weak Ring Stability analysis for N=3

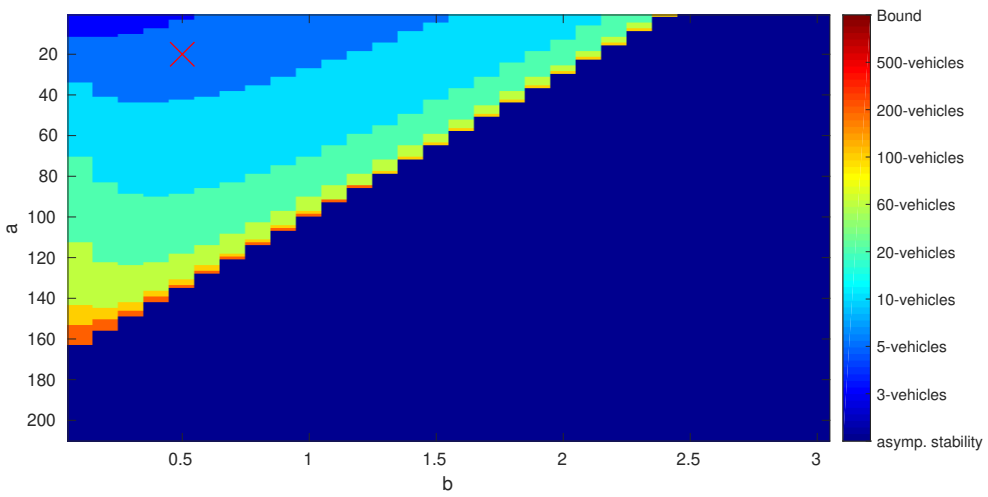

Figure 4-4: The $\times$ illustrates the position of $a = 20$, $b = 0.5$ in the (a,b)-plane. See also figure 4-3 for the complete description.

In this section, N is fixed equal to 3, and, after ensuring Lyapunov stability at the equilibrium, WRS is analyzed. The values of a and b are chosen

$$a = 20 \quad b = 0.5. \tag{4-38}$$

The $\times$ in Fig 4-4 shows the position of (4-38) in the (a,b)-plane and additionally Fig 4-5 the poles distribution in the complex plane for (4-37) with $N = 3$. All the poles are in the LHP denoting a Lyapunov stable equilibrium.

Once determined Lyapunov stability is possible to inquiry WRS. Let us recall Definition 7 for weak ring stability: given $F_i^{(N)}(s)$ in (4-37) with all the poles in the LHP for a fixed N, the peaks of (4-37) for $i \in \{1, \dots, N\}$ should decrease in their magnitude moving throughout the platoon from vehicle N to 1. Without knowledge on the structure of $F_i^{(N)}(s)$ in (4-37) is difficult to provide a rigorous sufficient condition of WRS. However, fixing N and defining

$$W_\Gamma = \{w \quad s.t. \quad |\Gamma(jw)| > 1\}, \tag{4-39}$$

$$W_F = \{w \quad s.t. \quad |F_N^{(N)}(jw)| > 1\}, \tag{4-40}$$

$$w_\Gamma = \arg\max_w |\Gamma(jw)|, \tag{4-41}$$

$$w_F = \arg\max_w |F_N^{(N)}(jw)|, \tag{4-42}$$

can be said, as a rule of thumb, that WRS is ensured if

$$W_\Gamma \cap W_F \approx \emptyset. \tag{4-43}$$

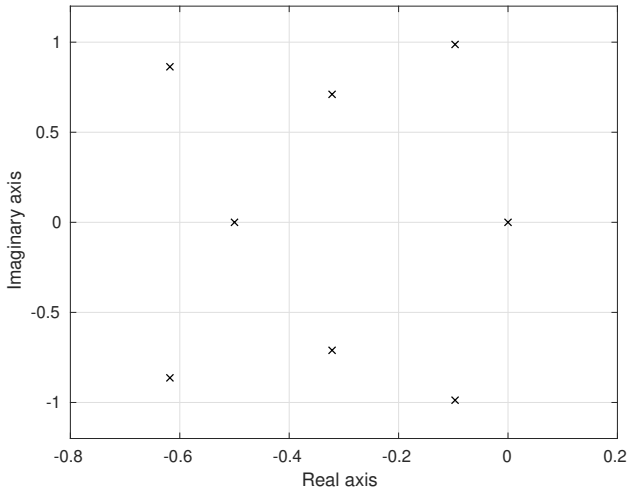

Figure 4-5: Poles distribution in the complex plane for $F_i^{(N)}(s)$ in (4-37) with $N = 3$, $a = 20$ and $b = 0.5$.

Fig 4-6 depicts $|\Gamma(jw)|$ and $|F_N^{(N)}(jw)|$ for $N = 3$ and $w \in \mathbb{R}$. Clearly, in this case (4-43) is met.

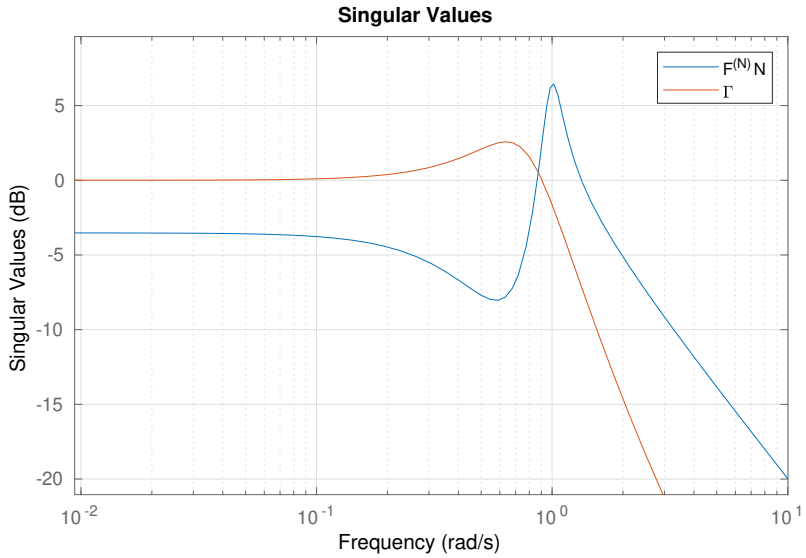

Figure 4-6: With $N = 3$, $a = 20$ and $b = 0.5$, the orange line is $|\Gamma(jw)|$ while the blue one is $|F_N^{(N)}(jw)|$, $w \in \mathbb{R}$. From these magnitude bodes it is expected a weak ring stable equilibrium.

In addition, the critical number of vehicles $\bar{N}$ after which the platoon becomes weak ring unstable can also be computed

$$\bar{N} > \frac{\log(|F_N^{(N)}(jw_f)|) - \log(|F_N^{(N)}(jw_\Gamma)|)}{\log(|\Gamma(jw_\Gamma)|)}. \tag{4-44}$$

Note that, at least for homogeneous HV platoons, most likely $\bar{N} > N$ and therefore weak ring instability cannot actually occur in reality. Figures 4-8a shows $|F_i^{(N)}(jw)|$ with $w \in \mathbb{R}$ and $i \in \{1, 2, 3\}$. Clearly, the peaks decrease while moving from veh-3, where the disturbance acts, to veh-1. Furthermore, Fig. 4-8b shows how after the 6-th vehicle $||F_{-3}^{(3)}||_\infty > ||F_3^{(3)}||_\infty$. As already mentioned, this result is not feasible in reality.
Finally, Fig. 4-7 depicts the non-linear simulation for the $N = 3$ HVs homogeneous platoon with an impulse disturbance acting on veh-3 at $t = 60s$. The disturbance is not amplified between vehicles and its effects are exacerbated in about $40s$. Eventually, the platoon asymptotically stabilizes at the equilibrium. As a matter of fact, for $N = 3$ the platoon equilibrium is both Lyapunov stable and Weak Ring stable.

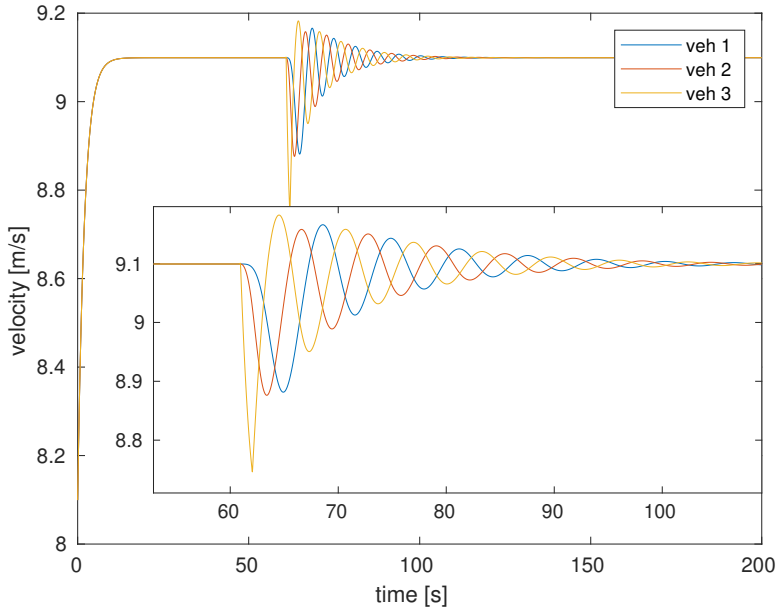

Figure 4-7: Non-linear simulation of the platoon with $N = 3$, $a = 20$ and $b = 0.5$. An impulse disturbance acts at $t = 60s$ and it is not amplified denoting ring stability.

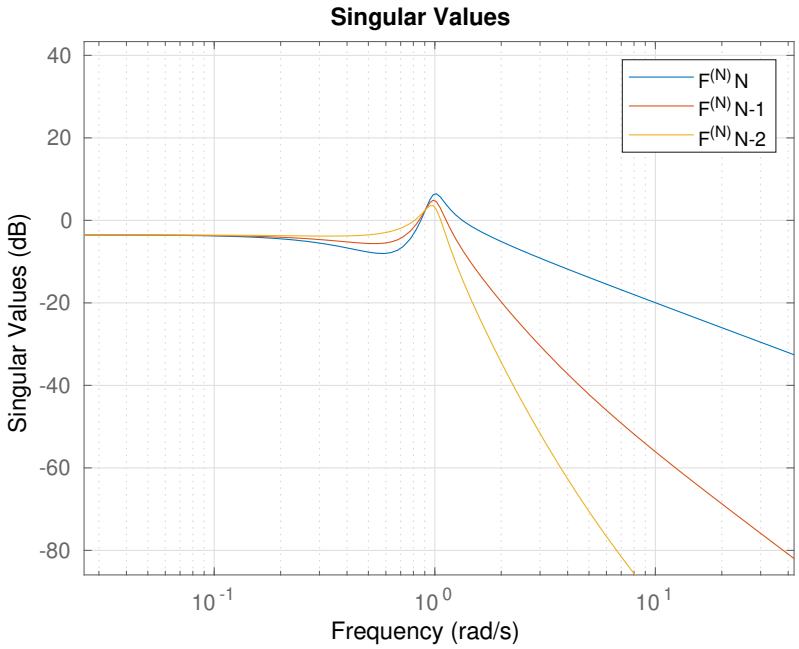

(a)

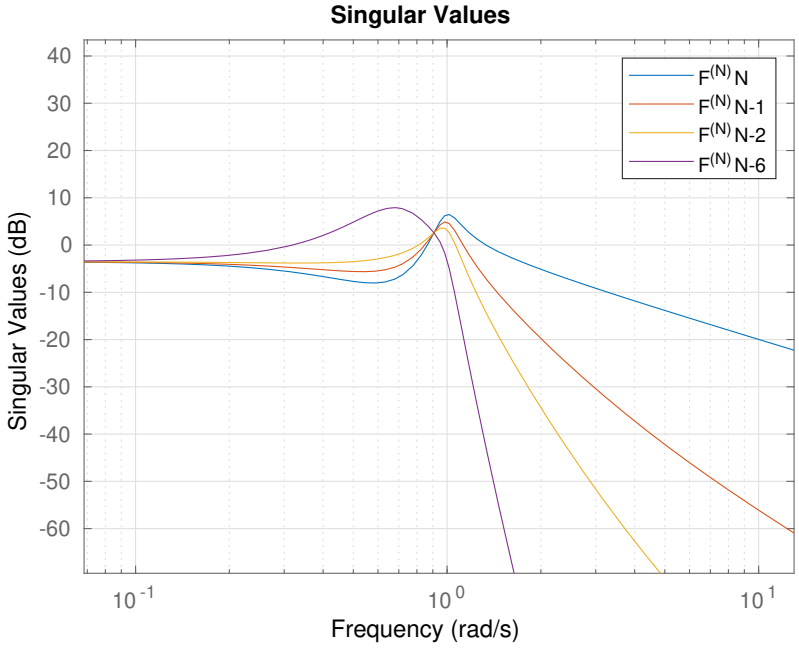

(b)

Figure 4-8: WRS analysis for $N = 3$, $a = 20$ and $b = 0.5$. Figure 4-8a shows $|F_3^{(3)}(jw)|$,$|F_2^{(3)}(jw)|$ and $|F_1^{(3)}(jw)|$, $w \in \mathbb{R}$. The purple bode in Fig. 4-8b is the $|F_{-3}^{(3)}(jw)|$ which represents an hypothetical $6th$ vehicle in the platoon which would actually amplify the disturbance.

4-5-4 Weak Ring Stability analysis for N=22

It is important to highlight that WRS frequency domain analysis can be done only once Lyapunov stability is ensured. This section provides another example for $N = 22$ and

$$a = 140 \quad b = 0.1. \tag{4-45}$$

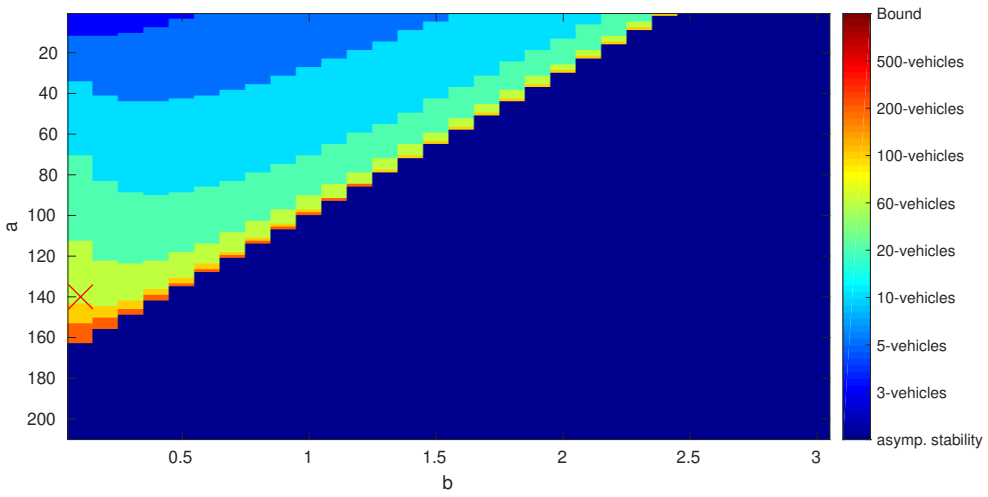

Figure 4-9: The $\times$ shows the position of $a = 140$ and $b = 0.1$ in the (a,b)-plane. See also Figure 4-3 for the complete description.

The $\times$ in Fig 4-9 shows the position of (4-45) in the (a,b)-plane and Fig 4-10 the poles distribution in the complex plane of (4-37) for $N = 22$. All the poles are again in the LHP denoting a Lyapunov stable equilibrium.

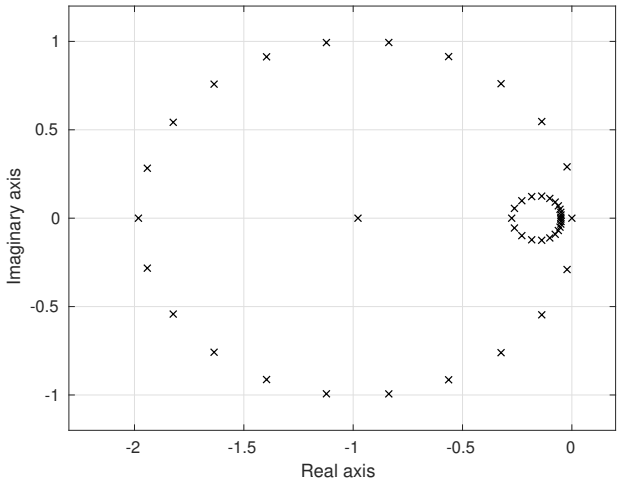

Figure 4-10: Poles distribution in the complex plane for $F_i^{(N)}(s)$ in (4-37) with $N = 22$, $a = 140$ and $b = 0.1$.

Fig 4-11 depicts $|\Gamma(jw)|$ and $|F_N^{(N)}(jw)|$ for $N = 22$ and $w \in \mathbb{R}$. In this case, $|\Gamma(jw)|$ appears remarkably flat with respect to $|F_N^{(N)}(jw)|$. As a consequence, (4-43) is once again met.

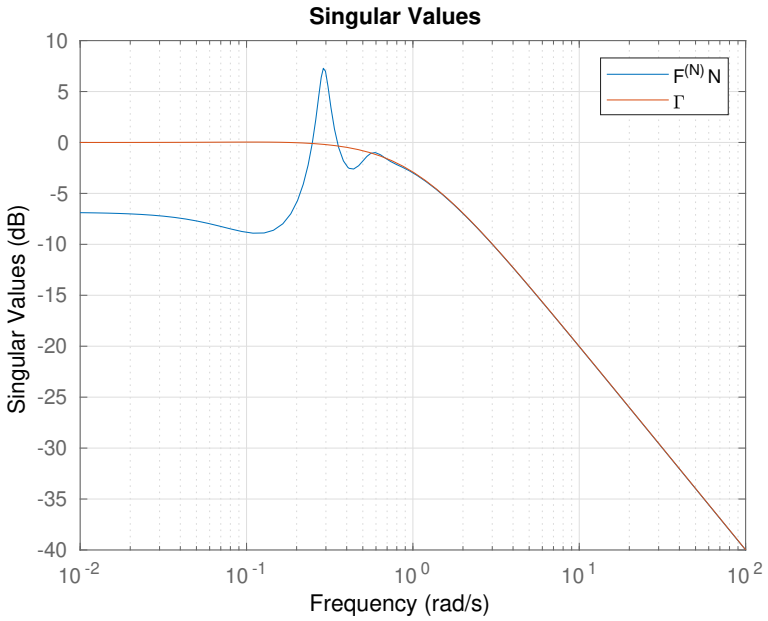

Figure 4-11: With $N = 22$, $a = 140$ and $b = 0.1$, the orange line is $|\Gamma(jw)|$ while the blue one is $|F_N^{(N)}(jw)|$, $w \in \mathbb{R}$. From these magnitude bodes it is expected a weak ring stable equilibrium.

Figures 4-12 shows $|F_i^{(N)}(jw)|$ with $w \in \mathbb{R}$ and $i \in \{1, \dots, 22\}$. For sake of clarity, only vehicles 22, 21, 20 and 16 are plotted. As predicted, the peaks are decreasing moving throughout the platoon.

Finally, Fig. 4-13 depicts the non-linear simulation with an impulse disturbance acting on veh-22 at $t = 60s$. Also in this case the disturbance is not amplified and the platoon asymptotically stabilizes at its equilibrium.

4-5-5 Conclusion on the Ring interconnection

The previous two examples are indicative since consider the Strong string unstable region in Fig. 4-2, with $||\Gamma||_\infty > 1$, but they turn out both Lyapunov and weak ring stable. Based on these examples, a first conclusion can be drawn. As also highlighted in [36], the cyclic/ring interconnection with a Lyapunov stable equilibrium has few advantages in terms of disturbance rejection with respect to a string interconnection with the same number of vehicles. This because the perturbation is detected and compensated by every member of the formation. As a result, despite $||\Gamma||_\infty > 1$, the same Type III disturbance has different effects on the ring and on the string. Indeed, in Fig. 4-14, an impulse disturbance acting at $t = 60s$ on the ring interconnection is not amplified throughout the platoon. Whilst, the same disturbance acting on the string results in a braking increase throughout the platoon (Fig. 4-15). In conclusion, strong string instability does not imply weak ring instability.

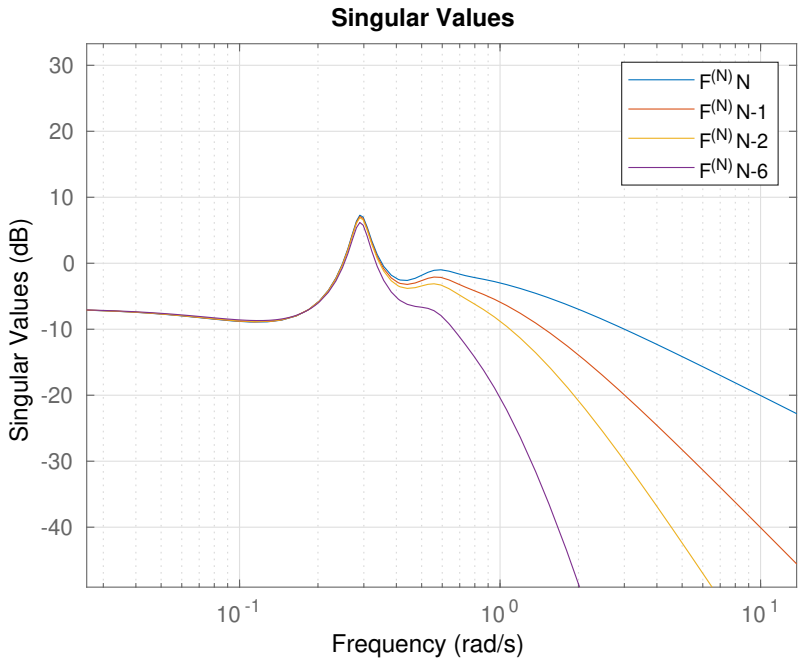

Figure 4-12: WRS analysis for $N = 22$, $a = 140$ and $b = 0.1$. Figure 4-8a shows $|F_2 2^{(22)}(jw)|$,$|F_2 1^{(22)}(jw)|$, $|F_2 0^{(22)}(jw)|$ and $|F_1 6^{(22)}(jw)|$ $w \in \mathbb{R}$. The peaks decrease moving throughout the platoon denoting weak ring stability.

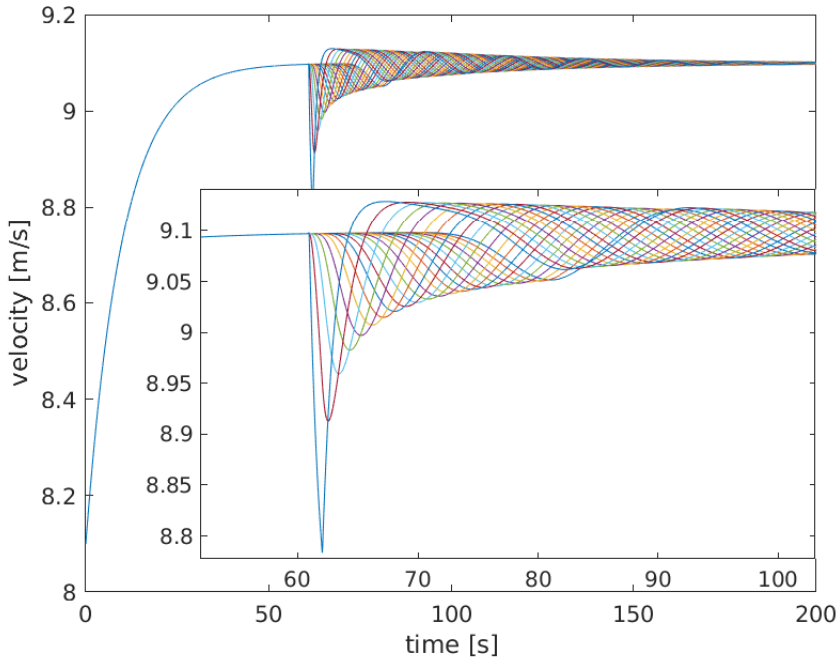

Figure 4-13: Non-linear simulation of the platoon with $N = 22$, $a = 140$ and $b = 0.1$. An impulse disturbance acts at $t = 60s$ and it is not amplified denoting ring stability.

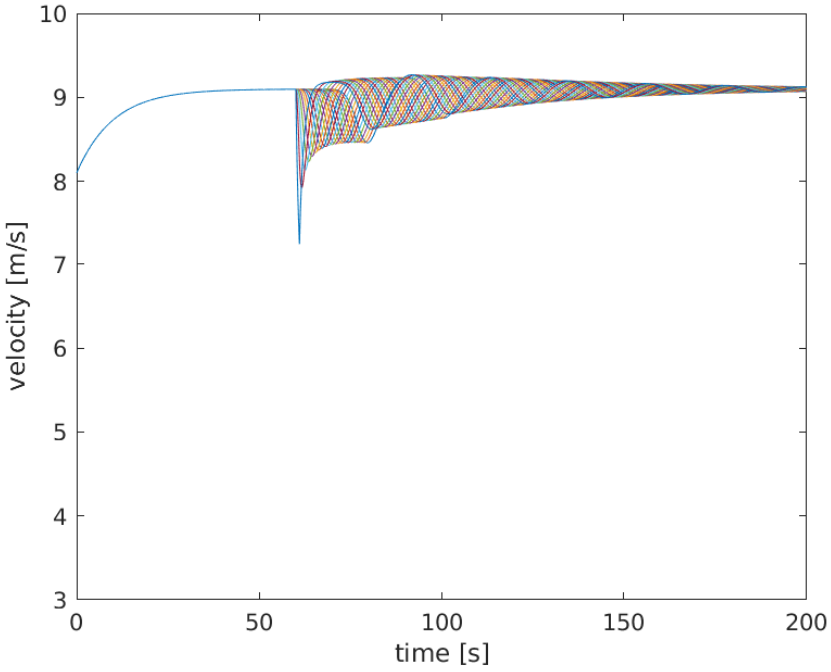

Figure 4-14: Non-linear simulation for $N = 22$, $a = 140$ and $b = 0.1$ for a ring roadway. An impulse disturbance acts at $t = 60s$ and it is not amplified denoting ring stability.

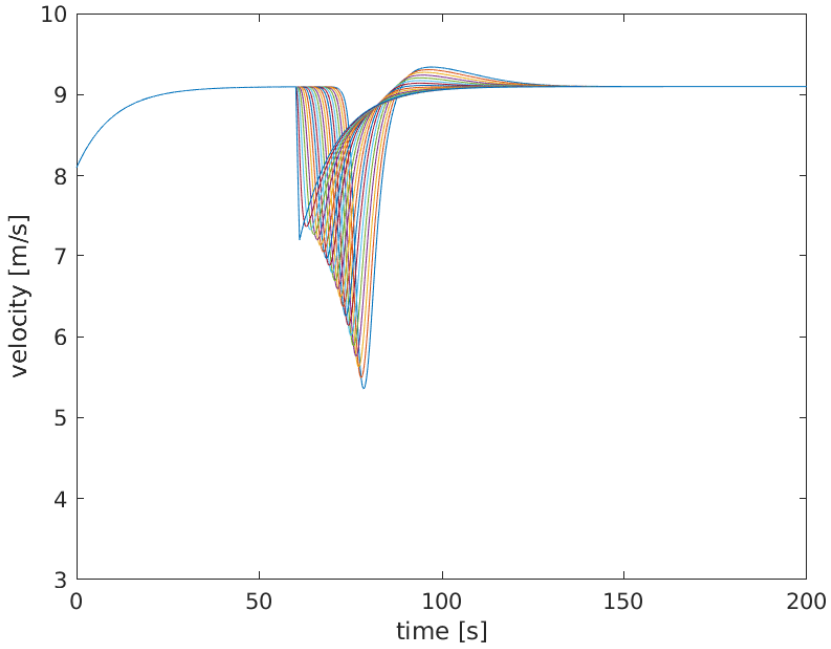

Figure 4-15: Non-linear simulation for $N = 22$, $a = 140$ and $b = 0.1$ for a string roadway. An impulse disturbance acts at $60s$ and it is amplified denoting string stability.

4-6 Sugiyama Experiment

This last section explains the Sugiyama experiment [1] and, from a theoretical point of view, what kind of instability is observed. Considering the calibration of the human model (2-25) described in [11], a and b are chosen as in Fig. 4-4

$$a = 20 \quad b = 0.5. \tag{4-46}$$

For $N = 22$, the eigenvalues of A in (4-3) which correspond to the roots of $1 - \Gamma^{22}(s) = 0$ with Γ in (4-2) are illustrated in Fig. 4-16. Clearly, from this numerical analysis turns out that there are poles in the RHP which means that the equilibrium is Lyapunov unstable. Therefore, the stop-and-go waves observed in [1] arise because of a condition of instability in Lyapunov sense.

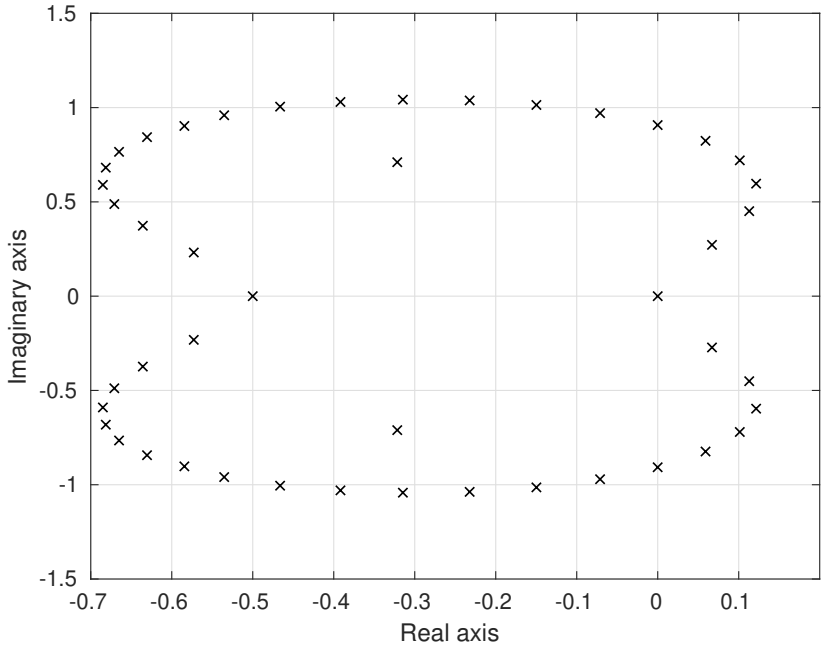

Figure 4-16: Poles distribution in the complex plane for $F_i^{(N)}(s)$ in (4-37) with $N = 22$, $a = 20$ and $b = 0.5$.

Fig. 4-17a and 4-17b illustrate the non-linear simulations obtained in this particular case. The dynamics used for the HVs is in (2-25). As observable, a small impulse disturbance acting at $t = 60s$ is enough to generate perpetual oscillations in the velocity of the platoon. Such fluctuations do not go to infinite because of the non-linearities which constraint the vehicles velocity between 0 and v_{max}. In Fig. 4-17b, where the evolution in time of the positions is illustrated, the slopes of the curves provides information on the vehicle velocities. It can be observed how the waves propagate in the platoon with the opposite direction of the traffic flow. This phenomenon is observed analogously in [1].

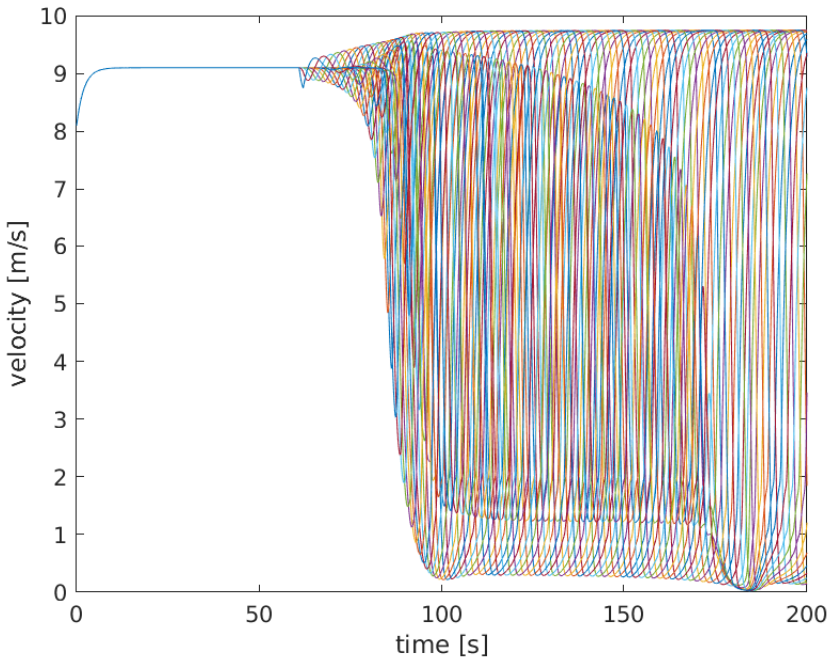

(a) Velocities of the N vehicles.

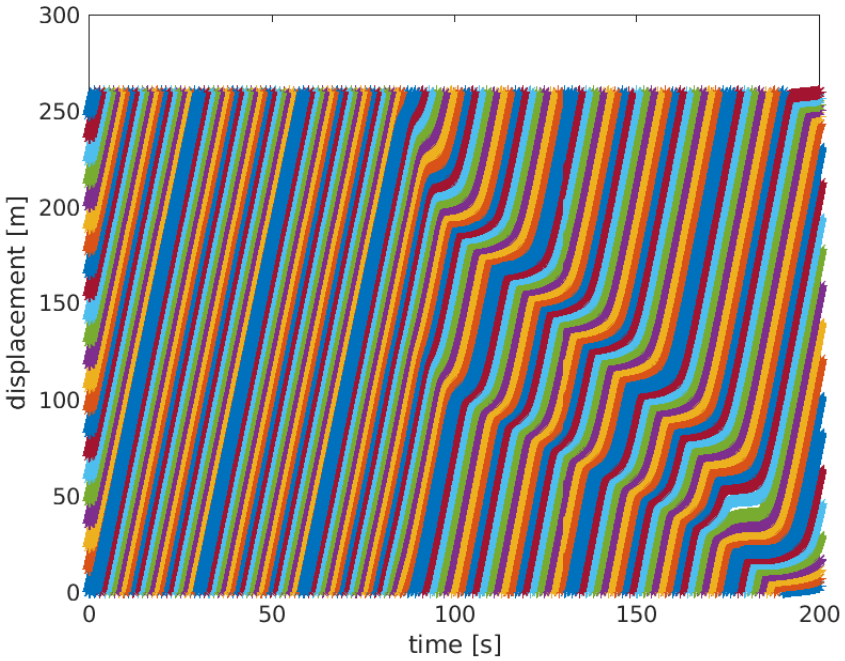

(b) Positions of the N vehicles.

Figure 4-17: Non-linear simulation of the platoon with $N = 22$, $a = 20$ and $b = 0.5$. An impulse disturbance acts at $t = 60s$ and it is enough to cause perpetual oscillations in the velocities (Fig. 4-17a) that do not decay for $t \to \infty$ denoting Lyapunov instability. This oscillations are bounded only because of the non-linearities. Fig. 4-17b illustrates a plot position-time, a stop-and-go wave proceeding in the opposite direction of the traffic flow occurs in the simulation as well as it is observed in [1].

Conclusion on the experiment

The conclusions that can be drawn by this analysis are:

- What observed in [1] is a typical case of Lyapunov unstable equilibrium. As a result, an AV should be able to first stabilize the equilibrium in Lyapunov sense, i.e. place the modes of the matrix A in (4-3) in the LHP and only afterwards dealing with WRS.
- The first point implies that in the field experiment [11] the AV stabilizes the system in Lyapunov sense.

4-7 Discussion

The main problem addressed in this chapter is the analysis of [1] by means of Linear Time Invariant (LTI) systems theory in order to provide a theoretical framework of what is observed in the experiment. The original contributions of this chapter are the necessary and sufficient condition to determine Lyapunov stability (Theorem 2) in Section 4-3 and the Weak Ring stability evaluation in Section 4-5. At the end of the chapter, the ring interconnection disturbance rejection properties are compared with those of a string and finally, few observations are made concerning the equilibrium of the Sugiyama's experiment.

Chapter 5

Mixed Traffic Scenario

This chapter explores the experimental evidence in [11], where a Human-driven Vehicle (HV) is replaced by a single Autonomous Vehicle (AV) and the platoon is stabilized. First of all, in Section 5-1 the controllability of the linearized system (4-3) at the equilibrium (4-1) is investigated. Once confirmed that the linearization is at least stabilizable, in Section 5-2 a sufficient condition to determine Lyapunov stability for a mixed-platoon is formulated and afterwards, different AVs are designed for a platoon with an otherwise Lyapunov unstable equilibrium. Namely, a PI with saturation controller in Sections 5-3 and 5-4 and a full state H_∞ controller in Section 5-5 have been developed and evaluated for both Lyapunov and weak ring stability and eventually validated by means of non-linear simulations. Limitations and possibilities of the different designs are eventually pointed out. Note that the performance of the different designs in time domain will vary according to the disturbance applied to the platoon. As mentioned, the disturbances more adopted in literature are:

- Type I: Initial condition perturbations for the leading vehicles;
- Type II: Initial condition perturbations for all vehicles;
- Type III: External disturbances for leading vehicle;
- Type IV: External disturbances for all the vehicles;
- Type V: a combination of the previous ones.

5-1 Controllability analysis

In this section the controllability analysis on a mixed HV-AV is done similarly to [25]. The necessary modifications are made in order to make it suitable for the considered platoon. First of all, the state space formulation for the linearized platoon with $N-1$ HVs and a single AV is

$$\dot{\chi} = A\chi + Bu_r, \tag{5-1}$$

$$\begin{bmatrix} \dot{\chi}_1 \\ \vdots \\ \dot{\chi}_{N-1} \\ \dot{\chi}_N \end{bmatrix} = \underbrace{\begin{bmatrix} A_1 & A_2 & & O \\ & \ddots & \ddots & \\ & & A_1 & A_2 \\ O & \dots & O & C_{AV} \end{bmatrix}}_{A} \begin{bmatrix} \chi_1 \\ \vdots \\ \chi_{N-1} \\ \chi_N \end{bmatrix} + \underbrace{\begin{bmatrix} 0 \\ 0 \\ \vdots \\ B_r \end{bmatrix}}_{B} u_r, \tag{5-2}$$

$$A_1 = \begin{bmatrix} 0 & 1 \\ -\bar{b}\bar{k} & -\bar{a}-\bar{b} \end{bmatrix} \quad A_2 = \begin{bmatrix} 0 & 0 \\ \bar{b}\bar{k} & \bar{a} \end{bmatrix} \quad B_r = \begin{bmatrix} 0 \\ 1 \end{bmatrix} \quad C_{AV} = \begin{bmatrix} 0 & 1 \\ 0 & 0 \end{bmatrix}. \tag{5-3}$$

Note that $\chi_i = [x_i, v_i]^T$ with x_i the front position of the i-th vehicle and v_i its velocity.

Lemma 1. *Consider the linear state space in* (5-2)*, the system is controllable for all* $N \in \mathbb{N}$.

Proof. Few lemmas stated in [37] are here introduced because useful for the proof. These are

Lemma 2 (Controllability)**.** *The linear system* (A, B) *is controllable if and only if* $[B, AB, \dots, A^{2n-1}B] = 2n$.

Lemma 2 is the known Kalman's controllability rank test in [37] which provides a necessary and sufficient condition for controllability. Additionally, the controllability of a state space is invariant both under state feedback and linear transformation. The following two lemmas underline these properties:

Lemma 3 (Invariance under state feedback)**.** *The linear system (A,B) is controllable if and only if* $(A - BK, B)$ *is controllable. Given* K *with compatible dimension.*

Lemma 4 (Invariance under linear transformation)**.** *The linear system (A,B) is controllable if and only if* $(T^{-1}AT, T^{-1}B)$ *is controllable for every nonsingular* T.

Thus, is possible to introduce the following state feedback, keeping the same controllability properties of (5-2) (lemma 3). The state feedback is

$$\hat{u}_r = u_r - A_1\chi_1 - A_2\chi_N, \tag{5-4}$$

the linear system (5-1) becomes

$$\begin{bmatrix} \dot{\chi}_1 \\ \vdots \\ \dot{\chi}_{N-1} \\ \dot{\chi}_N \end{bmatrix} = \begin{bmatrix} A_1 & A_2 & & O \\ & \ddots & \ddots & \\ & & A_1 & A_2 \\ A_2 & \dots & O & A_1 \end{bmatrix} \begin{bmatrix} \chi_1 \\ \vdots \\ \chi_{N-1} \\ \chi_N \end{bmatrix} + \begin{bmatrix} 0 \\ 0 \\ \vdots \\ B_r \end{bmatrix} \hat{u}_r. \tag{5-5}$$

State-space (5-5) can be rewritten as follows without losing generality for lemma 4

$$\begin{bmatrix} \dot{\chi}_N \\ \dot{\chi}_1 \\ \vdots \\ \dot{\chi}_{N-1} \end{bmatrix} = \underbrace{\begin{bmatrix} A_2 & O & \dots & A_1 \\ A_1 & A_2 & & O \\ & \ddots & \ddots & \\ O & & A_1 & A_2 \end{bmatrix}}_{\hat{A}} \begin{bmatrix} \chi_N \\ \chi_1 \\ \vdots \\ \chi_{N-1} \end{bmatrix} + \underbrace{\begin{bmatrix} B_r \\ 0 \\ \vdots \\ 0 \end{bmatrix}}_{B} \hat{u}_r, \tag{5-6}$$

$$\dot{\chi} = \hat{A}\chi + B\hat{u}_r. \tag{5-7}$$

$\hat{A}$ is a block circulant matrix and Theorem 5 (Appendix A) on the diagonalization of a block circulant matrix can be used to diagonalize it

$$\begin{aligned} \tilde{A} &= (E_N^H \otimes I_2)\hat{A}(E_N \otimes I_2) = \text{diag}(\Lambda_1, \Lambda_2, \dots, \Lambda_N), \\ \tilde{B} &= (E_N^H \otimes I_2)B, \end{aligned} \tag{5-8}$$

$$\tilde{B} = (E_N^H \otimes I_2)B = \frac{1}{\sqrt{N}} \begin{bmatrix} I_2 & 1 & I_2 & \dots & I_2 \\ I_2 & w_N I_2 & \bar{w}_N^2 I_2 & \dots & \bar{w}_N^{N-1} I_2 \\ I_2 & w_N^2 I_2 & \bar{w}_N^4 I_2 & \dots & \bar{w}_N^{2(N-1)} I_2 \\ \vdots & \vdots & \vdots & \ddots & \vdots \\ I_2 & \bar{w}_N^{N-1} I_2 & \bar{w}_N^{2(N-1)} I_2 & \dots & \bar{w}_N^{(N-1)(N-1)} I_2 \end{bmatrix} \begin{bmatrix} B_r \\ 0 \\ \vdots \\ 0 \end{bmatrix} = \frac{1}{\sqrt{N}} \begin{bmatrix} B_r \\ B_r \\ \vdots \\ B_r \end{bmatrix}, \tag{5-9}$$

$$\dot{\tilde{\chi}} = \tilde{A}\tilde{x} + \tilde{B}\hat{u} = \begin{bmatrix} \Lambda_1 & & & \\ & \Lambda_2 & & \\ & & \ddots & \\ & & & \Lambda_N \end{bmatrix} \tilde{\chi} + \frac{1}{\sqrt{N}} \begin{bmatrix} B_r \\ B_r \\ \vdots \\ B_r \end{bmatrix} \hat{u}, \tag{5-10}$$

where

$$\Lambda_i = \sum_{k=1}^{N} C_k w_k^{(k-1)(i-1)} = A_2 + A_1 w^{(N-1)(i-1)}, \tag{5-11}$$

$$\Lambda_i = \begin{bmatrix} 0 & 0 \\ \alpha_1 & \alpha_3 \end{bmatrix} + \begin{bmatrix} 0 & w^{(N-1)(i-1)} \\ -\alpha_1 w^{(N-1)(i-1)} & -\alpha_2 w^{(N-1)(i-1)} \end{bmatrix} \tag{5-12}$$

$$= \begin{bmatrix} 0 & w^{(N-1)(i-1)} \\ \alpha_1(1 - w^{(N-1)(i-1)}) & \alpha_3 - \alpha_2 w^{(N-1)(i-1)} \end{bmatrix}. \tag{5-13}$$

System (5-10) can be decoupled in N independent sub-systems ($i = 1, 2, \dots, N$), with the new states variables defined as $\tilde{\chi} = [\tilde{\chi}_{11}, \tilde{\chi}_{12}, \tilde{\chi}_{21}, \tilde{\chi}_{22}, \dots, \tilde{\chi}_{n1}, \tilde{\chi}_{n2}]^T$:

$$\frac{d}{dt} \begin{bmatrix} \tilde{\chi}_{i1} \\ \tilde{\chi}_{i2} \end{bmatrix} = \Lambda_i \begin{bmatrix} \tilde{\chi}_{i1} \\ \tilde{\chi}_{i2} \end{bmatrix} + \begin{bmatrix} 0 \\ \frac{1}{\sqrt{N}} \end{bmatrix} \hat{u} \tag{5-14}$$

$$= \begin{bmatrix} 0 & w^{(N-1)(i-1)} \\ \alpha_1(1 - w^{(N-1)(i-1)}) & \alpha_3 - \alpha_2 w^{(N-1)(i-1)} \end{bmatrix} \begin{bmatrix} \tilde{\chi}_{i1} \\ \tilde{\chi}_{i2} \end{bmatrix} + \begin{bmatrix} 0 \\ \frac{1}{\sqrt{N}} \end{bmatrix} \hat{u}. \tag{5-15}$$

Applying lemma 2, the controllability matrix for each sub-system becomes

$$Q_{c,i} = \begin{bmatrix} 0 & w^{(N-1)(i-1)} \frac{1}{\sqrt{N}} \\ \frac{1}{\sqrt{N}} & (\alpha_3 - \alpha_2 w^{(N-1)(i-1)}) \frac{1}{\sqrt{N}} \end{bmatrix}. \tag{5-16}$$

Clearly, $\det(Q_{c,i}) = (\frac{1}{N})(w^{(N-1)(i-1)}) \neq 0 \quad \forall i \in \{1, \dots, N\}$ and $\forall N \in \mathbb{N}$. As a result, the system in (5-1) is controllable. □

Remark 4. Ensuring that the linear system (5-1) is controllable for all N means that through a single AV is possible to stabilize the equilibrium of whichever platoon of N vehicles, $N \in \mathbb{N}$, in Lyapunov sense. However, as underlined in [22], Lyapunov stability implies that each single perturbation will decay for $t \to \infty$ which in reality does not constitute a desirable result. Hence, although is always possible to find a stabilizing AV design, the performance of the controllers is evaluated also considering the time required for the complete decay of the perturbations.

5-2 Sufficient Condition for Lyapunov stability

This section illustrates a sufficient condition for the mixed-platoon in order to ensure Lyapunov stability [22], as well as Theorem 3 in Section 4-4 does for the HVs homogeneous platoon. Eq. (5-17) is then exploited for the different AVs designs.

Proposition 1. *Consider* $\Gamma(s)$ *as in* (4-2) *and* $\Gamma_{AV}(s)$ *the transfer function of the AV dynamics at the equilibrium. The mixed HV-AV platoon is Lyapunov stable if*

$$|\Gamma(iv)|^{1-\gamma} \cdot |\Gamma_{AV}(iv)|^{\gamma} \leq 1 \quad \textit{for} \quad v \in \mathbb{R}. \tag{5-17}$$

With γ *in* (5-17) *the AV penetration rate, i.e. the ratio between HVs and AVs.*

Proof. Condition (4-26) for a homogeneous platoon asserts that the eigenvalues position of matrix $\hat{A}$ in (5-6) depends on the number of vehicles N in the ring. However, although the actual modes position on the complex plane changes, it has been observed that, regardless the number of vehicles N, all the modes lie dense in a curve $\mathcal{C} \subset \mathbb{C}$ which is independent from N. A graphical representation of this for a homogeneous platoon is given in Fig 5-1.

Moreover, from (4-26) analysis is known that the eigenvalues of (5-5) are by definition defined as the roots of $|H(z)| = 1$ with $|H(z)|$ in (4-27). As a result, the curve $\mathcal{C}$ in Fig. 5-1 is defined as

$$\mathcal{C} = \{z \in \mathbb{C} \quad : \quad |H(z)| = 1\}. \tag{5-18}$$

If for all z satisfying (5-18), $\mathfrak{Re}(z) \leq 0$ the equilibrium is Lyapunov stable. As a matter of fact, the stability criterion can be rewritten

$$\text{The equilibrium is stable if } \mathcal{C} \subset \mathbb{C}^- \tag{5-19}$$

$$\mathbb{C}^- = \{z \in \mathbb{C} \quad : \quad \mathfrak{Re}(z) \leq 0\}. \tag{5-20}$$

For a homogeneous platoon, condition in (5-19) is ensured if

$$|H(iv)| \leq 1 \quad \text{for} \quad v \in \mathbb{R}. \tag{5-21}$$

Whereas, for a mixed-platoon, $\mathcal{C}$ in (5-18) becomes

$$\mathcal{C} = \{z \in \mathbb{C} \quad : \quad |H(z)|^{1-\gamma} \cdot |\Gamma_{AV}(z)|^{\gamma} = 1\}. \tag{5-22}$$

Therefore, (5-19) becomes

$$|H(iv)|^{1-\gamma} \cdot |\Gamma_{AV}(iv)|^{\gamma} \leq 1 \quad \text{for} \quad v \in \mathbb{R}. \tag{5-23}$$

The variable γ in (5-23) is called the AV penetration rate and it defines the ratio between HVs and AVs. □

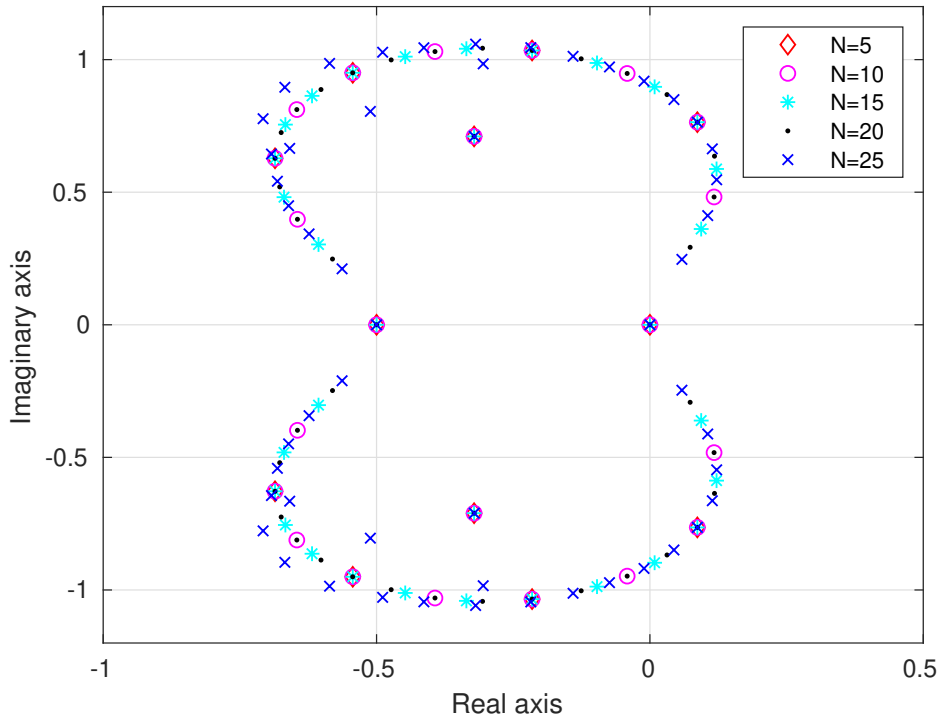

Figure 5-1: Poles distribution of a homogeneous platoon in the complex plane for different N vehicles. The modes are obtained as roots of $1 - \Gamma^N = 0$ where Γ is the HV transfer function at the equilibrium in 4-2.

Remark 5. Being in this case the AV unique, $\gamma = 1/N$ with N the overall number of vehicles driving on the ring. $H(z)$ is the HVs transfer function obtained at the defined equilibrium, in this specific case $H(iv) = \Gamma(iv)$ with Γ in (4-2). Similarly, $\Gamma_{AV}(iv)$ is the AV transfer function obtained at the equilibrium. Just to recall, the equilibrium is defined in (4-1).
At this point is possible to redefine the problem to solve: in real scenarios the HVs are prone to show string instability that, considering the Strong frequency domain string stability (SFSS) definition, means $||H(iv)||_\infty > 1$.
Given therefore $||H(iv)||_\infty > 1$ for all the $N-1$ HVs on the ring,

- which is a design for $\Gamma_{AV}(s)$ such that the condition (5-17) is met?

In addition to this, in Section 4-5, the conservativeness of the sufficient condition for Lyapunov stability in a homogeneous platoon is pointed out. Hence, another relevant question becomes:

- to what extent is (5-17) conservative?

5-3 AV design: PI with saturation

The first controller considered in our analysis is the PI with saturation AV introduced in [12]. A note on the notation, as already specified in the controllability analysis, the AV is the N-th

vehicle (see also the state-space notation in (5-2)). Since the platoon is on a ring, the AV follows the $1st$ vehicle and precedes the $N-1$-th. The non-linear dynamics of the AV is

$$\begin{aligned} \dot{x}_N &= v_N \\ \dot{v}_N &= K_{veh}(\alpha \cdot v_{target} + (1-\alpha)v_1 - v_N), \end{aligned} \tag{5-24}$$

where v_{target} and α are

$$\begin{aligned} v_{target} &= V_d + \min\Big(\max\Big(\frac{x_1 - x_N - h_{AV*}}{\delta}, 0\Big), 1\Big) \\ V_d &= \Big(\frac{v_N + v_1}{2}\Big) \\ \Delta x_s &= \max\Big(2 \cdot (v_1 - v_N), 4\Big) \\ \alpha &= \min\Big(\max\Big(\frac{x_1 - x_N - \Delta x_s}{\gamma}, 0\Big), 1\Big). \end{aligned} \tag{5-25}$$

Remark 6 (AV linearization constraints). A remark on the linearization, as for the HV model, the linearization is performed at the equilibrium $(h_*, 0, v_*)$ with h_* and v_* defined in (4-1). Furthermore, also (5-24) is a Car-Following (CF) model and then its linearization can be generalized as

$$\begin{aligned} \dot{v}_N &= (D_h f)(h_N - h_*) + (D_{\dot{h}} f)(\dot{h}_N - 0) + (D_v f)(v_N - v_*) \\ \dot{v}_N &= (D_h f)h_N - (D_{\dot{h}} f - D_v f)v_N + D_{\dot{h}} f v_1 - (D_v f v_* + D_h f h_*) \\ \dot{v}_N &= \beta_1 h_N - \beta_2 v_N + \beta_3 v_1 - \beta_4. \end{aligned} \tag{5-26}$$

Also for the AV the necessary constraints for rational driver behavior are

$$D_h f, D_{\dot{h}} f \geq 0 \quad \text{and} \quad D_v f \leq 0, \tag{5-27}$$

where $D_h f, D_{\dot{h}} f$ and $D_v f$ are the partial derivatives to respectively the headway, the difference in velocity with the vehicle ahead and the AV velocity. Finally, is required that the AV does not trigger string instability itself, which means it complies with the SFSS definition. In other words, given Γ_{AV} the transfer function obtained from (5-24) linearization, it is expected that $||\Gamma_{AV}||_\infty \leq 1$. Condition met if and only if

$$\beta_2^2 - \beta_3^2 - 2\beta_1 \geq 0. \tag{5-28}$$

Condition (5-28) is obtained for a HV in Section 4-4 (Theorem 3) and it is also valid for the AV as long as it has a CF model dynamics.

Considering (5-24) and (5-25), according to the value of δ two linearizations are possible: a first order and a second order.

5-3-1 AV first order (P Controller)

Considering a $\delta < x_1 - x_N - 7$ the controller (5-24) can be linearized as

$$\begin{aligned} \dot{x}_N &= v_N \\ \dot{v}_N &= K_{veh}\Big((1-\alpha)v_1 + \alpha\Big(\frac{v_N + v_1}{2}\Big) - v_N\Big) \\ &= K_{veh}\Big(1 - \frac{\alpha}{2}\Big)(v_1 - v_N) = \beta_3 v_1 - \beta_2 v_N. \end{aligned} \tag{5-29}$$

Leading to the following first order transfer function:

$$\Gamma_{AV}(s) = \frac{v_N(s)}{v_1(s)} = \frac{K_{veh}(1-\frac{\alpha}{2})}{s + K_{veh}(1-\frac{\alpha}{2})} = \frac{K_\alpha}{s+K_\alpha} = \frac{\beta_3}{s+\beta_2}. \tag{5-30}$$

Given $\alpha \approx 1$ and $K_{veh} > 0$, (5-29) meets both the requirements in (5-27) and (5-28).
At this point, a condition on Γ_{AV} such that (5-17) is assured can be computed.

Result 1. *Condition* (5-17) *of Lyapunov stability, for the AV in (5-30) and the HVs in (4-2) with* $||\Gamma||_\infty \geq 1$ *is met if:*

$$K_\alpha < v_\Gamma \sqrt{\frac{1}{Peak_\Gamma^{2(N-1)} - 1}}. \tag{5-31}$$

Proof. The HV transfer function in (4-2) is here recalled

$$\Gamma(s) = \frac{\bar{a}s + \bar{b}\bar{k}}{s^2 + (\bar{a}+\bar{b})s + \bar{b}\bar{k}}. \tag{5-32}$$

Considering condition (5-17), the most critical point is given by $||\Gamma||_\infty$ that is the peak of (5-32) and it occurs at the frequency v_Γ. Therefore, (5-17) can be rewritten as:

$$\left(\sqrt{\frac{K_\alpha^2}{v_\Gamma^2 + K_\alpha^2}}\right)^{1/N} \cdot Peak_\Gamma^{(N-1)/N} \leq 1, \tag{5-33}$$

$$\left(\frac{K_\alpha^2}{v_\Gamma^2 + K_\alpha^2}\right) \cdot Peak_\Gamma^{2(N-1)} \leq 1, \tag{5-34}$$

as $K_\alpha > 0$ lead to the following condition:

$$K_\alpha < v_\Gamma \sqrt{\frac{1}{Peak_\Gamma^{2(N-1)} - 1}}. \tag{5-35}$$

□

Remark 7. For certain HV configurations, (4-2) has a zero at really higher frequencies with respect to its poles. Because of this, in many cases (4-2) can be considered a second order system with complex poles

$$\Gamma(s) = \frac{\bar{a}s + \bar{b}\bar{k}}{s^2 + (\bar{a}+\bar{b})s + \bar{b}\bar{k}} \approx \frac{\bar{b}\bar{k}}{s^2 + (\bar{a}+\bar{b})s + \bar{b}\bar{k}} = \frac{\alpha_1}{s^2 + \alpha_2 s + \alpha_1}. \tag{5-36}$$

Thus, the resonance peak $Peak_\Gamma$ and its frequency v_Γ can be computed as

$$v_\Gamma = \omega_n \sqrt{1 - 2\xi^2}, \tag{5-37}$$

$$Peak_\Gamma = |\Gamma(jv_\Gamma)| = \frac{1}{2\xi\sqrt{1-\xi^2}}, \tag{5-38}$$

with

$$\xi = \frac{\alpha_2}{2\sqrt{\alpha_1}}, \tag{5-39}$$

$$\omega_n = \sqrt{\alpha_1}. \tag{5-40}$$

5-3-2 AV second order (PI controller)

Commonly in [12] $\delta > x_1 - x_N - 7$. Given the referential values to compute the equilibrium in tab. 4-2, this second order linearization is obtained

$$\begin{aligned}
\dot{x}_N &= v_N \\
\dot{v}_N &= K_{veh}\Big((1-\alpha)v_1 + \alpha\Big(\frac{v_N + v_1}{2}\Big) + \alpha\frac{(x_1 - x_N - h_{AV*})}{\delta} - v_N\Big) \\
&= \frac{K_{veh}\alpha}{\delta}(x_1 - x_N) - K_{veh}\Big(1 - \frac{\alpha}{2}\Big)v_N + K_{veh}\Big(1 - \frac{\alpha}{2}\Big)v_1 - \frac{K_{veh}\alpha}{\delta}h_{AV*} \\
&= \beta_1 h_N - \beta_2 v_N + \beta_3 v_1 - \beta_4.
\end{aligned} \tag{5-41}$$

From (5-41) the following second order transfer function is obtained:

$$\Gamma_{AV}(s) = \frac{v_N(s)}{v_1(s)} = \frac{K_{veh}[(1 - \frac{\alpha}{2})s + \frac{\alpha}{\delta}]}{s^2 + K_{veh}(1 - \frac{\alpha}{2})s + K_{veh}\frac{\alpha}{\delta}} = \frac{\beta_3 s + \beta_1}{s^2 + \beta_2 s + \beta_3}. \tag{5-42}$$

Condition (5-28), which ensures $||\Gamma_{AV}||_\infty \leq 1$ states that

$$\beta_2^2 - \beta_3^2 - 2\beta_1 \geq 0 \tag{5-43}$$

and unfortunately this is not the case. Taken β_1,β_2 and β_3 in (5-41), (5-43) becomes

$$-2\beta_1 < 0 \tag{5-44}$$

which means that $||\Gamma_{AV}||_\infty > 1$ and that this linearization is strong frequency domain unstable (cf. SFSS definition in Chapter 2).
Under these conditions, $||\Gamma_{AV}||_\infty > 1$ might have a detrimental effect on the controller performance. This does not mean that the AV is not able to stabilize the platoon equilibrium. Making β_1 very small for instance, would allow to approximately meet condition (5-43); however, it is intuitive to understand why this condition is not ideal. Hypothetically, a platoon with only AVs in (5-41) would most likely result string unstable which is clearly not ideal. Therefore, a modification in the non-linear controller in (5-24) is introduced in order to face this issue.

5-4 Modified non-linear PI with saturation AV

In order to improve the second order linearization of the PI with saturation AV in [12], a small modification in (5-24) is introduced. The non-linear dynamics of the AV becomes

$$\begin{aligned}
\dot{x}_N &= v_N \\
\dot{v}_N &= K_{veh}(\alpha \cdot v_{target} + (1-\alpha)v_1 - v_N) + c(v_{AV*} - v_N)
\end{aligned} \tag{5-45}$$

with

$$\begin{aligned} v_{target} &= V_d + \min\Big(\max\Big(\frac{x_1 - x_N - h_{AV*}}{\delta}, 0\Big), 1\Big) \\ V_d &= \Big(\frac{v_N + v_1}{2}\Big) \\ \Delta x_s &= \max\Big(2 \cdot (v_1 - v_N), 4\Big) \\ \alpha &= \min\Big(\max\Big(\frac{x_1 - x_N - \Delta x_s}{\gamma}, 0\Big), 1\Big). \end{aligned} \tag{5-46}$$

As in the previous section, $\delta > x_1 - x_N - 7$ lead to the following second order linearization

$$\begin{aligned} \dot{x}_N &= v_N \\ \dot{v}_N &= K_{veh}\Big((1-\alpha)v_1 + \alpha\Big(\frac{v_N + v_1}{2}\Big) + \alpha\frac{(x_1 - x_N - h_{AV*})}{\delta} - v_N\Big) + c(v_{AV*} - v_N) \\ &= \frac{K_{veh}\alpha}{\delta}(x_1 - x_N) - \Big(K_{veh}\Big(1 - \frac{\alpha}{2}\Big) + c\Big)v_N + K_{veh}\Big(1 - \frac{\alpha}{2}\Big)v_1 - \Big(\frac{K_{veh}\alpha}{\delta}h_{AV*} - cv_{AV*}\Big) \\ &= \beta_1 h_N - \beta_2 v_N + \beta_3 v_1 - \beta_4. \end{aligned} \tag{5-47}$$

From (5-47) the following second order transfer function is obtained:

$$\Gamma_{AV}(s) = \frac{v_N(s)}{v_1(s)} = \frac{K_{veh}[(1 - \frac{\alpha}{2})s + \frac{\alpha}{\delta}]}{s^2 + \Big(K_{veh}(1 - \frac{\alpha}{2}) + c\Big)s + K_{veh}\frac{\alpha}{\delta}} = \frac{\beta_3 s + \beta_1}{s^2 + \beta_2 s + \beta_3}. \tag{5-48}$$

Condition (5-28), which ensures $||\Gamma_{AV}||_\infty \leq 1$, becomes

$$\begin{aligned} \Big(K_{veh}\Big(1 - \frac{\alpha}{2}\Big) + c\Big)^2 - K_{veh}^2\Big(1 - \frac{\alpha}{2}\Big)^2 - 2K_{veh}\frac{\alpha}{\delta} &\geq 0 \\ c^2 + 2cK_{veh}\Big(1 - \frac{\alpha}{2}\Big) - 2K_{veh}\frac{\alpha}{\delta} &\geq 0 \\ c > -K_{veh}\Big(1 - \frac{\alpha}{2}\Big) + \sqrt{K_{veh}^2\Big(1 - \frac{\alpha}{2}\Big)^2 + 2K_{veh}\frac{\alpha}{\delta}} & \end{aligned} \tag{5-49}$$

(5-49) provides a condition on c in order to ensure SFSS of the AV. At this point, a condition on Γ_{AV} such that the sufficient condition for Lyapunov stability (5-17) is assured can be computed.

Result 2. *Condition* (5-17) *of Lyapunov stability, for the AV in (5-30) and the HVs in (4-2) with* $||\Gamma||_\infty \geq 1$ *is met if:*

$$\begin{aligned} K_{veh} < &\frac{\Big(1 - \frac{\alpha}{2}\Big)cv_\Gamma^2 - \frac{\alpha}{\delta}v_\Gamma^2}{\Big[\frac{\alpha^2}{\delta^2} + \Big(1 - \frac{\alpha}{2}\Big)^2 v_\Gamma^2\Big](Peak_\Gamma^{2(N-1)} - 1)} + \\ &\frac{v_\Gamma\sqrt{\Big(1 - \frac{\alpha}{2}\Big)^2(-v_\Gamma^4) - \frac{\alpha}{\delta}\Big[2(1 - \frac{\alpha}{2})cv_\Gamma^2 + \frac{\alpha}{\delta}c\Big] + (v_\Gamma^2 + c^2)\Big[\frac{\alpha^2}{\delta^2} + \Big(1 - \frac{\alpha}{2}\Big)^2 v_\Gamma^2\Big]Peak_\Gamma^{2(N-1)}}}{\Big[\frac{\alpha^2}{\delta^2} + \Big(1 - \frac{\alpha}{2}\Big)^2 v_\Gamma^2\Big](Peak_\Gamma^{2(N-1)} - 1)}. \end{aligned} \tag{5-50}$$

Proof. The proof on this theorem is substantially identical to Theorem 1. Indeed, condition (5-17) of Lyapunov stability for Γ_{AV} in (5-47) leads to the following inequality to solve

$$\left(\frac{K_{veh}^2[(1-\frac{\alpha}{2})^2 v_\Gamma^2 + \frac{\alpha^2}{\delta^2}]}{(\frac{K_{veh}\alpha}{\delta} - v_\Gamma^2)^2 + v_\Gamma^2[K_{veh}(1-\frac{\alpha}{2})+c]^2}\right) \cdot Peak_\Gamma^{2(N-1)} < 1. \tag{5-51}$$

By developing (5-51), the following second order inequality is obtained

$$K_{veh}^2\left[\frac{\alpha^2}{\delta^2} + \left(1-\frac{\alpha}{2}\right)^2 v_\Gamma^2\right](Peak_\Gamma^{2(N-1)}-1) + 2K_{veh}\left(\frac{\alpha}{\delta}v_\Gamma^2 - \left(1-\frac{\alpha}{2}\right)cv_\Gamma^2\right) - (v_\Gamma^4 + v_\Gamma^2 c) < 0, \tag{5-52}$$

which yields

$$K_{veh} < \frac{\left(1-\frac{\alpha}{2}\right)cv_\Gamma^2 - \frac{\alpha}{\delta}v_\Gamma^2 + \sqrt{\left(\frac{\alpha}{\delta}v_\Gamma^2 - \left(1-\frac{\alpha}{2}\right)cv_\Gamma^2\right)^2 + (v_\Gamma^4 + v_\Gamma^2 c^2)\left[\frac{\alpha^2}{\delta^2} + \left(1-\frac{\alpha}{2}\right)^2 v_\Gamma^2\right](Peak_\Gamma^{2(N-1)}-1)}}{\left[\frac{\alpha^2}{\delta^2} + \left(1-\frac{\alpha}{2}\right)^2 v_\Gamma^2\right](Peak_\Gamma^{2(N-1)}-1)}. \tag{5-53}$$

Simplifying (5-53) leads to (5-50). □

Remark 8. For practical applications with a number of vehicles N which is higher then 5 and by considering $\delta > x_1 - x_N - 7$, the value of $\frac{\alpha}{\delta} \approx 0$. By means of this approximation, (5-50) turns

$$K_{veh} < \frac{c + \sqrt{(c^2 + v_\Gamma^2)\cdot Peak_\Gamma^{2(N-1)} - v_\Gamma^2}}{(1-\frac{\alpha}{2})(Peak_\Gamma^{2(N-1)}-1)}. \tag{5-54}$$

Condition (5-54) is easier to handle and approximates quite well the result in Theorem 2.

Remark 9. Given $||\Gamma||_\infty > 1$ and therefore $Peak_\Gamma > 1$, from (5-53) is clear that the root square in (5-50) is always greater than zero.

To summarize, a modified version of the PI with saturation controller in [12] has been proposed and motivated by the issues that its second order linearization has shown. Additionally, given the second order linearization of this modified PI, a sufficient condition on its gains in order to ensure Lyapunov stability on a platoon of N vehicles on a ring has been developed. The following sections investigate numerically the conservativeness of Result 2 and to what extent this design is able to deal with Weak Ring Stability (WRS).

5-4-1 Conservativeness of the sufficient condition of Lyapunov stability

For the homogeneous platoon with only HVs, Section 4-5 and in particular 4-5-1 illustrates numerically how the sufficient condition for Lyapunov stability on the ring, i.e. $||\Gamma||_\infty < 1$, is conservative. Similarly, this section investigates the conservativeness of condition (5-50) in Result 2 for a mixed platoon with a single AV. In coherence with the homogeneous case, tab. 4-1 reports the values used for this numerical analysis and tab. 4-2 provides the referential values to compute the equilibrium in (4-1). In addition to this, the HVs dynamics in (2-25) is considered with

$$a = 20 \quad b = 0.5, \tag{5-55}$$

which are the values used in [11] to validate the Optimal Velocity-Follow the Leader (OV-FTL) model for the Sugiyama's experiment [1]. These values are in the $||\Gamma||_\infty > 1$ region (see Fig. 4-4). In this scenario, in order to determine the discrepancy between the gain K_{veh} in (5-47) obtained with an only sufficient condition and a necessary and sufficient condition for Lyapunov stability; condition (5-50) (sufficient) is checked together with the indirect Lyapunov method (Theorem 1, sufficient and necessary) for A in (5-56) which contains the AV linearized dynamics as N-th row. As previously, $\chi_i = [x_i, v_i]^T$ with x_i vehicle i front position and v_i its velocity.

$$\begin{bmatrix} \dot{\chi}_1 \\ \vdots \\ \dot{\chi}_{N-1} \\ \dot{\chi}_N \end{bmatrix} = \underbrace{\begin{bmatrix} A_1 & A_2 & & O \\ & \ddots & \ddots & \\ & & A_1 & A_2 \\ A_{AV1} & \dots & 0 & A_{AV2} \end{bmatrix}}_{A} \begin{bmatrix} \chi_1 \\ \vdots \\ \chi_{N-1} \\ \chi_N \end{bmatrix} + \underbrace{\begin{bmatrix} 0 \\ 0 \\ \vdots \\ B_r \end{bmatrix}}_{B} u_r, \tag{5-56}$$

A_1, A_2 and B_r are in (5-3), while A_{AV1} and A_{AV2} are

$$A_{AV1} = \begin{bmatrix} 0 & 0 \\ \frac{\alpha K_{veh}}{\delta} & K_{veh}(1-\frac{\alpha}{2}) \end{bmatrix} \quad A_{AV2} = \begin{bmatrix} 0 & 1 \\ -\frac{\alpha K_{veh}}{\delta} & -\Big(K_{veh}(1-\frac{\alpha}{2})+c\Big) \end{bmatrix}. \tag{5-57}$$

The fixed variables for the AV are

$$\delta = 23 \quad \alpha = 0.9 \quad c = 0.5. \tag{5-58}$$

The numerical analysis returns the results in Fig. 5-2.

Clearly, for N around 20, which is the scope of interest of both [1, 11], eq. (5-50) and the indirect Lyapunov method applied to (5-56) provide really close conditions for K_{veh} in order to ensure Lyapunov stability of the equilibrium.

5-4-2 Ring Stability and non-linear simulations

This section investigates WRS (Definition 7, Chapter 2) for the mixed platoon with a single AV. The block diagram representation of the linearized mixed platoon is given in Fig. 5-3. The capacity of preventing both Lyapunov and ring stability is evaluated for an AV designed by using Result 2. Fig. 5-3 depicts a type III disturbance acting on the AV, the transfer function $F_i^{AV(N)}(s)$ for a general vehicle i from disturbance to velocity is

$$F_i^{AV(N)}(s) = \frac{\Gamma^{N-i}(s)}{1-\Gamma_{AV}(s)\Gamma^{N-1}(s)} P_N(s) \tag{5-59}$$

Lyapunov stability is ensured by Result 2. For $N = 22$, K_{veh} in Fig. 5-2 is

$$K_{veh} = 0.0029. \tag{5-60}$$

The rest of the numerical values are provided in tabs. 4-1, 4-2 and eq. (5-55) for the HVs and in (5-58) for the AV. For the sake of transparency Fig. 5-4 illustrates how the poles location of the linearized ring change with the AV ($F_i^{AV(N)}$ in (5-59)) and without ($F_i^{(N)}$ in (4-37)).

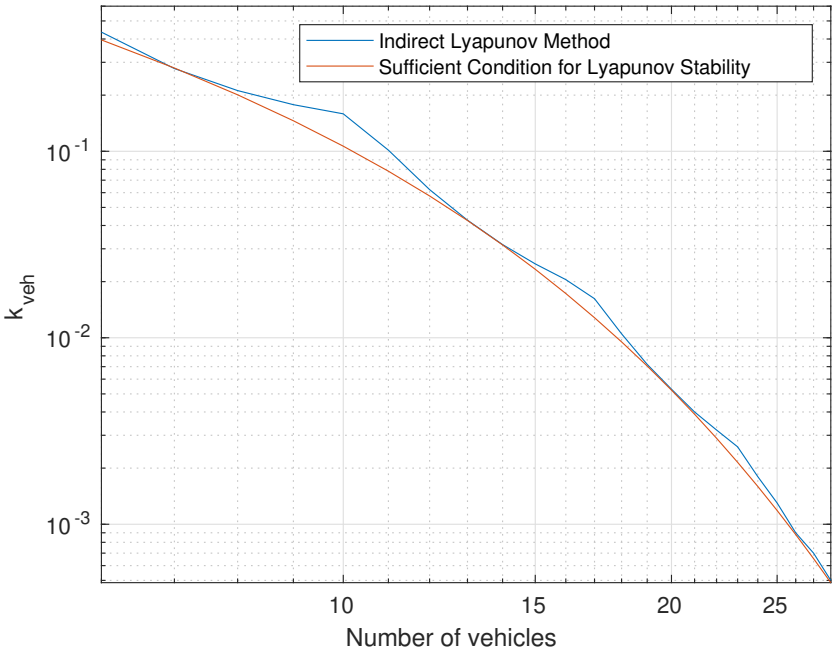

Figure 5-2: This figure compares the K_{veh} obtained in condition (5-50) with the maximum K_{veh}, obtained using the Indirect Lyapunov method (Theorem 1), able to keep the modes of A in (5-56) in the LHP.

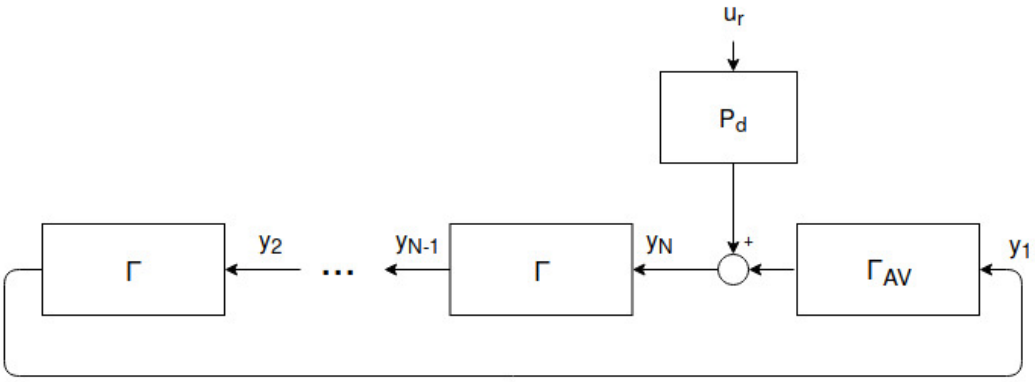

Figure 5-3: Block Diagram representation of a mixed-platoon with a single AV and the remaining HVs. With respect to Fig. 3-4, in this figure the AV transfer function $\Gamma_{AV}(s)$ is present; while, the rest of the transfer functions for the HVs is $\Gamma(s)$.

Similarly to the homogeneous platoon in Chapter 4, a rule of thumb to determine WRS is

$$W_\Gamma \cap W_{F(AV)} \approx \emptyset, \tag{5-61}$$

with

$$W_\Gamma = \{w \quad s.t. \quad |\Gamma(jw)| > 1\} \tag{5-62}$$

$$W_{F(AV)} = \{w \quad s.t. \quad |F_N^{AV(N)}(jw)| > 1\}. \tag{5-63}$$

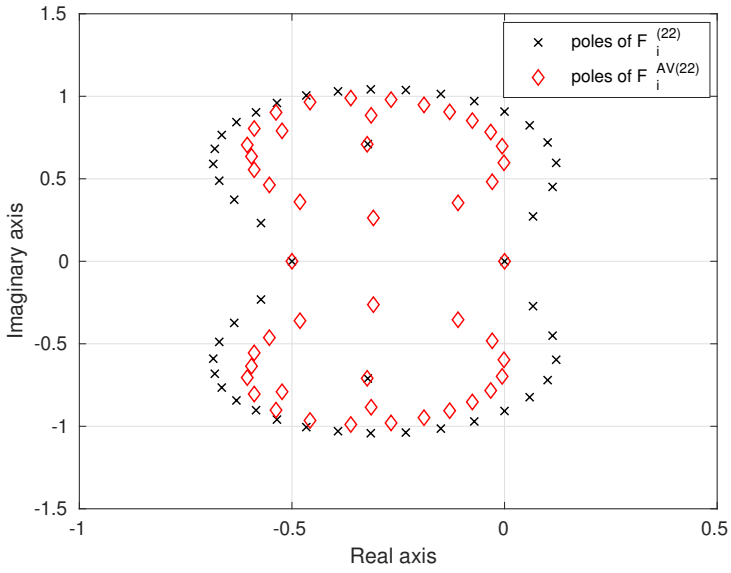

Figure 5-4: Poles distribution of $F_i^{(N)}$ in (4-37) and $F_i^{AV(N)}$ in (5-59) for $N = 22$, $a = 20$ and $b = 0.5$. Clearly the presence of the AV stabilizes the equilibrium in Lyapunov sense.

As Fig. 5-5a shows, this is in fact not the case and consequentially, Fig. 5-5b depicts the typical increase of the frequency peaks moving throughout the platoon. The weak ring instability result is confirmed by the non linear simulations. As Fig. 5-6b illustrates, the transient from initial condition to the v_{AV*} in (5-45), which in this case is exactly the same as the v_* in (4-1), is well damped and the effects of an initial velocity $v_0 = 0$ are almost null. This is mainly because of the choice of $c = 0.5$ which is motivated by the study of the linearized human vehicle dynamics (2-27). Indeed, a reasonable value of c is $c = \bar{b}$ which is also in compliance with (5-49). On the other hand, a small impulse disturbance on the AV acceleration acting at $t = 100s$ for $1s$ is enough to have a remarkable amplification over the vehicles (Fig. 5-6b). The propagation of the wave is also visible in Fig. 5-6a.

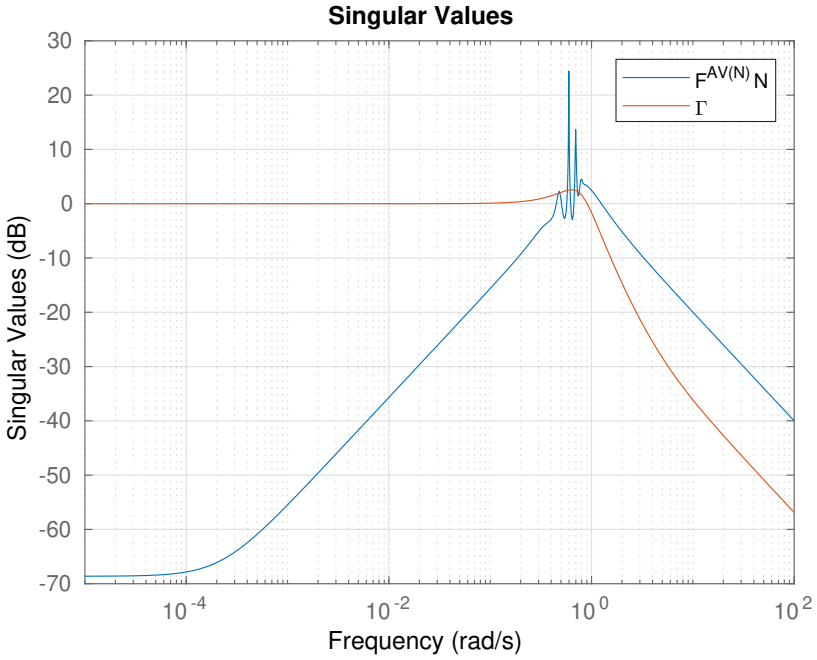

(a)

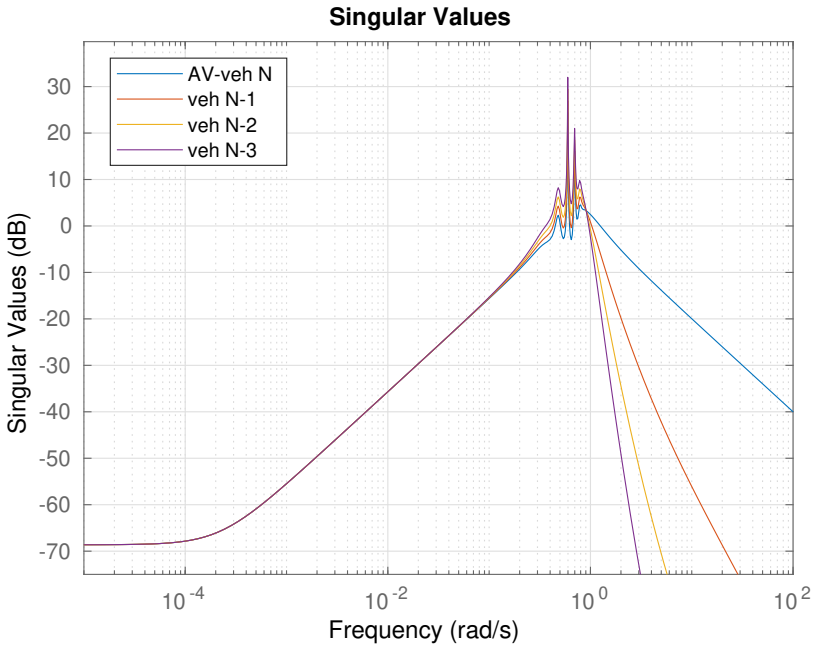

(b)

Figure 5-5: WRS analysis. Fig. 5-5b shows $|F_{22}^{AV(22)}(jw)|$, $|F_{21}^{AV(22)}(jw)|$, $|F_{20}^{AV(22)}(jw)|$ and $|F_{19}^{AV(22)}(jw)|$ with $F_i^{AV(N)}(jw)$ in (5-59), $w \in \mathbb{R}$. The peaks are amplified from vehicle 22 to 19 denoting a ring unstable scenario. Weak ring stability is predicted looking at Fig. 5-5a where $||\Gamma||_\infty$ and $||F_N^{AV(N)}(jw)||_\infty$ $(N = 22)$ occur roughly at the same frequencies.

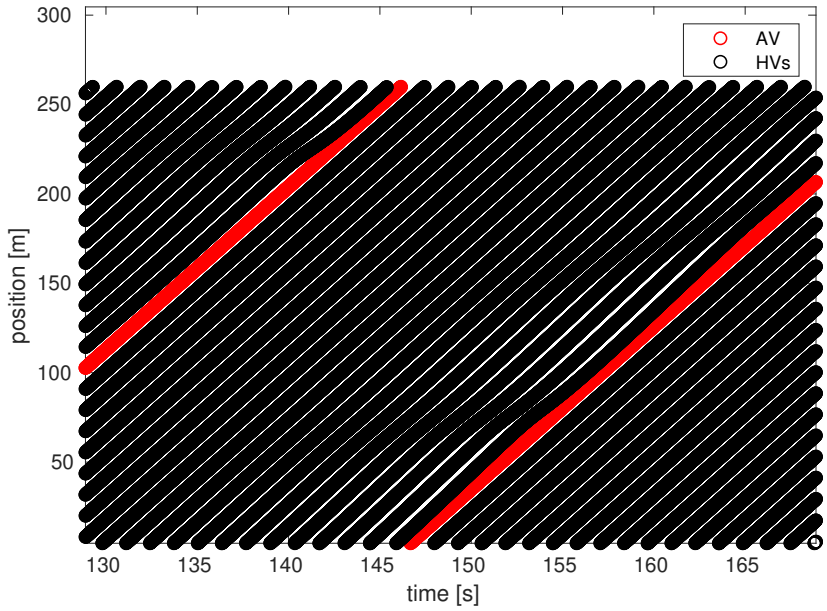

(a) Positions of the N vehicles for $N = 22$, $a = 20$ and $b = 0.5$ for a mixed traffic scenario with a single PI with saturation modified AV in (5-45). The red position is the AV's.

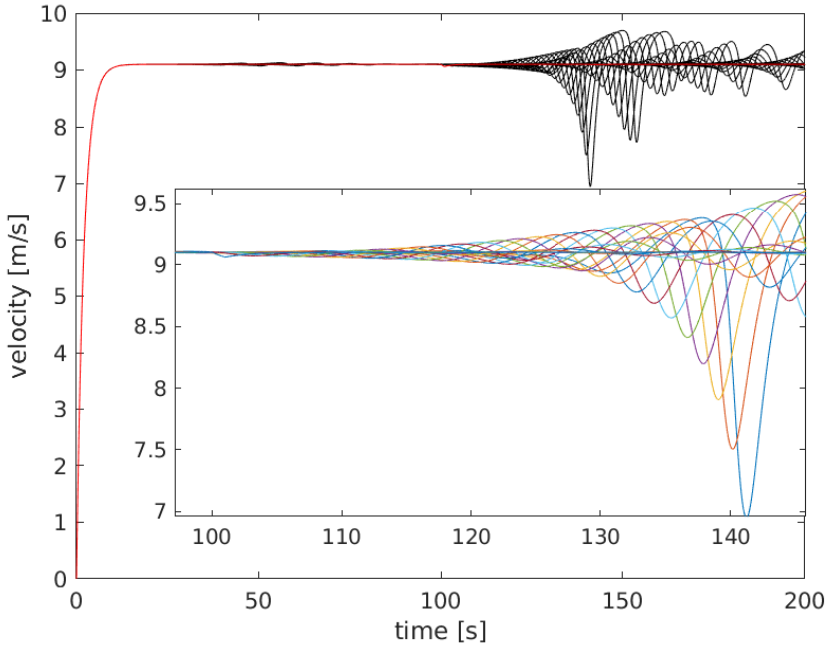

(b) Velocities of the N vehicles for $N = 22$, $a = 20$ and $b = 0.5$ for a mixed traffic scenario with a single PI with saturation modified AV in (5-45). The red velocity is the AV's.

Figure 5-6: Non-linear simulations for $N = 22$, $a = 20$ and $b = 0.5$ for a mixed traffic scenario with a single PI with saturation modified AV in (5-45). Lyapunov stability and rejection of initial conditions perturbations is achieved. An impulse disturbance acts at $t = 60s$ and is amplified throughout the platoon denoting ring instability.

5-4-3 Change the equilibrium of the system

At parity of disturbance a possible way to decrease the ring instability effect is to increase the velocity equilibrium of the overall platoon [25]. The natural equilibrium of the homogeneous platoon is obtained in (4-1) and for the specific case in tabs 4-1 and 4-2, $v_* = 9.09m/s$. Increasing v_{AV*} at $9.3m/s$ for instance, makes the AV reach a smaller equilibrium headway ($h_{AV*} < h_*$) and, in this way, makes the ring "bigger" for the HVs which translates in higher h_*. The linearization obtained for this new equilibrium point shows a decrease in $||\Gamma||_\infty$ as illustrated in Fig 5-7.

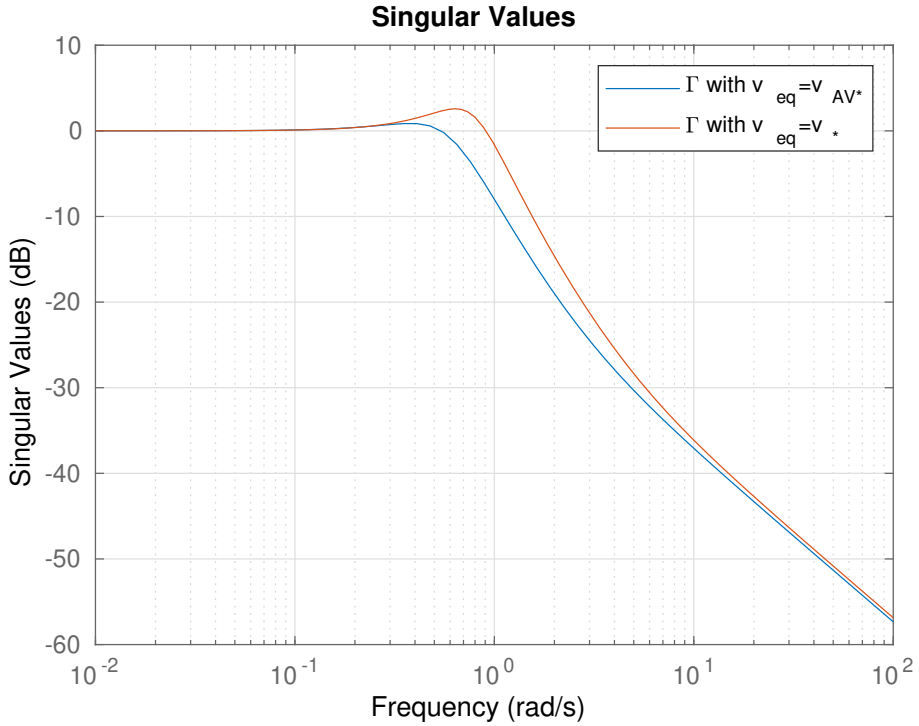

Figure 5-7: Evolution of the HV transfer function $|\Gamma(jw)|$ with $a = 20$ and $b = 0.5$ for different equilibrium points.

This decrease reflects remarkably in the amplification of the disturbance. As in the case of Fig. 5-6b, a small impulse disturbance acts on the AV acceleration at $t = 100s$ for $1s$; however, Fig. 5-8b shows how the amplification is really negligible with respect to what happens in the previous section. However, steering the system to a higher equilibrium velocity pays a price in the transient which in Fig. 5-8b is not as smooth as in Fig. 5-6b.

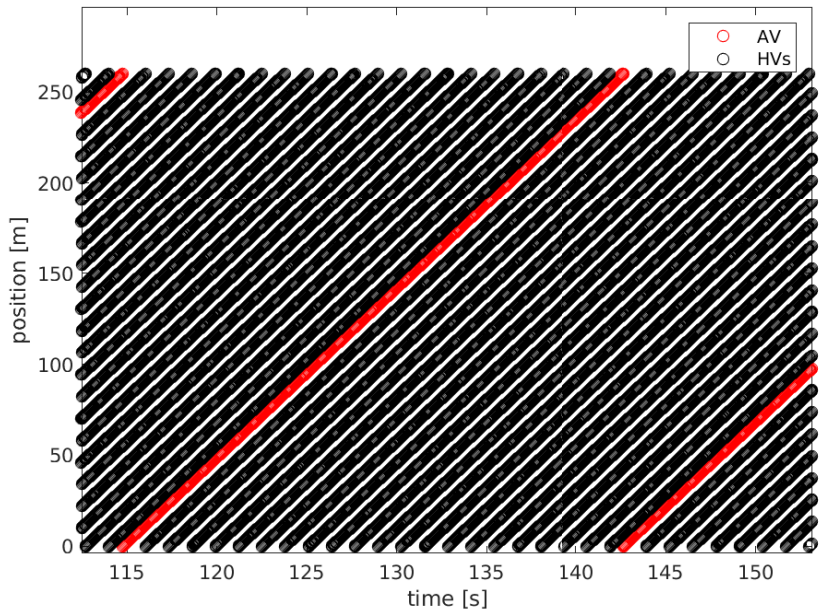

(a) Positions of the N vehicles for $N = 22$, $a = 20$ and $b = 0.5$ for a mixed traffic scenario with a single PI with saturation modified AV in (5-45) and $v_{AV*} = 9.3m/s$. The red position is the AV's.

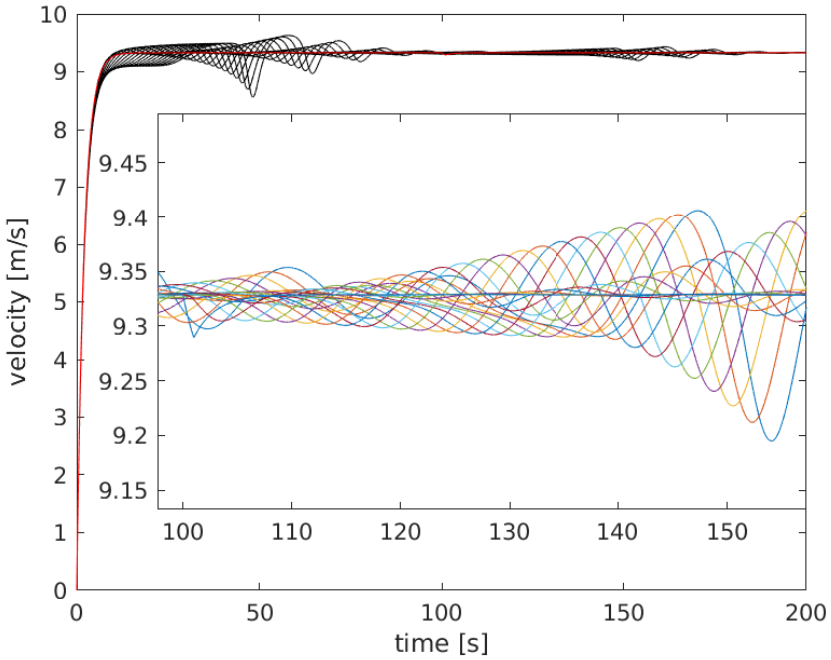

(b) Velocities of the N vehicles for $N = 22$, $a = 20$ and $b = 0.5$ for a mixed traffic scenario with a single PI with saturation modified AV in (5-45) and $v_{AV*} = 9.3m/s$. The red velocity is the AV's.

Figure 5-8: Enabling the AV reaching a new equilibrium velocity $v_{AV*} > v_*$ reduces the headway between the AV and its preceding vehicle. As a result, the ring becomes bigger for the HVs which become "less string unstable" and the same disturbance acting in Fig. 5-6 is better attenuated.

5-4-4 How to accomplish both Lyapunov and Ring stability

In the previous sections, for $N = 22$, and HVs'dynamics (2-25) with $a = 20$ and $b = 0.5$, an AV able to achieve Lyapunov stability have been designed. However, although few strategies to improve the disturbance rejection have been illustrated, Weak Ring stability has not been accomplished. The reasons why the platoon equilibrium ends up weak ring unstable are hereby explained.
In particular, Fig. 5-2 shows the values of K_{veh} in (5-45) able to guarantee Lyapunov stability for $a = 20$, $b = 0.5$ and $N \geq 6$. Regardless the method, $K_{veh} < 0.5$. With such a small value of K_{veh} is not possible to accomplish $W_\Gamma \cap W_{F(AV)} \approx \emptyset$ with W_Γ and $W_{F(AV)}$ defined respectively in (5-62) and (5-63) resulting impossible to achieve weak ring stability. This is because the only way to move $||F_N^{AV(N)}(jw)||_\infty$ at higher frequency ($F_i^{AV(N)}$ in (5-59)) is to increase the value of K_{veh}, which however is constrained to ensure Lyapunov stability. Consequentially, it has been observed that this AV cannot accomplish weak ring stability for $N \geq 5$,$a = 20$ and $b = 0.5$.
Weak ring stability is instead achievable for $N = 4$, $a = 20$ and $b = 0.5$.
The poles of the homogeneous HVs platoon for this scenario are illustrated in Fig. 5-9

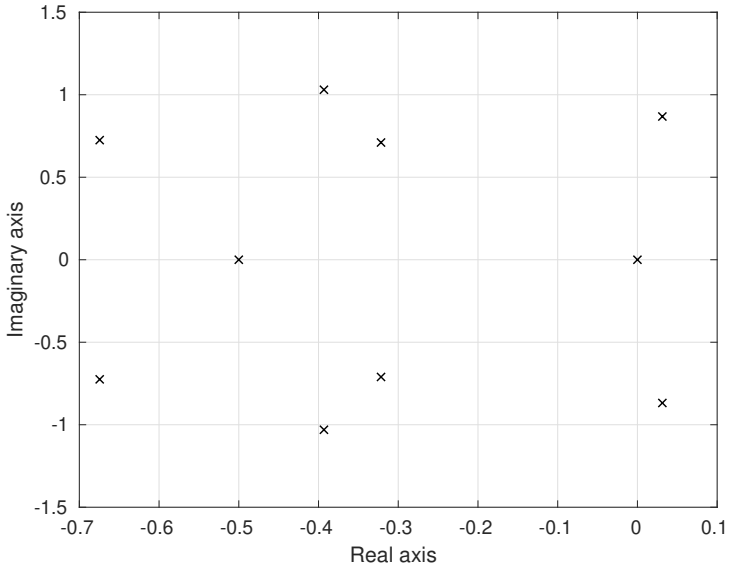

Figure 5-9: Poles distribution in the complex plane for the homogeneous-platoon with $N = 4$ HVs with $a = 20$ and $b = 0.5$.

Clearly, the equilibrium results Lyapunov unstable since Fig. 5-9 shows poles in the Right Half Plane (RHP). At this point, a HV is replaced with a modified PI with saturation AV (5-45); the K_{veh} obtained by using condition (5-51) in Result 2 returns

$$K_{veh} = 0.8723. \tag{5-64}$$

However, applying the indirect Lyapunov method to (5-56) shows that also for $K_{veh} = 15$ all the poles are in the LHP. Fig. 5-10 shows the poles distribution in the complex plane for the

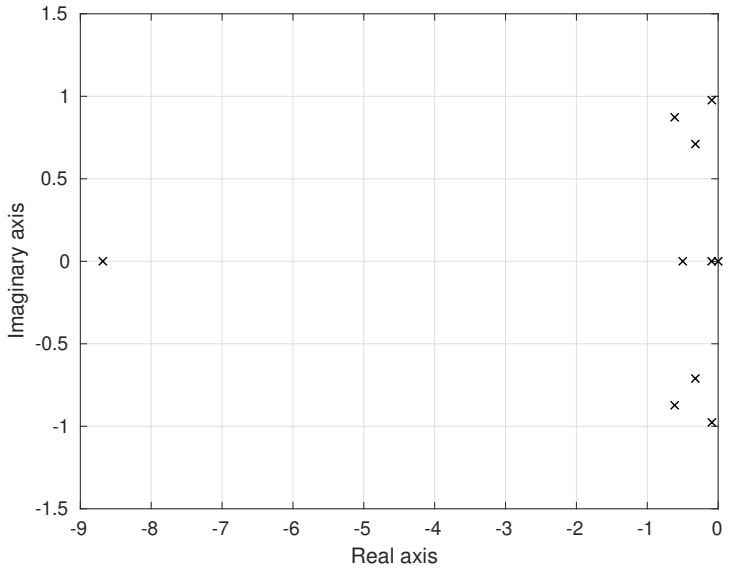

Figure 5-10: Poles distribution in the complex plane for the mixed-platoon with an AV in (5-45) with $K_{veh} = 15$ and the remaining 3 HVs with $a = 20$ and $b = 0.5$.

mixed-platoon with an AV in (5-45) with $K_{veh} = 15$ and the remaining 3 HVs with $a = 20$ and $b = 0.5$.

With $K_{veh} = 15$, $W_\Gamma \cap W_{F(AV)} \approx \emptyset$ (Fig. 5-11b) is accomplished, which means that the equilibrium is weak ring stable. Indeed, Fig. 5-11d depicts a decrease of the frequency peaks moving throughout the platoon. On the other hand, Fig. 5-11a shows that $|F_4^{AV(4)}(jw)|$ in (5-59), $w \in \mathbb{R}$, for $K_{veh} = 0.8723$ has a peak which approaches the same frequencies of $||\Gamma||_\infty$ leading to weak ring instability of the mixed-platoon equilibrium. Weak ring instability for $K_{veh} = 0.8723$ can be visualized in Fig. 5-11c where the peaks increase moving throughout the platoon.

Finally, Fig. 5-12 shows the non-linear simulation for the weak ring stable case, an impulse disturbance occurring at $t = 100s$ is well attenuated and not amplified.

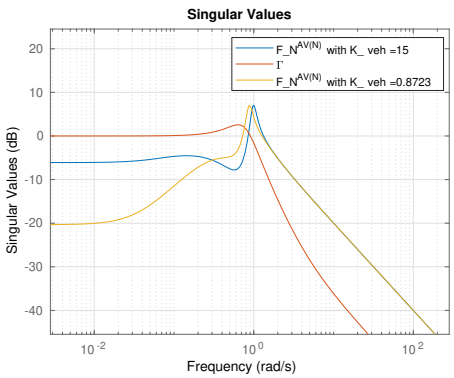

(a) The figure illustrates $|F_4^{AV(4)}(jw)|$ for $K_{veh} = 0.8723$ and $K_{veh} = 15$ and $|\Gamma(jw)|$, $w \in \mathbb{R}$. Clearly, with $K_{veh} = 15$, $||F_4^{AV(4)}||_\infty$ can be moved at higher frequency leading to weak ring stability.

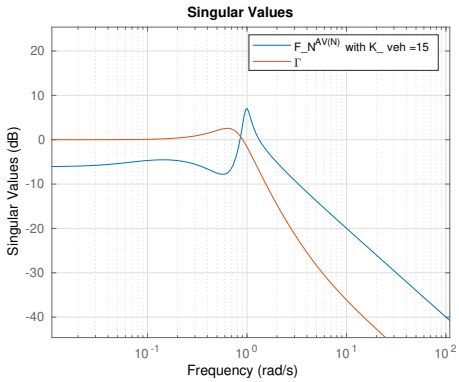

(b) The figure illustrates $|F_4^{AV(4)}(jw)|$ for $K_{veh} = 15$ and $|\Gamma(jw)|$, $w \in \mathbb{R}$. In this case $W_\Gamma \cap W_{F(AV)} \approx \emptyset$.

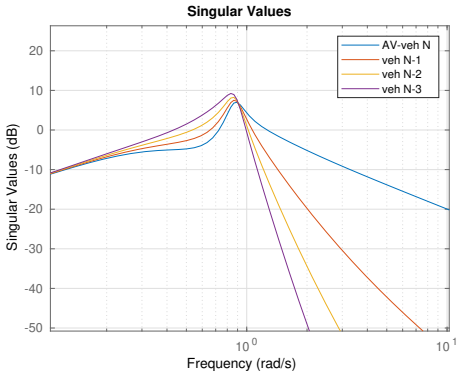

(c) Weak ring unstable case with $K_{veh} = 0.8723$.

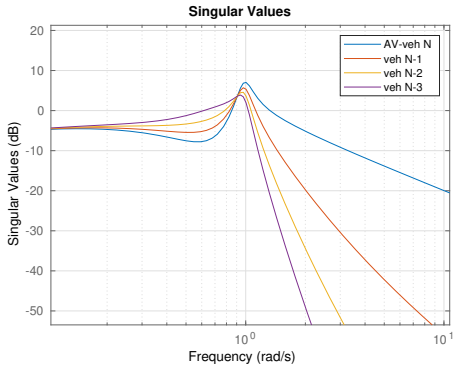

(d) Weak ring stable case with $K_{veh} = 15$.

Figure 5-11: WRS analysis. Fig. 5-11d shows $|F_4^{AV(4)}(jw)|$, $|F_3^{AV(4)}(jw)|$, $|F_2^{AV(4)}(jw)|$ and $|F_1^{AV(4)}(jw)|$ with $F_i^{AV(N)}(jw)$ in (5-59), $w \in \mathbb{R}$. The peaks decrease from vehicle 4 to 1 denoting a ring stable scenario. Weak ring stability is predicted looking at Fig. 5-11b where $||\Gamma||_\infty$ and $||F_N^{AV(N)}(jw)||_\infty$ $(N = 4)$ occur at different frequencies. Fig 5-11c shows instead the weak ring unstable scenario for $K_{veh} = 0.8723$.

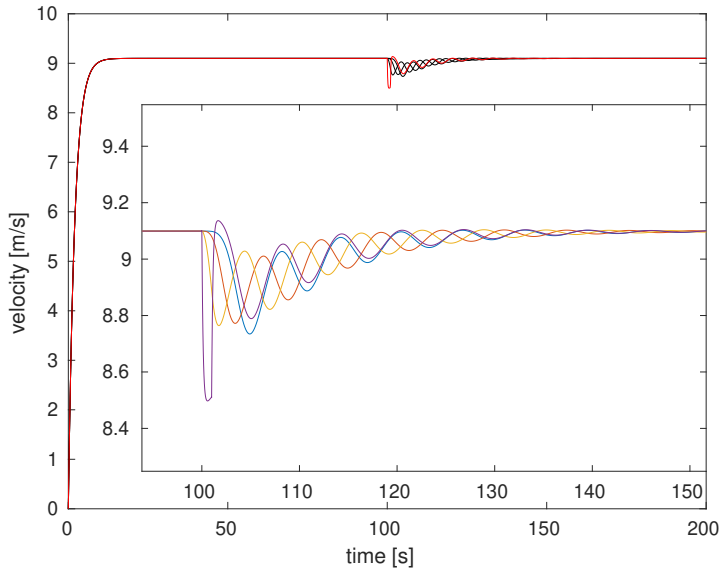

Figure 5-12: Non-linear simulation for the weak ring stable case. An impulse disturbance occurs at $t = 100s$ and it is not amplified throughout the platoon. The red velocity is the AV.

In conclusion, this numerical analysis shows that weak ring stability can be obtained for the modified PI with saturation AV only with a higher penetration rate. For small penetration rates, such as $\gamma = 1/22$ as in [11], only Lyapunov stability can be accomplished.

5-5 Full state H_∞ controller

The second controller developed is a full state H_∞ AV [34, 38, 39]. This controller assumes the knowledge of all the states of the vehicles in the platoon, which means knowing position x_i and velocity v_i for each vehicle i driving on the ring. This can be made possible only by means of communications among the HVs and the AV; as a result, this controller is harder to be practically implemented with respect to a PI with saturation controller that requires only information about its preceding vehicle. The main focus of this section is to understand to what extent eventual communications can improve the controller performance.
For the H_∞ problem, the linearized state-space model at the equilibrium (4-1) for the N-HVs (2-27) on the ring is

$$\dot{\chi} = A\chi + B_1 u_r + B_2 d, \tag{5-65}$$
$$z = QC\chi, \tag{5-66}$$

$$\begin{bmatrix} \dot{\chi}_1 \\ \vdots \\ \dot{\chi}_{N-1} \\ \dot{\chi}_N \end{bmatrix} = \underbrace{\begin{bmatrix} A_1 & A_2 & & O \\ & \ddots & \ddots & \\ & & A_1 & A_2 \\ A_2 & & & A_1 \end{bmatrix}}_{A} \begin{bmatrix} \chi_1 \\ \vdots \\ \chi_{N-1} \\ \chi_N \end{bmatrix} + \underbrace{\begin{bmatrix} 0 \\ 0 \\ \vdots \\ B_r \end{bmatrix}}_{B_1} u_r + \underbrace{\begin{bmatrix} B_r & & & \\ & \ddots & & \\ & & B_r & \\ & & & B_r \end{bmatrix}}_{B_2} \begin{bmatrix} d_1 \\ \vdots \\ d_{N-1} \\ d_N \end{bmatrix}, \quad (5\text{-}67)$$

$$\begin{bmatrix} z_1 \\ \vdots \\ z_{N-1} \\ z_N \end{bmatrix} = \underbrace{\begin{bmatrix} q_1 & & & \\ & \ddots & & \\ & & q_{N-1} & \\ & & & q_N \end{bmatrix}}_{Q} \underbrace{\begin{bmatrix} C_1 & & & \\ & \ddots & & \\ & & C_1 & \\ & & & C_1 \end{bmatrix}}_{C} \begin{bmatrix} \chi_1 \\ \vdots \\ \chi_{N-1} \\ \chi_N \end{bmatrix}, \quad (5\text{-}68)$$

with $\chi_i = [x_i, v_i]^T$ and

$$A_1 = \begin{bmatrix} 0 & 1 \\ & -\bar{a} - \bar{b} \end{bmatrix} \quad A_2 = \begin{bmatrix} 0 & 0 \\ \bar{b}\bar{k} & \bar{a} \end{bmatrix} \quad B_r = \begin{bmatrix} 0 \\ 1 \end{bmatrix} \quad C_1 = \begin{bmatrix} 0 & 1 \end{bmatrix}. \quad (5\text{-}69)$$

Q denotes the matrix of the states weights ($q_i > 0$). It is assumed that there exists a disturbance signal $d(t)$ in each vehicle acceleration signal

$$\dot{v}_i = -\bar{b}\bar{k}x_i - (\bar{a} + \bar{b})v_i + \bar{b}\bar{k}x_{i+1} + \bar{a}v_{i+1} + d_i. \quad (5\text{-}70)$$

Whereas, the control input u_r, which is the AV controller, acts only on the last vehicle N as in the previous section.

$$\dot{v}_N = -\bar{b}\bar{k}x_N - (\bar{a} + \bar{b})v_N + \bar{b}\bar{k}x_1 + \bar{a}v_1 + u_r + d_N. \quad (5\text{-}71)$$

An optimal control input $u = -K\chi$ which stabilizes the equilibrium and minimizes the disturbance influence d_i is the goal of the H_∞ design. Mathematically it becomes

$$\min_K ||G_{dz}||_\infty \quad (5\text{-}72)$$

$$\text{subject to } u_r = -K\chi, \quad (5\text{-}73)$$

where G_{dz} is the transfer function from disturbance signal $d = [d_1, d_2, \ldots, d_N]^T$ to the vehicles velocities $z = [q_1 v_1, q_2 v_2, \ldots, q_N v_N]^T$; the vehicles velocities are considered as traffic performance indexes. For this design, the weights applied to the traffic performance indexes are monotonically decreasing going from 1 to N. This in order penalize more what is far from the AV and try in this way to achieve weak ring stability, which means that the disturbances do not amplify throughout the platoon. On the other hand, no specific weights are applied to the control action.

5-5-1 Numerical evaluation

In order to compare the H_∞ controller with the PI with saturation AV the same case scenario depicted in Section 5-4-2 is also taken here. Hence

$$N = 22 \quad a = 20 \quad b = 0.5. \quad (5\text{-}74)$$

For the sake of clarity, given the linear vehicle dynamics Γ, as in (4-2), and a type III disturbance acting on the N-th vehicle (see Fig. 3-4 for the block diagram representation), the transfer function $F_i^{(N)}(s)$ from disturbance to i-th vehicle velocity for the only HVs homogeneous platoon on the ring is

$$F_i^{(N)}(s) = \frac{\Gamma^{N-i}(s)}{1-\Gamma^N(s)} P_N(s). \tag{5-75}$$

While, considering the AV as well, the transfer function $F_i^{AV(N)}(s)$ for a general vehicle i from disturbance to velocity is

$$F_i^{AV(N)}(s) = \frac{\Gamma^{N-i}(s)}{1-\Gamma_{AV}(s)\Gamma^{N-1}(s)} P_N(s), \tag{5-76}$$

with $\Gamma_{AV}(s)$ the AV transfer function resulting from the H_∞ optimization problem. Fig.5-13 shows $|F_i^{(N)}(jw)|$ in (5-75) for the vehicles $i \in \{17,\dots,22\}$, $w \in \mathbb{R}$. Whereas, Fig. 5-14 shows $|F_i^{AV(N)}(jw)|$ in (5-76) for the same vehicles $i \in \{17,\dots,22\}$; clearly the effects of the H_∞-AV are evident and the peaks related to the disturbance effect (visible in Fig.5-13) are remarkably smoothed. In Fig. 5-14 the frequency range is the same as Fig.5-13 in order to ease the comparison before and after the AV action. Fig 5-15 instead depicts $||F_i^{AV(N)}||_\infty$ for $i \in \{17,\dots,22\}$ which in this case occurs at lower frequencies; the peaks have the same magnitude and therefore moving throughout the platoon no amplification or really marginal is expected denoting therefore a weak ring stability scenario.

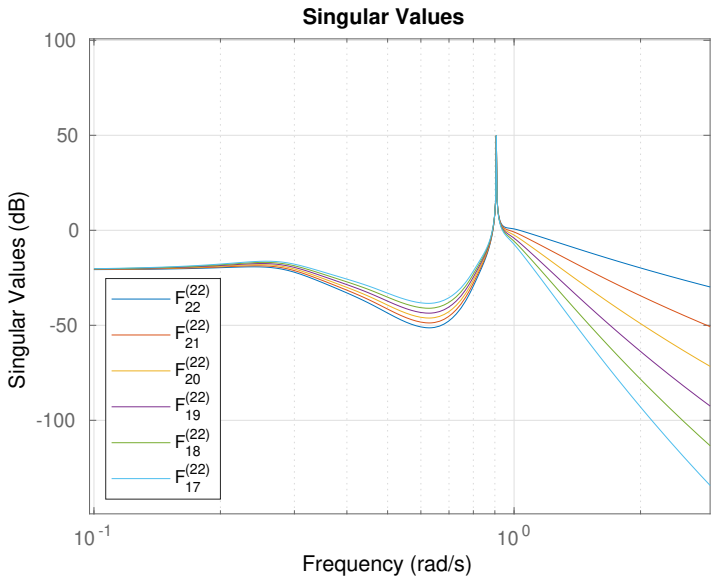

Figure 5-13: $|F_i^{(N)}(jw)|$ in (5-75) for the vehicles $i \in \{17,\dots,22\}$, $w \in \mathbb{R}$.

This AV achieves remarkable performance in terms of both tracking and disturbance rejection and weak ring stability is indeed observed.
Fig. 5-16 shows an impulse disturbance acting on the 21st HV at $t = 10s$, while Fig. 5-17 shows an impulse disturbance acting on the AV again at $t = 10s$. As the figures show the AV

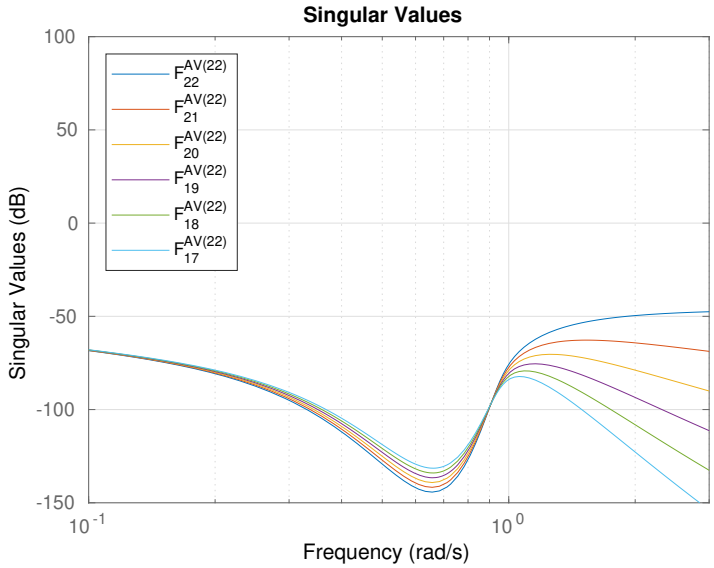

Figure 5-14: $|F_i^{AV(N)}(jw)|$ in (5-76) for vehicles $i \in \{17, \dots, 22\}$. The AV is designed by solving the H_∞ optimization problem in (5-72) and (5-73).

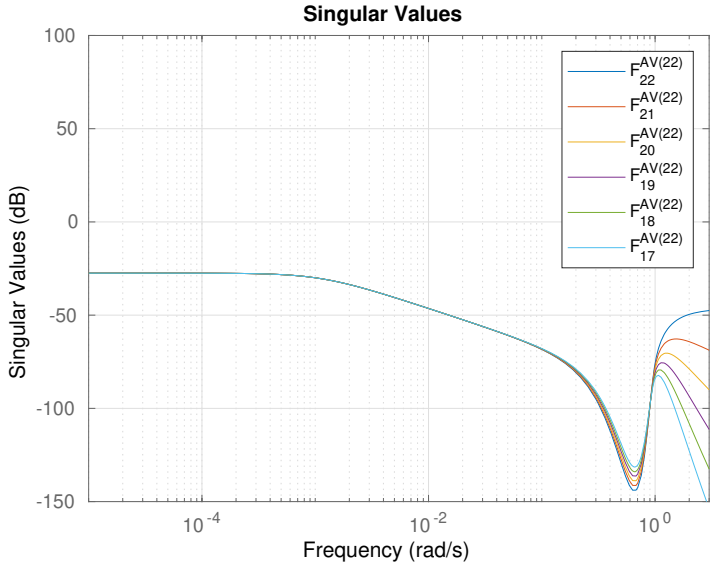

Figure 5-15: This figure is the same as Fig. 5-14 just for a bigger frequency range which allows to see $||F_i^{AV(N)}||_\infty$ for $i \in \{17, \dots, 22\}$.

is able to quickly compensate for the perturbations accomplishing good rejection and avoiding the amplification of the disturbances throughout the vehicles in the platoon.

In conclusion, the strong assumption of full communication AV-HVs and a H_∞ controller properly designed are able to guarantee weak ring stability for this HVs dynamics and with a penetration rate of $1/22$.

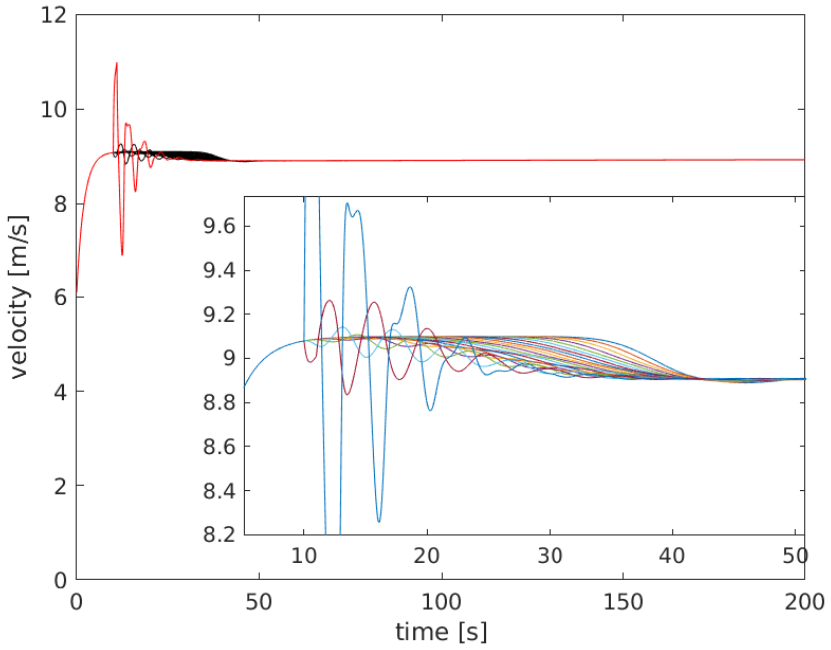

Figure 5-16: Non-linear simulations velocities for the $N = 22$ mixed-platoon with a full state H_∞ AV and HVs with $a = 20$ and $b = 0.5$. An impulse disturbance acts on the HVs at $t = 10s$ and is slightly amplified throughout the platoon. The red velocity is the AV.

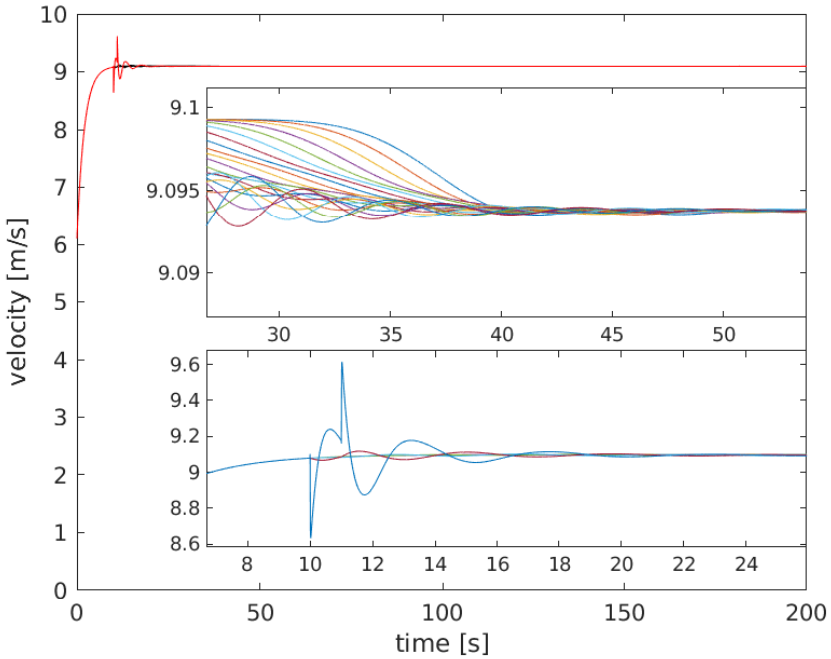

Figure 5-17: Non-linear simulations velocities for the $N = 22$ mixed-platoon with a full state H_∞ AV and HVs with $a = 20$ and $b = 0.5$. An impulse disturbance acts on the AV at $t = 10s$ and is slightly amplified throughout the platoon. The red velocity is the AV.

5-6 Discussion

To summarize, this chapter contains the highest number of contributions and, inspired by the experimental evidence in [11], this chapter provides a theoretical support for the design of an AV able to stabilize the ring.
First of all, a controllability analysis is performed on the linearized state-space (5-2), in a similar fashion to [34] and endorsing the result obtained in [22] which states that a single AV is always able to stabilize the platoon for $t \to \infty$ and for any arbitrary number N of HVs. Secondly, the chapter provides a sufficient condition for stability in Lyapunov sense for the mixed AV-HV platoon (Proposition 1), such condition is then exploited in the AV design.
Afterwards, the PI with saturation controller developed in [12] is analyzed and the need for a new modified version is theoretically supported.
By means of numerical analysis, conservativeness of the sufficient condition for Lyapunov stability and weak ring stability for the realistic scenario in [11] are estimated. In addition to this, two sides results are presented: how to improve the disturbance rejection properties of the platoon by changing the AV equilibrium and how to achieve weak ring stability by increasing the AV penetration rate.
Finally, in order to determine to what extent enabling communications among vehicles would improve the AV performance, a full-state H_∞ is designed. Note that the H_∞ is not a casual choice, since it is able to asymptotically stabilize the equilibrium while minimizing the disturbance effects. Conversely, other full-state feedback controllers would have only ensured asymptotic stability. The conclusion of this analysis is that, enabling communications of the AV with the HVs improve the performance and also for a small penetration rate such as those in [11], it is able to guarantee weak ring stability.

Chapter 6

Conclusion

This thesis proposed to address the following open problems:

- An *absence of a theoretical framework* by means of Linear Time Invariant (LTI) systems theory *for the two experiments* [1, 11].
- To what extent *the more common definitions adopted for the stability on a string can be actually used on a ring road topology.*
- Identify the stability problems that an Autonomous Vehicle (AV) has to face on a ring roadway and propose methods for a stabilizing design also for a really small penetration rate.

In order to do so, the work has been divided in two main macro-sections: a first theoretical analysis of the relevant field experiments [1, 11] and a second which discusses how to design an AV that, with a small penetration rate, is able to stabilize the traffic flow on a ring road setup for any number N of vehicles.
During the literature study, it has been realized that a theoretical analysis by means of LTI systems theory of the mentioned field experiments was missing, with the exception of [34] that was published at survey almost finished. As a result, such analysis was considered relevant in order to determine and motivate a method to design a stabilizing AV which can be exploited for traffic control.

- In the first macro-section, the instability observed in [1] has been determined to be in Lyapunov sense; since, for the given Human-driven Vehicle (HV)s dynamics, the ring road state-space at the equilibrium was showing modes in the Right Half Plane (RHP).
- Furthermore, it has been discovered that Strong frequency domain string stability (SFSS), which means amplification of disturbances throughout the platoon on a string, does not imply asymptotic instability of the ring roadway equilibrium. From this study arose that, for certain number N of string unstable HVs, the equilibrium of the ring was

though appearing asymptotically stable. In order to deal with this unpublished cases, the definition of Weak Ring Stability (WRS) has been formulated and introduced in the experiments analysis providing new insights on the ring road scenario.

- The goal of the second macro-section was to determine, with the help of analytical results, a design for an AV useful to stabilize a platoon which would have been otherwise unstable. As first controller, a PI with saturation, already adopted in [11, 12] and empirically designed and tested, was in first instance considered. By analyzing the controller at the equilibrium, the need for a modified version has been theoretically supported. Based on this new version, an analytical result (Result 2) has been formulated in order to ensure Lyapunov stability for an arbitrary number N of vehicles. Concerning WRS, it was not accomplished by means of the modified PI with saturation AV for a small penetration rate such as the $\gamma = 1/22$ depicted in [11]. However, for higher penetration rate ($\gamma = 1/4$) it has been shown how both asymptotic and weak ring stability can be obtained.
- Finally, in order to determine the eventual positive effects of communications between AV and HVs, an H_∞-AV has been designed and tested on the same setup of the previous controller and for a penetration rate of $1/22$. With this AV the performance improved and weak ring stability was accomplished for $\gamma = 1/22$.

In conclusion, the WRS requirement appeared too demanding for small penetration rates and for controllers with a limited amount of information. On the other hand, communications AV-HVs and a proper H_∞-AV design were able to mitigate the disturbances effects and accomplish both Lyapunov and Weak ring stability on the ring roadway.

Future works could consider testing the different controllers on a real field experiment, this in order to validate the obtained results. Additionally, algorithm for real time estimation of the HVs dynamics can be developed and an AV, able to adaptively change its behavior, designed. Eventually, the implementation of traffic control strategies by means of AV in a more complex scenarios, such as multi-lane highways, could represent eventual future research topics.

Appendix A

Circulant Matrices

Definition 8 (**Circulant Matrix**.). *[33] A NxN circulant matrix is generated from the N-vector* $\{c_1, c_2, \ldots, c_n\}$ *by cyclically permuting its entries, and is of the form:*

$$C = \begin{bmatrix} c_1 & c_2 & \ldots & c_N \\ c_N & c_2 & \ldots & c_{N-1} \\ \vdots & \vdots & \ddots & \vdots \\ c_2 & c_3 & \ldots & c_1 \end{bmatrix}. \tag{A-1}$$

Definition 9 (**Block Circulant Matrix**.). *Let* C_i *be a* MxM *matrix for each* $i = 1, 2, \ldots N$. *Then a* $NMxNM$ *block circulant matrix is generated from the ordered set* $\{C_1, C_2, \ldots, C_n\}$ *and is of the form:*

$$C = \begin{bmatrix} C_1 & C_2 & \ldots & C_N \\ C_N & C_1 & \ldots & C_{N-1} \\ \vdots & \vdots & \ddots & \vdots \\ C_2 & C_3 & \ldots & C_1 \end{bmatrix}. \tag{A-2}$$

Definition 10 (**Generating Matrices**.). *Let the* $NMxNM$ *block circulant* C *be given by definition 9 then the elements of the ordered set*

$$\{C_1, C_2, \ldots, C_N\} \tag{A-3}$$

are said to be generating matrices of C.

A block circulant is therefore defined completely by its generating matrices. The matrix array given by Definition 9 is said to be a block circulant of type (M, N). The set of all such matrices is denoted by $\mathcal{BC}_{M;N}$.

A-1 Diagonalization of a Circulant matrix

A unitary transformation involving the Fourier matrix is used to diagonalize general block circulant matrices.

Nth roots of Unity.

A root of unity is any complex number that results in 1 when raised to some integer $N \in Z_+$. More generally, the Nth roots of a complex number $z_0 = r_0 e^{j\theta_0}$ are given by a nonzero number $z = re^{j\theta_0}$ such that

$$z^N = 0 \quad \text{or} \quad r^N e^{jN\theta} = r_0 e^{j\theta_0} \tag{A-4}$$

where $j = \sqrt{-1}$. Eq. (A-4) holds if and only if $r^N = r_0$ and $N\theta = \theta_0 + 2\pi k$ with $k \in \mathbb{Z}$. Therefore,

$$\begin{aligned} r &= \sqrt[N]{r_0} \\ \theta &= \frac{\theta_0 + 2\pi k}{N} \quad k \in \mathbb{Z} \end{aligned} \tag{A-5}$$

and the Nth roots are

$$z = \sqrt[N]{r_0} \exp\left(j\frac{\theta_0 + 2\pi k}{N}\right) \quad k \in \mathbb{Z}. \tag{A-6}$$

Eq. (A-6) shows that the roots all lie on a circle of radius $\sqrt[N]{r_0}$ centered at the origin in the complex plane, and that they are equally distributed every $2\pi/N$ radians. Thus, all of the distinct roots correspond to $k = 0, 1, 2, \ldots, N-1$.

Definition 11 (**Distinct Nth Roots of Unity**). *The distinct Nth roots of unity follow from Eq.(A-6) by setting $r_0 = 1$ and $\theta_0 = 0$ and are denoted by*

$$w_N^{(k)} = w_N^k = e^{j\frac{2\pi k}{N}} \tag{A-7}$$

for integers $k = 0, 1, 2, \ldots, N-1$.

A-1-1 The Fourier Matrix

This section introduces the complex Fourier matrix and its relevant proprieties, including the symmetric structure of the $N-$vectors that compose its columns. A key result is that the Fourier matrix is unitary, which is systematically developed and proved.

Definition 12 (**Fourier Matrix**.). *The NxN Fourier matrix is defined as*

$$E_N = \frac{1}{\sqrt{N}} \begin{bmatrix} 1 & 1 & 1 & \ldots & 1 \\ 1 & w_N & w_N^2 & \ldots & w_N^{N-1} \\ 1 & w_N^2 & w_N^4 & \ldots & w_N^{2(N-1)} \\ \vdots & \vdots & \vdots & \ddots & \vdots \\ 1 & w_N^{N-1} & w_N^{2(N-1)} & \ldots & w_N^{(N-1)(N-1)} \end{bmatrix}_{NxN} \tag{A-8}$$

where w_N is the primitive Nth root of unity and $N \in \mathbb{Z}_+$.

Theorem 4 (**Diagonalization of a Circulant**.). *Let $C \in \mathcal{C}_N$ have generating elements $c_1, c_2, \ldots, c_N$. Then if E_N is the NxN Fourier matrix,*

$$E_N^H C E_N = \begin{bmatrix} \lambda_1 & & & 0 \\ & \lambda_2 & & 0 \\ & & \ddots & \\ 0 & & & \lambda_N \end{bmatrix}, \tag{A-9}$$

is a diagonal matrix. $(\cdot)^H = \bar{(\cdot)}^T$ is the conjugate transpose. For $i = 1, 2, \ldots, N$, the diagonal elements are

$$\lambda_i = \sum_{k=1}^{N} c_k w_N^{(k-1)(i-1)}, \tag{A-10}$$

where w_N is the primitive Nth root of unity.

Theorem 5 (**Block Diagonalization of a Block Circulant**.). *Let $C \in \mathcal{BC}_{M,N}$ and denote its MxM generating matrices by $C_1, C_2, \ldots, C_N$. Then if E_N is the NxN Fourier matrix and I_M is the identity matrix of dimension M,*

$$(E_N^H \otimes I_M) C (E_N \otimes I_M) = \begin{bmatrix} \Lambda_1 & & & 0 \\ & \Lambda_2 & & 0 \\ & & \ddots & \\ 0 & & & \Lambda_N \end{bmatrix} \tag{A-11}$$

is a $NMxNM$ block diagonal matrix. For $i = 1, 2, \ldots, N$, the MxM diagonal blocks are

$$\Lambda_i = \sum_{k=1}^{N} C_k w_k^{(k-1)(i-1)} \tag{A-12}$$

where w_N is the primitive Nth root of unity.

References

[1] Yuki Sugiyama, Minoru Fukui, Macoto Kikuchi, Katsuya Hasebe, Akihiro Nakayama, Katsuhiro Nishinari, Shin-ichi Tadaki, and Satoshi Yukawa. "Traffic jams without bottlenecks experimental evidence for the physical mechanism of the formation of a jam". In: *New journal of physics* 10.3 (2008), p. 033001.

[2] Hyun Keun Lee, Robert Barlovic, Michael Schreckenberg, and Doochul Kim. "Mechanical restriction versus human overreaction triggering congested traffic states". In: *Physical review letters* 92.23 (2004), p. 238702.

[3] Wolfgang Knospe, Ludger Santen, Andreas Schadschneider, and Michael Schreckenberg. "Human behavior as origin of traffic phases". In: *Physical Review E* 65.1 (2001), p. 015101.

[4] Markos Papageorgiou and Apostolos Kotsialos. "Freeway ramp metering: An overview". In: *IEEE transactions on intelligent transportation systems* 3.4 (2002), pp. 271–281.

[5] Lakshmi Dhevi Baskar, Bart De Schutter, J Hellendoorn, and Zoltan Papp. "Traffic control and intelligent vehicle highway systems: a survey". In: *IET Intelligent Transport Systems* 5.1 (2011), pp. 38–52.

[6] Simone Baldi, Iakovos Michailidis, Elias B Kosmatopoulos, Antonis Papachristodoulou, and Petros A Ioannou. "Convex design control for practical nonlinear systems". In: *IEEE Transactions on Automatic Control* 59.7 (2014), pp. 1692–1705.

[7] LC Davis. "Effect of adaptive cruise control systems on traffic flow". In: *Physical Review E* 69.6 (2004), p. 066110.

[8] Florian Knorr, Daniel Baselt, Michael Schreckenberg, and Martin Mauve. "Reducing traffic jams via VANETs". In: *IEEE Transactions on Vehicular Technology* 61.8 (2012), pp. 3490–3498.

[9] Maxime Guériau, Romain Billot, Nour-Eddin El Faouzi, Julien Monteil, Frédéric Armetta, and Salima Hassas. "How to assess the benefits of connected vehicles? A simulation framework for the design of cooperative traffic management strategies". In: *Transportation research part C: emerging technologies* 67 (2016), pp. 266–279.

[10] Youssef Abou Harfouch, Shuai Yuan, and Simone Baldi. "An Adaptive Switched Control Approach to Heterogeneous Platooning With Intervehicle Communication Losses". In: *IEEE Transactions on Control of Network Systems* 5.3 (2018), pp. 1434–1444.

[11] Raphael E Stern, Shumo Cui, Maria Laura Delle Monache, Rahul Bhadani, Matt Bunting, Miles Churchill, Nathaniel Hamilton, Hannah Pohlmann, Fangyu Wu, Benedetto Piccoli, et al. "Dissipation of stop-and-go waves via control of autonomous vehicles: Field experiments". In: *Transportation Research Part C: Emerging Technologies* 89 (2018), pp. 205–221.

[12] Maria Laura Delle Monache, Thibault Liard, Anais Rat, Raphael Stern, Rahul Badhani, Benjamin Seibold, Jonathan Sprinkle, Daniel Work, and Benedetto Piccoli. "Feedback control algorithms for the dissipation of traffic waves with autonomous vehicles". In: (2017). to appear.

[13] Masako Bando, Katsuya Hasebe, Akihiro Nakayama, Akihiro Shibata, and Yuki Sugiyama. "Dynamical model of traffic congestion and numerical simulation". In: *Physical review E* 51.2 (1995), p. 1035.

[14] Kai Nagel and Michael Schreckenberg. "A cellular automaton model for freeway traffic". In: *Journal de physique I* 2.12 (1992), pp. 2221–2229.

[15] Louis Albert Pipes. "Car following models and the fundamental diagram of road traffic". In: *Transportation Research/UK/* (1966).

[16] R Eddie Wilson. "Mechanisms for spatio-temporal pattern formation in highway traffic models". In: *Philosophical Transactions of the Royal Society A: Mathematical, Physical and Engineering Sciences* 366.1872 (2008), pp. 2017–2032.

[17] Masako Bando, Katsuya Hasebe, Ken Nakanishi, and Akihiro Nakayama. "Analysis of optimal velocity model with explicit delay". In: *Physical Review E* 58.5 (1998), p. 5429.

[18] Martin Treiber, Ansgar Hennecke, and Dirk Helbing. "Congested traffic states in empirical observations and microscopic simulations". In: *Physical review E* 62.2 (2000), p. 1805.

[19] Denos C Gazis, Robert Herman, and Richard W Rothery. "Nonlinear follow-the-leader models of traffic flow". In: *Operations research* 9.4 (1961), pp. 545–567.

[20] Gábor Orosz, R Eddie Wilson, and Gábor Stépán. *Traffic jams: dynamics and control*. 2010.

[21] Dirk Helbing, Hans J Herrmann, Michael Schreckenberg, and Dietrich E Wolf. *Traffic and granular flow99: social, traffic, and granular dynamics*. Springer Science & Business Media, 2012.

[22] Shumo Cui, Benjamin Seibold, Raphael Stern, and Daniel B Work. "Stabilizing traffic flow via a single autonomous vehicle: Possibilities and limitations". In: *2017 IEEE Intelligent Vehicles Symposium (IV)*. IEEE. 2017, pp. 1336–1341.

[23] R Eddie Wilson and Jonathan A Ward. "Car-following models: fifty years of linear stability analysis–a mathematical perspective". In: *Transportation Planning and Technology* 34.1 (2011), pp. 3–18.

[24] Hassan K Khalil and Jessy W Grizzle. *Nonlinear systems*. Vol. 3. Prentice hall Upper Saddle River, NJ, 2002.

[25] Shuo Feng, Yi Zhang, Shengbo Eben Li, Zhong Cao, Henry X Liu, and Li Li. "String stability for vehicular platoon control: Definitions and analysis methods". In: *Annual Reviews in Control* (2019).

[26] L Peppard. "String stability of relative-motion PID vehicle control systems". In: *IEEE Transactions on Automatic Control* 19.5 (1974), pp. 579–581.

[27] Kai-ching Chu. "Decentralized control of high-speed vehicular strings". In: *Transportation science* 8.4 (1974), pp. 361–384.

[28] Jeroen Ploeg, Nathan Van De Wouw, and Henk Nijmeijer. "Lp string stability of cascaded systems: Application to vehicle platooning". In: *IEEE Transactions on Control Systems Technology* 22.2 (2014), pp. 786–793.

[29] Maziar E Khatir and EJ Davidson. "Bounded stability and eventual string stability of a large platoon of vehicles using non-identical controllers". In: *2004 43rd IEEE Conference on Decision and Control (CDC)(IEEE Cat. No. 04CH37601)*. Vol. 1. IEEE. 2004, pp. 1111–1116.

[30] Andrés A Peters, Richard H Middleton, and Oliver Mason. "Cyclic interconnection for formation control of 1-D vehicle strings". In: *European Journal of Control* 27 (2016), pp. 36–44.

[31] Jin Ge. "Connected Cruise Control Design in Mixed Traffic Flow Consisting of Human-Driven and Automated Vehicles". In: (2017).

[32] Jonathan A Rogge and Dirk Aeyels. "Vehicle platoons through ring coupling". In: *IEEE Transactions on Automatic Control* 53.6 (2008), pp. 1370–1377.

[33] Brian J Olson, Steven W Shaw, Chengzhi Shi, Christophe Pierre, and Robert G Parker. "Circulant matrices and their application to vibration analysis". In: *Applied Mechanics Reviews* 66.4 (2014), p. 040803.

[34] Yang Zheng, Jiawei Wang, and Keqiang Li. "Smoothing traffic flow via control of autonomous vehicles". In: *arXiv preprint arXiv:1812.09544* (2018).

[35] Robert B Burckel. *An introduction to classical complex analysis*. Vol. 1. Academic Press, 1980.

[36] Andrés A Peters. "Stability and String Stability Analysis of Formation Control Architectures for Platooning." PhD thesis. National University of Ireland Maynooth, 2015.

[37] Rudolf Emil Kalman. "Mathematical description of linear dynamical systems". In: *Journal of the Society for Industrial and Applied Mathematics, Series A: Control* 1.2 (1963), pp. 152–192.

[38] Sigurd Skogestad and Ian Postlethwaite. *Multivariable feedback control: analysis and design*. Vol. 2. Wiley New York, 2007.

[39] Anton Stoorvogel. *The H infinity control problem: a state space approach*. Citeseer, 1990.

Glossary

List of Acronyms

AV	Autonomous Vehicle
HV	Human-driven Vehicle
LTI	Linear Time Invariant
PI	Proportional-Integral
LHP	Left Half Plane
RHP	Right Half Plane
CF	Car-Following
OVM	Optimal Velocity Model
FTL	Follow-The-Leader
IDM	Intelligent Driver Model
OSS	Original definition of String Stability
PF	Predecessor Following
SFSS	Strong frequency domain string stability
ESS	Eventual Stability Definition
LPSS	L_p string stability
SRS	Strong Ring Stability
WRS	Weak Ring Stability
OV-FTL	Optimal Velocity-Follow the Leader